IRON OXIDE/SILICA CORE-SHELL NANOPARTICLES AS RECHARGEABLE SOURCES OF SINGLET OXYGEN FOR SYNTHETIC APPLICATIONS

A THESIS SUBMITTED TO

THE GRADUATE SCHOOL OF ENGINEERING AND SCIENCE

OF BILKENT UNIVERSITY

IN PARTIAL FULFILLMENT OF THE REQUIREMENTS FOR

THE DEGREE OF

MASTER OF SCIENCE

IN

CHEMISTRY

By

DENİZ YILDIZ

April 2017

IRON OXIDE/SILICA CORE-SHELL NANOPARTICLES AS RECHARGEABLE SOURCES OF SINGLET OXYGEN FOR SYNTHETIC APPLICATIONS
By DENİZ YILDIZ
April 2017

We certify that we have read this thesis and that in our opinion it is fully adequate, in scope and in quality, as a thesis for the degree of Master of Science.

Engin Umut AKKAYA(Advisor)

Bilge BAYTEKİN

Salih ÖZÇUBUKÇU

Approved for the Graduate School of Engineering and Science:

Ezhan KARASAN
Director of the Graduate School

ABSTRACT

IRON OXIDE/SILICA CORE-SHELL NANOPARTICLES AS RECHARGEABLE SOURCES OF SINGLET OXYGEN FOR SYNTHETIC APPLICATIONS

DENİZ YILDIZ
MSc. in Chemistry
Advisor: Engin Umut AKKAYA
April 2017

In the rapidly developing world of synthetic chemistry, there is a constant need for high-efficient catalyst. Besides this, reusable and easily removable catalysts are highly desired to reduce costs for environmentally friendly synthesis for both synthetic and manufacturing requirements. Magnetic nanoparticles (MNPs) are promising candidates for effortlessly removable structures due to their ability of being removed by magnetic field. Iron oxide nanoparticles have a well distinguished place among MNPs since they have unique properties and they can be prepared and functionalized easily.

Combination of photosensitizers with MNPs is a new approach for synthetic applications due to the fact that singlet oxygen is a reactive specie for various types of reactions. Herein, BODIPY with 2-pyridone moiety on silica coated iron oxide nanoparticle is designed as a magnetically removable nanostructure that can generate, store and release singlet oxygen. The efficiency is studied by the oxidation of organic sulfides to sulfoxides since they are at the core of many biological processes. Furthermore, this design can produce recyclable and reusable catalysts for additional transformations with high efficieny.

Keywords: BODIPY, SPIONs, endoperoxide, singlet oxygen, photo-oxidation, sulfoxide.

ÖZET

SENTETİK UYGULAMALAR İÇİN SİNGLET OKSİJEN DOLDURULABİLİR KAYNAKLAR OLARAK SİLİKA KAPLI DEMİR OKSİT NANOPARÇACIKLAR

DENİZ YILDIZ
Kimya, Yüksek Lisans
Tez Danışmanı: Engin Umut AKKAYA
Nisan 2017

Gelişmekte olan sentetik kimya dünyasında, yüksek verim ile çalışan katalizörlere her zaman ihtiyaç duyulmaktadır. Bunun yanı sıra, hem bilim hem de üretim dünyasında düşük maliyetli ve çevre dostu sentez koşulları için tekrar kullanılabilen ve ortamdan kolayca uzaklaştırılabilen katalizörler önem kazanmaktadır. Manyetik nanoparçacıklar (MNP'ler), sadece bir mıknatıs ile toplanabilmesinden ötürü kolayca uzaklaştırılması gereken yapılar için umut vaad etmektedirler. Kendilerine özgü önemli özelliklere sahip demir oksit nanoparçacıkları, kolayca hazırlanıp fonksiyonlandırılabildikleri için MNP'ler arasında özel bir yere sahiptir.

Singlet oksijen çeşitli tepkime türleri için uygun bir reaktif olduğundan, fotoduyarlaştırıcılar ile MNP'lerin kombinasyonu sentetik uygulamalar için yenilikçi bir yaklaşımdır. Bu noktada, silika kaplı demir oksit nanoparçacıkların üzerine 2-piridon bağlı BODIPY yerleştirilerek hem singlet oksijen üreten, hem depolayan hem de serbest bırakabilen mıknatıslanabilir bir nano-yapı tasarlanmıştır. Sülfoksitler birçok biyolojik prosesin çekirdeğini oluşturdukları için, bu tasarım, organik sülfitlerin sülfoksitlere oksitlenmesi izlenerek test edilmiştir. Dahası, bu tasarım reaksiyon sonunda geri toplanabilir ve yüksek verimlilikle sonraki tepkimeler için tekrar kullanılabilir.

Anahtar sözcükler: BODIPY, SPIONs, endoperoksit, singlet oksijen, fotooksidasyon, sülfoksit.

dedicated to my mother and father...

Acknowledgement

This thesis has been a result of combined efforts and dedication of many people. It was a pleasure to work with them and I am grateful to those who made this thesis possible.

First of all, I owe my warmest gratitude to Prof. Dr. Engin Umut Akkaya for his greatest support, patience and encouragement during my both master studies and senior project. Without his everlasting infectious enthusiasm about science, I could not perceive the world like I do now. I learned a lot from him and I will never forget the days I spent in EUA group.

It is a pleasure to thank Dr. İlke Şimşek Turan and Dr. Serdal Kaya for their guidance and support throughout my research. Without the knowledge I gather from them during the course of this research, it would be beyond the bounds of possibility for me to have this thesis.

I am also grateful to our past and present group members, Dr. Özlem Seven, Dr. Tuna Subaşı, Dr. Safacan Kölemen, Simay Aydonat, Seylan Ayan, Cansu Kaya, Nisa Yeşilgül, Yahya Fikry, Merve Canyurt, Özge Pehlivan, Beste Gündüz and rest of the EUA members for the great working ambiance in the laboratory. It was a pleasure for me to work with them and I thank them all for the helpful and supportive discussions. I would like to express my sincere thanks to Simay Aydonat, Pınar Erdil and Merve Canyurt for their valuable friendship and family atmosphere. Those days were meaningless without them.

I also owe gratitude to Zeynep Erdoğan for the endless help in HRMS and GCMS experiments, Cangül Akgül for XRD measurements, Dr. Gökçe Çelik for UV-Vis Spectroscopy, and Mustafa Güler for TEM analysis.

I would like to thank my dearest friends, Şayeste Çağıl İnal, Ecem Cansu Asan, Hilal Pat, Tolga Özkan for their eternal friendship since our childhood. They are very precious for me. Also I would like to thank Elif Perşembe and Merve Balcı for the greatest times in Bilkent University. I am also greatful to Nurcan Haştar,

Begüm Dikecoğlu, Fatih Yergöz and Ahmet Emin Topal for those joyful nigths spent in UNAM. Those nights would be meaningless and tedious without them.

I would like to express my special thanks to Abdurrahman Türksoy, for the continuous joy and his precious partnership in this research and all of my days in Bilkent University. He has made available his support in a number of ways and without him, those days would be colorless and futile.

Finally, I would like to show my gratitude to my mother, Melahat YILDIZ and father, Sedat YILDIZ for their patience, support, understanding and endless love. I owe them a lot for teaching me how to be an independent woman. Without their patience and hands on me, I would not be here today, writing this thesis. It is an honour for me to be their daughter.

List of Abbreviations

BODIPY: Boron-dipyrromethene

NMR: Nuclear Magnetic Resonance

GCMS: Gas Chromatography-Mass Spectrometry

TEM: Transmission Electron Microscopy

EDX: Energy Dispersive X-Ray

HRMS: High Resolution Mass Spectrometry

ESI: Electrospray Ionization

APCI: Atmospheric Pressure Chemical Ionization

XPS: X-Ray Photoelectron Spectroscopy

SPIONs: Superparamagnetic Iron Oxide Nanoparticles

MNPs: Magnetic Nanoparticles

PDT: Photodynamic Therapy

DPBF: 1,3 Diphenylisobenzofuran

DMSO: Dimethyl Sulfoxide

DCM: Dichloromethane

DMF: Dimethylformamide

THF: Tetrahydrofuran

MeOH: Methanol

HCl: Hydrochloric Acid

AcOH: Acetic Acid

NBS: N-Bromosuccinimide

Contents

List of Figures

List of Tables

Chapter I

Introduction

1.1 Oxidation of Sulfides

Preparation of organic sulfoxides from sulfides are essential for organic synthesis not only for rudimentary research but also for multifarious applications, especially for biological and synthetic applications[1-4]. Sulfoxides exist in many reactions as a key intermediate leading toward diversified compounds like cyclohexane-1,3-dione[5, 6] and allyl alcohol derivatives[7, 8]. Besides, they are useful in activation of substrates for enzymatic processes like glycosidation[9]. Many therapeutic reagents having anti-bacterial and anti-fungal activities contains sulfoxide group[10-14]. Also preparation of some cardiotonic[15] and vasodilator[16] drugs, which are important for cardiovascular diseases, requires high efficient sulfoxide synthetic methods.

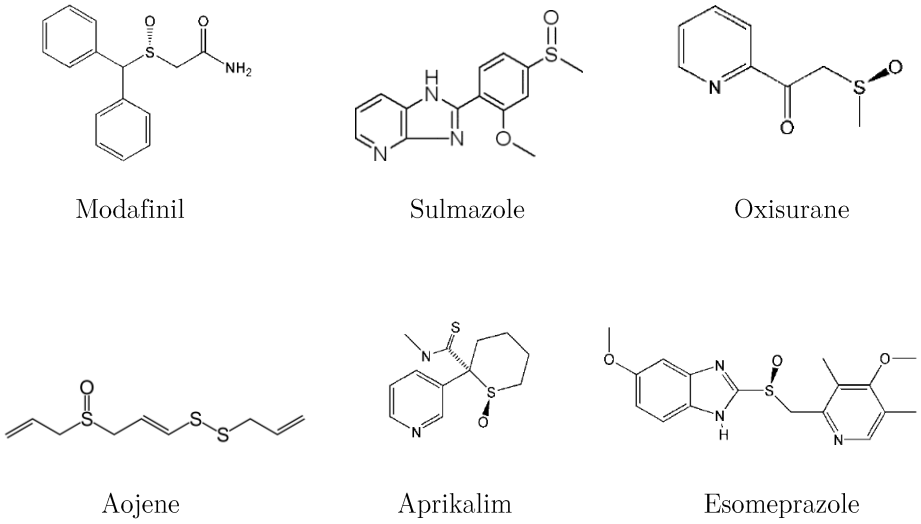

Figure 1: Examples of sulfoxides used as drugs.

Due to its significance, oxidation of sulfides has been drawing attention for many decades. Mild and high yielding conditions, which prevent side reactions including sulfone production have been desired and investigated in the synthetic and manufacturing manner. Although over oxidation of sulfide into sulfone is undesired, yet usually observed and hard to prevent. The reaction conditions, i.e. time, concentration, temperature should be set carefully to minimize the side products. Still there are many ongoing research for preparation of sulfoxides in high yields.

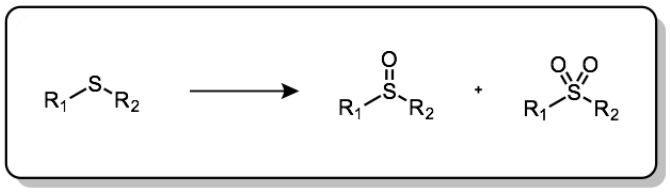

Figure 2: Oxidation of sulfide yielding sulfoxide and sulfone.

In 1865, Märcker is the one who first reported the oxidation of sulfoxides[17]. This work led to developments in oxidation methods for sulfides including usage of oxidants such as m-chloroperoxybenzoic acid[18], sodium metaperiodate[19],

oxygen derivatives i.e. ozone[20], singlet oxygen[21-24]. But the most convenient method using oxidants is the employment of hydrogen peroxide[25, 26].

Hydrogen peroxide is a cheap and green regent for oxidation since water is the only by-product and it is soluble in water as well as many organic solvents. In the meantime, oxidation of sulfides with hydrogen peroxide with mild conditions requires long time up to 24 h[27, 28]. To curtail time, reaction conditions are optimized with different solvents; for example, by changing the solvent into methanol as substitute for acetone decreases time from 24 h to 18 h[29]. Also, introducing some transition metals, specifically molybdenum, tungsten, and titanium with hydrogen peroxide increases the ability to selective oxidation of sulfides[30, 31].

Another common agents for oxidation of sulfoxides are halogen derivatives, which are not green solution for oxidation but with various advantages including ease of handling, high stability, and cheapness. To make it environmentally friendly, solvent-free conditions are developed with some halogen reagents like $NaBrO_3$–$Mg(HSO_4)_2$[32]or alumina supported phenyliodine(III) diacetate (PIDA)[33]. Selective oxidation of sulfides in the presence of other oxidizable groups, such as carbonyl, nitrile, hydroxyl, can be accomplished with $Ca(ClO)_2$ in alumina with quite high yields[32].

1.1.1 Photo-oxidation of Sulfides

In the development of research in oxidation of sulfides, foremost difficulties encountered are the over-oxidation to sulfones, low yields, long reaction durations, formation of side products, especially for halogen-derivative oxidants. Herein, photocatalytic organic reactions introduce environmentally friendly, mild reactions with relatively high yields and lower production of by-products such as sulfones. As a consequence, photocatalytic oxidation of sulfides arouses great interest in recent years. The photocatalytic oxidation from sulfur atom was

reported for the first time with dialkyl sulfoxide by Schenck in 1962[34]. These photosensitizers, in that case chlorophyll, rose bengal, porphyrin derivatives etc., were called 'free-radical transferring' by Schenck and they propose a mechanism as following:

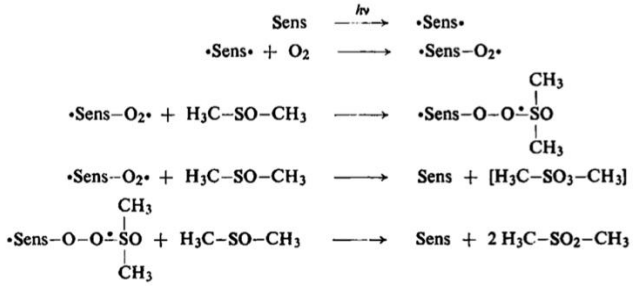

Figure 3: Proposed mechanism by Schenck for photooxidation of sulfoxide

Later, Schenk et al. made improvements in the mechanism, which is an unpublished result, quoted by Gollnick in 1968[23, 35], introducing the production of singlet oxygen, leading to the formation of diradical intermediates. In addition, these intermediates can act as nucleophiles or electrophiles in different solvents i.e., in protic solvents like methanol, radical intermediates behave like electrophile and in aprotic solvents like benzene, they act as nucleophile. From that point of view, it is clear that there is not only one mechanism under these kind of oxidations.

The fundamental intermediate formed during the oxidation of sulfides in the presence of a photosensitizer forming singlet oxygen is the persulfoxide. Persulfoxide is first suggested by Foote and co-workers in 1983[23]. It is generally described as having resonance hybrid structure bearing both diradical canonical and zwitterionic configuration. It has basic character on the oxygen end leading the production of varying structures with formation of hydroperoxy sulfurane, hydroperoxy sulforium ion, silicate anion, thiadioxirane, hydroperoxy sulfonium ylide, sulfoxide and addition of sulfide by adjusting the reaction media and conditions as seen in the Figure 4.

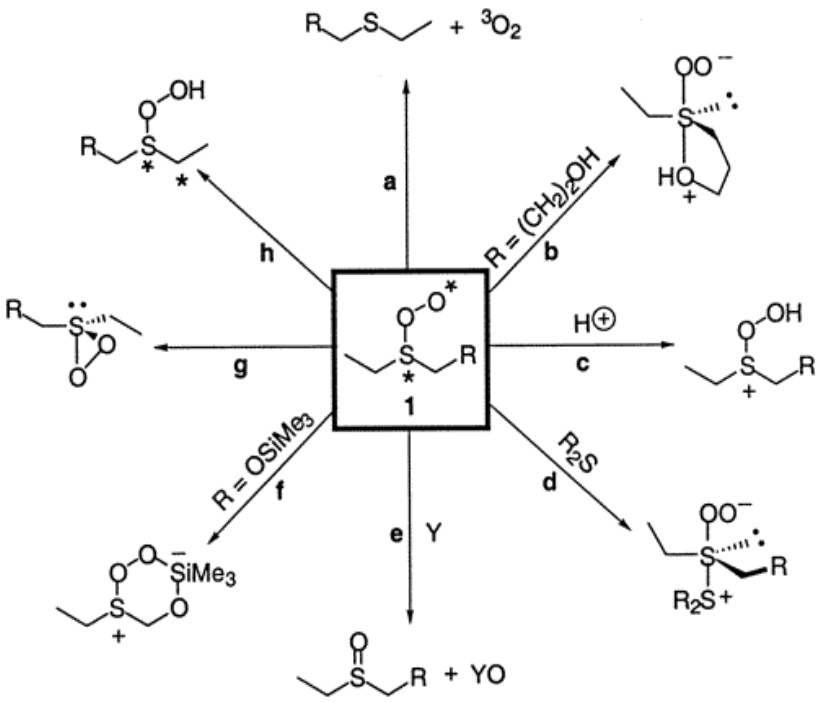

Figure 4: Persulfoxide reaction pathways. Reprinted with permission from reference[24]. Copyright ©2001 American Chemical Society.

The significant potential of persulfoxide that yield sulfoxide formation is the oxygen atom transfer to a substrate, i.e. same kind or different sulfur containing electrophiles, phosphites etc. In protic solvents such as methanol, nucleophilic character of persulfoxide decreases significantly, because of the hydrogen bonding with the solvent.[24] Thus, efficiency of the photooxidation of sulfides with singlet oxygen increases in most cases.

$$\text{Sens}^* + O_2 \rightarrow \text{Sens} + {}^1O_2$$

$${}^1O_2 + R_2S \rightarrow R_2S^+{-}O{-}O^-$$

$$R_2S^+{-}O{-}O^- + R_2S \rightarrow 2\,R_2SO$$

Figure 5: Photo-oxidation of sulfide into sulfoxide.

In the steadily developing research on photooxidation reactions, many catalyst species are reported in literature. A rubidium based organometallic complex was reported for oxidation of sulfides for the first time by Zen[36] in Figure 6. Some rubidium and iridium based photocatalysts are also developed in that manner[37-41]. Considering drawbacks of organometallic catalysts such as requirement of UV-light, high toxicity and cost, researchers tend to find new organic catalysts for oxidation reactions. 9,10-dicyanoanthracene, triphenylpyrylium tetrafluoroborate, n-methylquinolinium tetrafluoroborate as metal-free photocatalysts working in visible range gave promising results for that purpose[42-44].

Organic dyes also play a significant role acting as photocatalysts instead of metal containing catalysts ascribed to having advantageous properties such as low toxicity, ease of functionality and low cost. Photocatalytic efficiencies of organic dyes are examined by Zeitler for photoredox transformations with various simple, inexpensive organic dyes such as rhodamine B, alizarin red S, perylene and xanthene derivatives[45]. The most promising dyes because of their stability are found as fluorescein, eosin Y and perylene derivatives. Eosin Y shone amongst others with its favourable photochemical and photocatalytic properties. In other reported works, Rose Bengal show competent catalytic activity for α-oxyamination reactions[46]. Herein, BODIPY derivatives are promising due to having unique properties[47].

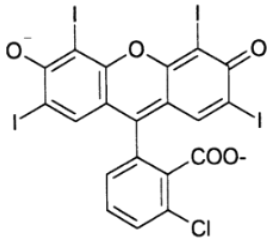

Rose Bengal

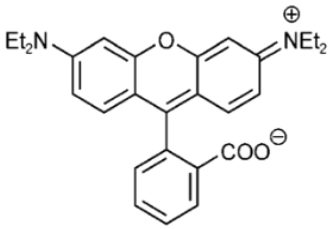

Rhodamine B

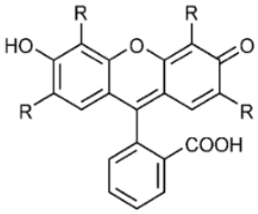

R = H Fluorescein
R = Br Eosin Y

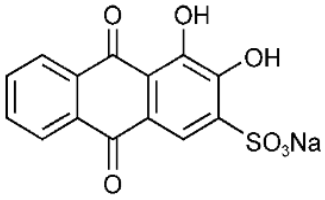

Alizarin Red S

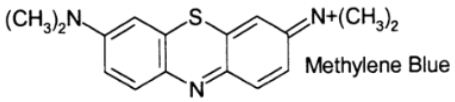

Methylene Blue

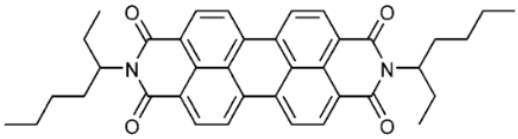

Perylene

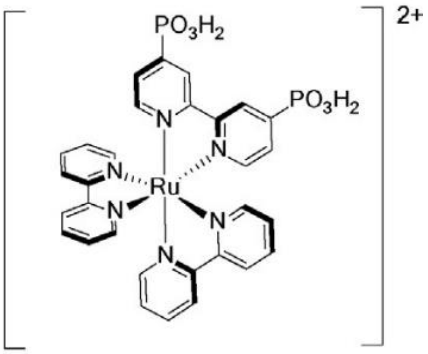

P-bpy-Ru$^{II,2+}$

Figure 6: Examples of photosensitizers used in photooxidation of sulfides.

1.2 BODIPY: A High Efficient Photosensitizer

Application of BODIPY (boron-dipyrromethene) dyes are expanding within the last ten years with functionalization and modification of Bodipy cores. By substitution of different functional groups to the Bodipy core, synthesis of longer wavelength absorbing/emitting fluorescent dyes can be achieved, which led to many applications including photodynamic therapy[48-50], light harvesters[51], solar cell sensitizers[52, 53], molecular logic systems[54, 55], supramolecular systems as well as photocatalytic oxidation[47, 56, 57].

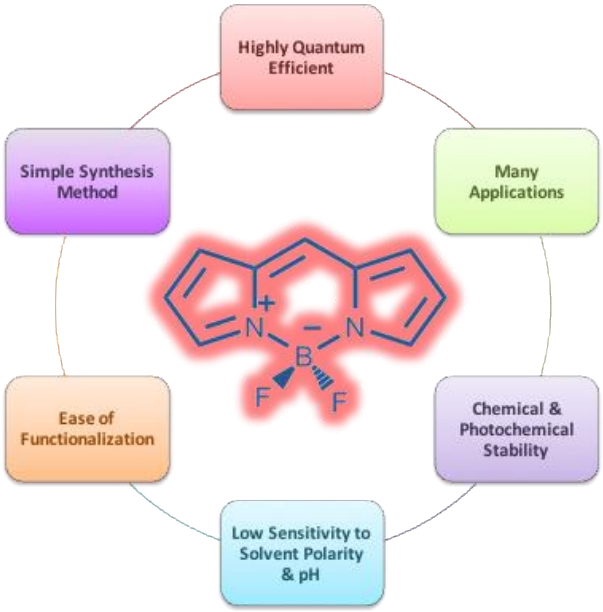

Figure 7: Properties of BODIPY

The highly fluorescent BODIPY (4,4-difluoro-4-borata-3a-azonia-4a-aza-s-indacene) unit which has similar structure with porphyrin was designed and synthesised by Kreuzer and his coworkers in 1968[58]. BODIPY's high fluorescence quantum yields (Φ_f), high molar extinction coefficients (ε), yielding high absorption, chemical and photophysical stability makes it unique and notable in the areas mentioned above. The parent BODIPY unit has a major absorption

peak (S_0-S_1 transition) near 500 nm; however, incorporation of fused aromatic rings and/or aryl substituents, ethynylaryl substitution, and aza-substitution at the meso (8) position push this peak into the red end of the visible spectrum[59]. All of these approaches may be useful in certain applications, nevertheless mono and distyryl modifications seem to offer a greater degree of versatility.

For functionalization of BODIPY core, there are certain ways to increase the conjugation or addition of functional groups. One of the notable methods for modification of BODIPY core is the Knoevenagel condensation. Knoevenagel first reports and gave his name to that condensation with the formaldehyde and diethyl malonate[60]. Buyukcakir et. al. developed Knoevenagel condensation in a convenient manner to modification of BODIPY core from 1,3,5,7th position[61]. The reaction is catalyzed by acetic acid and piperidine in benzene as solvent, and by adjusting the stoichiometry of aldehyde, mono, di, tri and tetra-styryl BODIPY derivatives can be synthesized leading to synthesis of a great variety of BODIPY derivatives absorbing at different wavelengths. The reaction conditions are improved by changing solvent, acid and stoichiometric ratios to have more varieties of functionalization.[62, 63]

The photosensitizing ability of the BODIPY dyes are far more significant than other properties due to its applicability in noninvasive therapeutic actions such as photodynamic therapy (PDT). PDT basically lies on three agents: photosensitizer, molecular oxygen and light. Under and appropriate wavelength, excited photosensitizer transfer its energy to molecular oxygen, exciting it to singlet oxygen. Singlet oxygen is cytotoxic, so it leads to tissue damage and cell death. Singlet oxygen is also a significant agent for photooxidation reactions. For these aforementioned reasons, singlet oxygen generation capability of the photosensitizer is desired to be enhanced by increasing spin-orbit coupling to allow spin forbidden transitions for oxygen from triple state to singlet state. This phenomena, called heavy atom effect, is introduced by O'Shea on BODIPY dyes by adding halogens (I, Br, Cl) on the 2nd and 6the position of BODIPY dyes[48]. This effect enhances the singlet oxygen efficiency by 1000-folds for BODIPY dyes.

1.2.1 BODIPY as photocatalyst

With the great degree of functionalization feasibility, BODIPY dyes are possible candidates for photooxidation reactions; photooxidation of hydroxynaphtalene and sulfide derivatives, and oxidative condensation of amines. The mechanism behind these photooxidation reactions depend on the high singlet oxygen generation ability of BODIPY dyes.

For oxidation of sulfides, singlet oxygen forms the persulfoxide intermediate to form sulfoxide as described before. Jing first reported the photooxidation of sulfides[47], here thioanisole, with BODIPY derivatives in 2011, and then improved the reaction conditions with synthesizing 4 different BODIPY derivatives (Figure 8) and examining the efficiency in different solvents. Wang et al. examined this catalytic reaction with 10 various BODIPY derivatives and thioanisole derivatives, proving this is a successful alternative for known photosensitizes such as Nile Red and Ru-based organometallic catalysis[64].

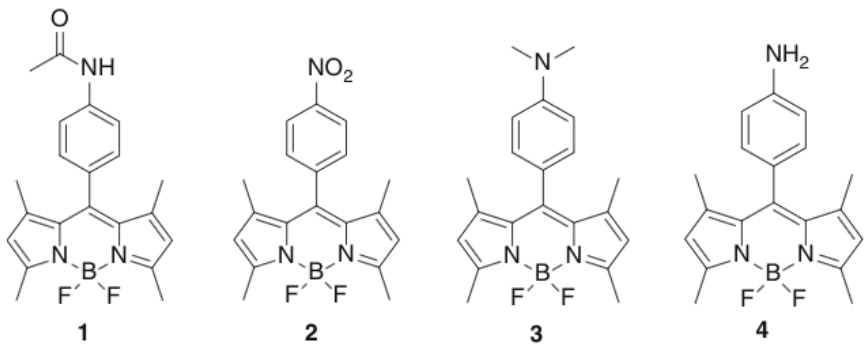

Figure 8: First BODIPY derivatives for photooxidation of sulfides. Adapted with permission from reference[47]. Copyright ©2013, Springer Science+Business Media New York.

For the oxidative condensation of amine, benzyl amine derivative was oxidized by singlet oxygen to form phenylmethanimine which is a reactive intermediate compound undergoing condensation reaction to give 2-aryl

benzothiazole derivatives[57,65]. Singlet oxygen also forms endoperoxide intermediate with hydroxynaphtalene derivatives yielding 1,4-naphtalenedione derivatives, for example juglone which is a chemical used as herbicides or coloring agent in cosmetics, food industry and cloth[56, 57].

An additional pathway for photooxidation was reported in the past decade for oxidative formation of amides with aromatic aldehydes and acids[66]. Consequential C-C bond formation such as, cross-dehydrogenative coupling reactions, acylation of thiophene and furane also follow the similar reaction mechanism including single electron transfer (SET) [67, 68]. For example, for cross-dehydrogenative coupling reactions, single electron is transferred to photosensitizer in its triplet excited state from amine group forming iminium intermediate, which will react with a nucleophilic group. The following figure shows the detailed mechanism under these kind of reactions:

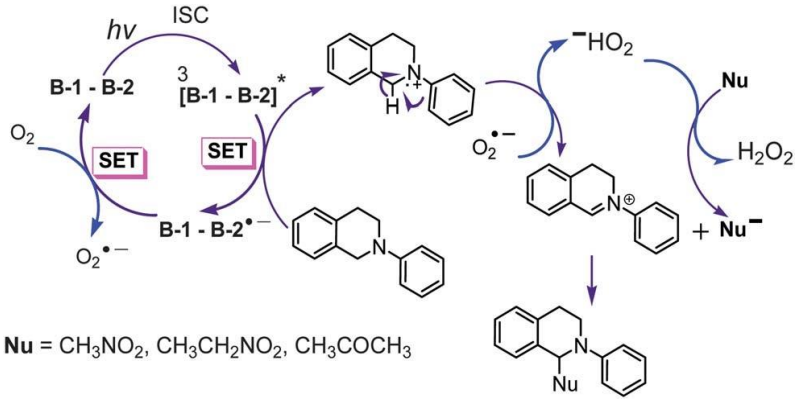

Figure 9: Proposed mechanism for cross-dehydrogenative coupling reactions with SET. Reprinted with permission from reference[68]. Copyright ©2013, Royal Society of Chemistry.

Photooxidation reactions with BODIPY dyes are also integrated with some tandem reactions including oxidation, [3+2] cycloaddition and aromatization following the similar mechanism. [66]

1.3 Singlet Oxygen and its Photophysical Formation

For the preparation of sulfoxides from sulfides with a photocatalyst, singlet oxygen is the key toward the persulfoxide formation as described in previous section. Singlet oxygen is a reactive oxygen species, having a short lifetime, 3.3µs in water, 101µs in DCM, 73 ms in CCl_4 as the longest lifetime[69]. To generate singlet oxygen, a high triplet yield photosensitizer is required although the singly excited states of oxygen ($^1\Delta_g$: 94 kJ/mol and $^1\Sigma_g^+$: 156 kJ/mol) have lower energy than first triplet excited state. The reason is that these transitions are not spin allowed according to the symmetry, spin and selection rules defined in literature[70]. To accomplish these spin-forbidden transitions of oxygen, the following pathway is utilized in the presence of photosensitizer:

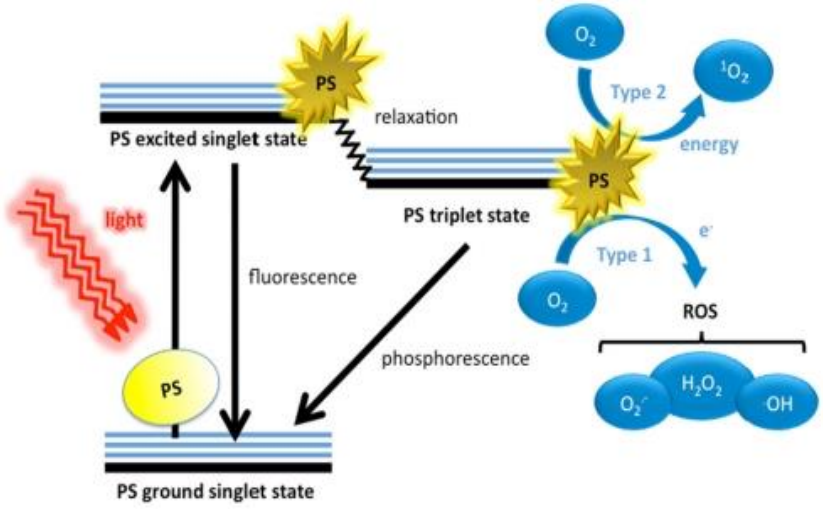

Figure 10: Schematic representation of generation of singlet oxygen by photosensitization on Jablonski Diagram. Reprinted from reference[71]. Copyright ©2012, Dai, Fuchs, Coleman, Prates, Astrakas, St. Denis, Ribeiro, Mylonakis, Hamblin and Tegos.

Upon exposure of a photosensitizer with an appropriate wavelength of light, single photon absorption excites the photosensitizer from ground state (S_0) to one of the vibrationally excited states of S_1. After vibrationally relaxed, it may

follow two relaxation pathways: it may relax back to S_0 state to emit light, called fluorescence, or it may do intersystem crossing to reach triplet state (T_1) in case of having high triplet quantum yield like halogenated BODIPY dyes[48]. Relaxation from T_1 state to S_0 is called phosphorescence which has comparably long lifetime than fluorescence in general. In the existence of molecular oxygen in the media, phosphorescence is quenched with the excitation of triplet oxygen into singlet oxygen.

1.3.1 Singlet Oxygen Storage with Polycyclic Aromatic Endoperoxides

Photosensitization is a convenient way to produce singlet oxygen in high yields, however for the applications where deep light penetration is a problem, photosensitizers are not functional. Also photosensitization needs dissolved molecular oxygen in the media to be used, otherwise, like in hypoxic environment in cancer cells, photosensitizer is not able to produce singlet oxygen due to lack of triplet oxygen. On the other hand, singlet oxygen shows antibacterial[72-74] (for gram-positive bacteria), antiviral (for some kinds of enveloped viruses)[74] besides the cytotoxic effects. For those aforementioned reasons, developments in strategies to store and deliver singlet oxygen is significant.

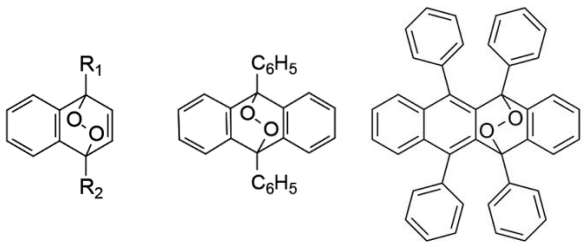

Figure 11: Examples of Polycyclic Aromatic Endoperoxides

Aromatic compounds such as anthracene, naphthaline, tetracene, 2-pyridone derivatives can undergo [4+2] cycloaddition to form endoperoxides as a source of

singlet oxygen which can be stored, delivered and released under certain conditions. This ability of tetracene derivatives was first reported by Moureu and Dufraisse in 1926[75], stating oxygen can covalently bind to rubrene and this reaction is reversible, i.e. then the compound is heated up to 120 °C, it starts to release oxygen forming its initial structure. Dufreaisse continue his research on anthracene derivatives, observing the same result. After 40 years, Wasserman worked with 9,10-diphenylanthracene and proved that oxygen is in its singlet excited state when it was generated with the cycloreversion of endoperoxide[76].

The reactivity and cycloreversion efficiency depends on many factors such as temperature, solvent, structure of organic compound. As the electron density on the aromatic compound increases, formation of endoperoxide generally increases. Thus electron donating groups on aromatic compound (dimethylamino, methoxy, methyl, phenyl) increases the reactivity toward singlet oxygen. Secondly, as temperature increases, amount of thermally activated cycloreversion generated singlet oxygen increases. The thermolysis of endoperoxides undergoes two main routes conversion as shown in the Figure 12.

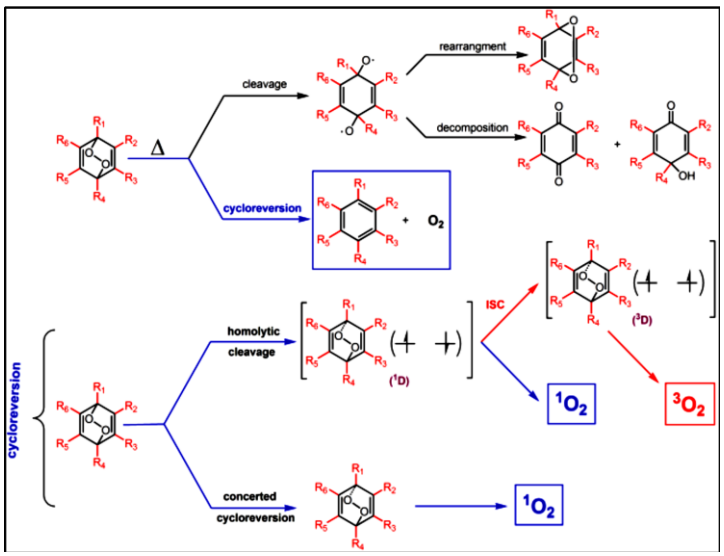

Figure 12: Thermolysis Pathways for Polycyclic Aromatic Endoperoxides

First pathway is the cleavage of the bond between oxygen atoms leading the formation of quinone and hydroxy ketone derivatives, besides it can undergo rearrangement to form endoperoxide again. Second route is the cycloreversion which yields to singlet or triplet oxygen.

Matsumoto reported N-pyridones also reacts with singlet oxygen to give endoperoxides and have high decomposition yields to give singlet oxygen[77]. Also N-pyridones decompose relatively low temperatures compared to anthracene derivatives, which enables biological applications giving better results than anthracene derivatives.

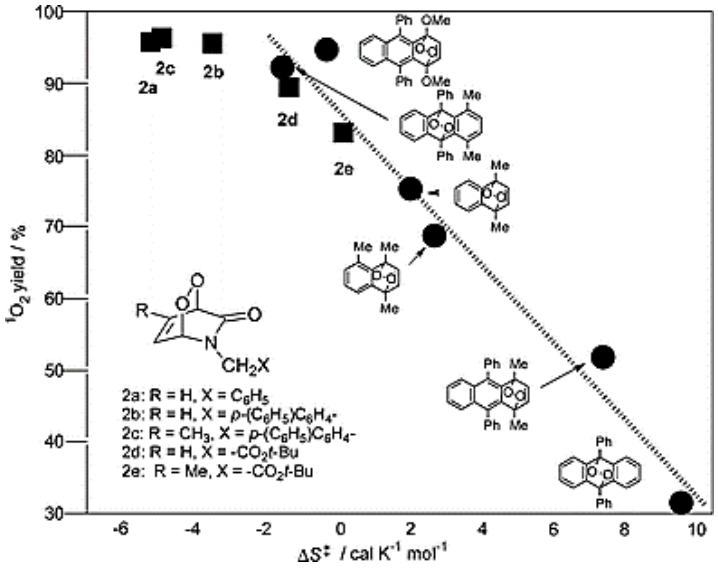

Figure 13: Comparison of singlet oxygen yield vs. activation entropy for thermolysis of polycyclic aromatic endoperoxides. Reprinted with permission from reference[77]. Copyright ©2004, Royal Society of Chemistry.

For example, in some tissue engineering applications where molecular oxygen supplies are required, some 2-pyridone derivatives are used to prevent cell deaths. Since 2-pyridone derivatives release singlet oxygen rather than triplet oxygen, undergoing retro-Diels Alder type reactions, some singlet oxygen quenchers such as vitamin C is used[78]. Also 2-pyridone endoperoxide containing structures are also introduced in some PDT[50] and synthetic applications[79].

1.4 Singlet Oxygen Delivery Strategies

For decades, many strategies have been developed for the delivery of singlet oxygen to the targeted media such as cancer cell for photodynamic therapy, or reaction media containing substrates, because singlet oxygen is highly reactive and has short lifetime. For the very reason, developing efficient $^1O_2$ carriers is significant in a way that only targeted substrates should be affected by the presence of singlet oxygen but others should stay unreacted. One way to achieve this goal is that the encapsulation of photosensitizers by nanostructures such as nanoparticles, dendrimers etc. which cause accumulation in certain targeted areas in biological systems or ease of handling in the case of singlet oxygen producing catalysis. On the other hand, using aromatic compounds as $^1O_2$ carriers in a form of endoperoxides helps remote control of release of singlet oxygen in desired media. Both strategies have its own beneficial and detrimental aspects, furthermore strategies combining those two lead new insights in delivery of singlet oxygen.

In the case of nanoparticles as delivery agent of singlet oxygen, photosensitizer or endoperoxide is encapsulated on nanoparticle surface and upon light irradiation or heat, production of $^1O_2$ is achieved. For efficient photosensitization with nanoparticles, $^3O_2$ should easily reach to the surface of nanoparticles where photosensitizer locates since concentration of molecular oxygen is an important limiting factor for singlet oxygen quantum yield. Also, the surface should not be too much steric so that the produced or released singlet oxygen can be dispersed away from the surface easily since $^1O_2$ had low diffusion distance around nm to mm scale. Another significant point is that surface of the nanoparticles should be chosen intentionally so that the surface will not react with singlet oxygen and quench it. Otherwise, both nanoparticles will degrade and the efficiency of singlet oxygen will be diminished. Taking note of the situations mentioned, a great variety of functionalized nanoparticles are developed for many applications.

1.4.1 Gold Nanoparticles

Gold nanoparticles are one of the most remarkable metal nanoparticles because of their unique properties that allows applicability in many areas such as diagnostics[80], photodynamic theraphy[81], molecular probes[82] etc. Singlet oxygen production by methylene blue[83], zinc-phthalocyanine[84], Rose Bengal[85] on gold nanoparticles has also been reported that gold nanoparticles are appropriate agents for singlet oxygen producing photosensitizers' delivery.

Moreover, gold nanoparticles are used in hyperthermia therapy in which nanoparticles absorbs light to yield emission of heat. Absorption wavelength of gold nanoparticles can be adjusted by varying the particle size, thus those gold nanoparticles can be used to kill cancer cells. Last year, Akkaya reported remotely controlled release of singlet oxygen with an anthracene derivative on gold nanorods[86]. The anthracene endoperoxide is linked to goldnanorods and photodynamic action is tested in HeLa cells. The gold nanorods are irradiated with 808 nm light, which is in therapeutic range, and with the heat released by gold nanorods, endoperoxides undergoes cycloreversion to give singlet oxygen. This aspect paves the way for solving the self-limiting feature of photodynamic therapy which uses the little amount oxygen in hypoxic cancer cells.

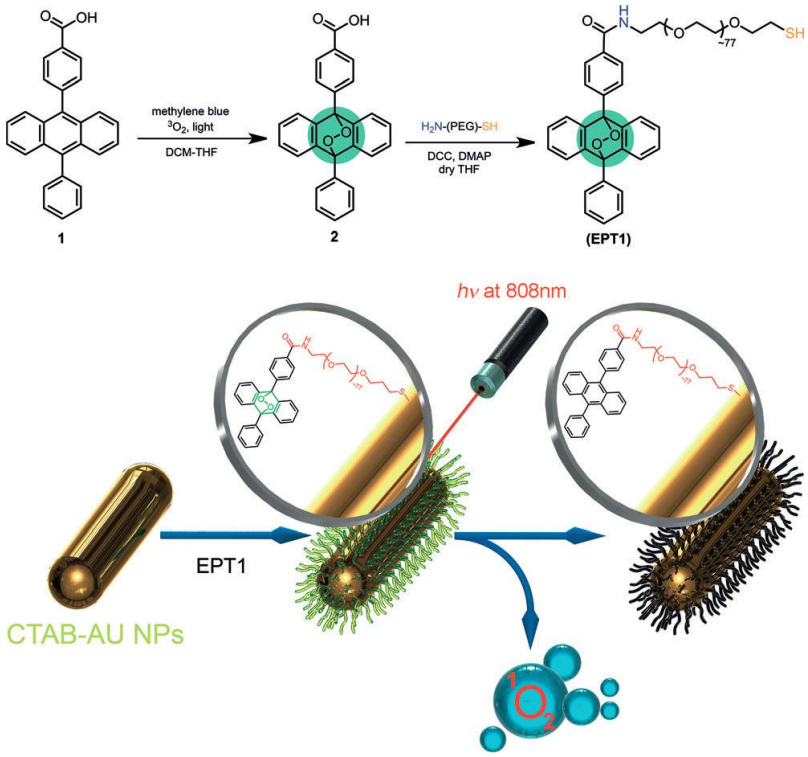

Figure 14: Design of the release of singlet oxygen by plasmonic heating of endoperoxide-modified gold nanorods. Reprinted with permission from reference[86]. Copyright ©2016 WILEY-VCH Verlag GmbH & Co. KGaA, Weinheim.

1.4.2 Carbon-Based Nanostructures

Graphene and carbon nanotube based agents are also another perspective for delivery for photosensitizers. Due to its organic structure, carbon nanotubes almost never shows cytotoxicity, so they are alternative candidates for carriers in biological systems. In 2009, pyrenyl functionalized BODIPY on single walled carbon nanotubes (SWNTs) are reported as viable source of singlet oxygen by photosensitization[87]. Additionally, besides the promising optical and electronic properties of graphene, it can be also used as singlet oxygen delivery agent. This

feature of graphene oxide nanostructures and composites are studied in literature with methylene blue[88], zinc-phthalocyanine[89], and chlorin e6 in 2013[90].

1.4.3 Iron-Oxide Nanoparticles

In the past few decades, superparamagnetic iron oxide nanoparticles (SPIONs) has attracted great attention in many applications including biomedical and imaging applications[91-93], data storage[94] and synthetic developments due to its unique properties such as low toxicity in biological systems, magnetization, and ease of functionalization with the help of varying coating techniques. There are three major iron oxide types which have superparamagnetism: Fe_3O_4 magnetite, Fe_2O_3 derivatives: maghemite and hematite. Magnetite has the biggest role in SPIONs researched due to biocompatibility[93].

The iron oxide nanoparticles are in many shapes and sizes varying according to usage. There are many synthetic ways to control some parameters such as size/shape, dispersibility, surface functionality by limiting reaction conditions. The remarkable techniques are co-precipitation, thermal decomposition, sol-gel method, microemulsion, sonochemical synthesis[95]. The mostly accepted method for the synthesis of magnetite is co-precipitation method. The method follows the mixing the ferric and ferrous salts in and stoichiometric ratio of 1:2 and adjusting the pH of the solution in alkali conditions. The elevation of the temperature leads to the nucleation and growth of the black iron oxide nanoparticles with a wide particle size distribution. The reaction atmosphere should be inert to prevent any oxidation reaction with oxygen in the air and the freshly growth SPIONs. Adjusting the pH, temperature, stirring rate, changing of the salts can affect the size of the nanoparticles.

Aggregation and oxidation are significant issues that should be dealt with while working with naked iron oxide nanoparticles. To facilitate the usage

conditions with iron oxide nanoparticles, surface coating is necessary and many coating techniques with different materials have been developed in the past few decades. Those coatings help in controlling the sizes of SPIONs and stabilizing the dispersion by repulsive forces, i.e. electrostatic and steric repulsions. The materials used are generally organic molecules such as polymers, carboxylates, surfactants, as well as inorganic materials such as silica.[95] The importance of the coating is not limited with the prevention of the aggregation and oxidation of nanoparticles, yet it provides the functionalization of the surface.

Silica is of choice in many magnetizable nanoparticles including iron oxides. The utilization of silica coating on SPIONs have a major advantage which make it mostly preferred, that is the ease of functionalization on silica layer. Any substrate having triethyl-orthosilicate group can be easily bound on the silica layer. Also silica shell reduces the toxicity levels in biological applications, which makes it more desirable in medical studies[96]. Silica nanosphere also solves the problem with the aggregation problem with electrostatic repulsions by having negatively charged character as well as shielding the magnetic dipoles of iron oxide cores[97]. All of those beneficial properties make the silica coated nanoparticles applicable to many various applications including singlet oxygen delivery strategies.

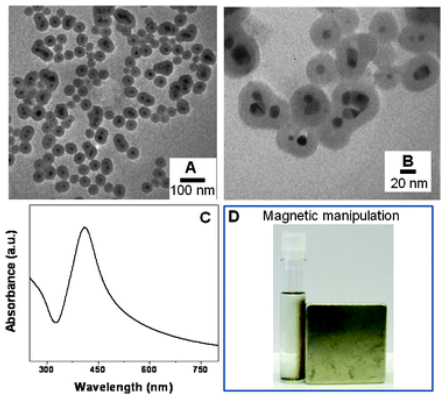

Figure 15: Silica coated SPIONs. Reprinted with permission from reference[98]. Copyright © 2008, Royal Society of Chemistry.

For PDT actions, pheophorbide-A, methylene blue and AlC_4Pc functionalized iron oxide nanoparticles with silica coating have been reported as sources of singlet oxygen by photosensitization[99, 100]. Also Rose Bengal integrated SPIONs are also reported in 2011[101]. Another study by Gu et al. demonstrates a bimodal therapy for cancer treatment integrating photodynamic therapy (PDT) and hyperthermia therapy (HT) using porphyrin derivative as photosensitizer[102].

1.4.4 Self-charging Designs

As mentioned before, combining the photosensitizer with endoperoxide moieties is powerful aspects in delivery of singlet oxygen. The self-photosensitization in the presence of molecular oxygen for the formation of endoperoxides wipes out the need for another photosensitizer. Moreover, endoperoxides can release oxygen to fulfil the photosensitizers' need for molecular oxygen in the oxygen depleted environment. This sort of new insight in delivery of singlet oxygen can be used in many areas including PDT, synthetic approaches etc.

A reported example is a phthalocyanine-palladium complex fused with four anthracene groups[103]. Anthracene endoperoxides are formed with the photosensitization of singlet oxygen by phthalocyanine-palladium complex. The system has photoreversibility with two photon absorption, i.e. endoperoxide can be formed and oxygen can be released from system reversibly. Also, thermally reversible anthracene and naphthalene substituted porphyrin or phthalocyanine derivatives are developed with the same manner[104-106].

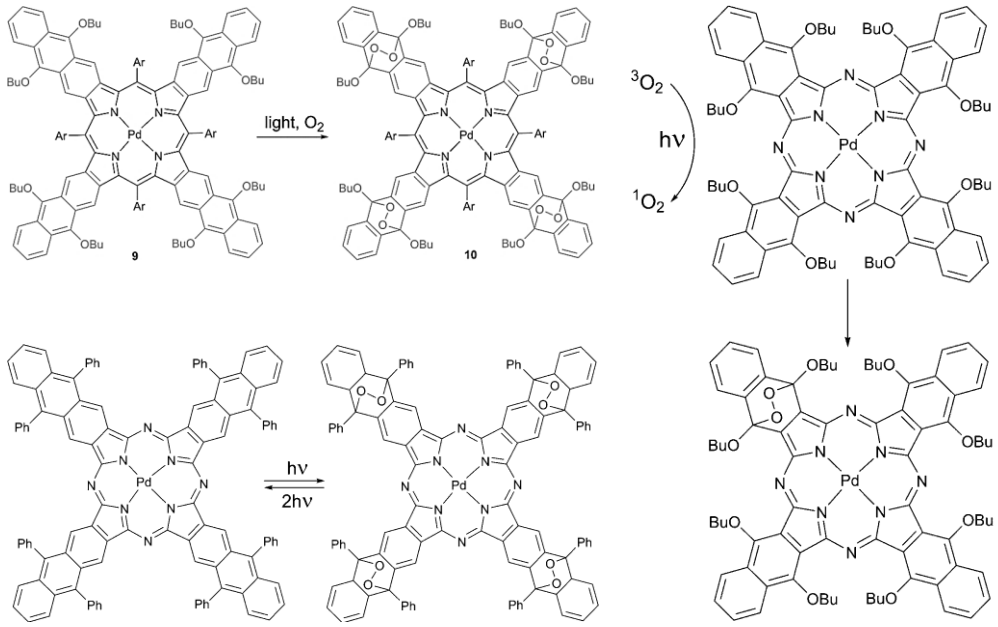

Figure 16: Examples of Self-charging designs

Another example is an example of synthetic approach from such kind of fused systems[79]. Again, a porphyrin derivative with four 2-pyridone moiety is used for oxidation reaction of mustard gas. The system is defined as it can "generate, trap, store, and release" singlet oxygen all by itself. As N-pyridone derivatives are introduced, the thermal cycloreversion of singlet oxygen can be attained at 40 °C which is a mild temperature.

Last year, Turan et al. introduced a new design for fractional photodynamic therapy, which is a combination of 2-pyridone moiety with BODIPY as photosensitizer[50]. Therefore, the self-diminishing effect of PDT in hypoxic conditions can be solved by introducing heating cycles between light irradiation periods to release oxygen from endoperoxide.

1.5 Magnetic Nanoparticles (MNP) as Synthetic Agents

By definition, catalyst is a reagent that takes place in the reaction but remain unaffected at the end. Thus theoretically, it can be collected and reused after reactions, but practically, collection of the catalysts is problematic with traditional methods like filtration, centrifugation, decantation etc. Herein, magnetic nanoparticles as catalysts is a promising approach, since collecting the catalysts by using just a magnet is handy. Magnetic nanoparticles can be nickel, cobalt, iron or other metals that can be manipulated by magnetic fields, but the most common one is the iron oxide nanoparticles due to its ease of preparing, coating and functionality. Some functional groups can be attached on the iron oxide nanoparticles, generally with silica coating, which can show catalytic activities.

There are many examples of iron oxide nanoparticles as analogues of catalysts like DMAP, which can be used in acylation reactions[107]. Not only it can be recovered by magnet but also undergo many cycles with great efficiencies. Another examples are the ones which can be used in acid or base catalyzed reactions by mimicking acidic or basic resins/catalysts[108, 109]. Also some MNPs can be used for oxidation of sulfides or in oxidative coupling reactions[109, 110]. Still, they can be recyclable and used with great yields.

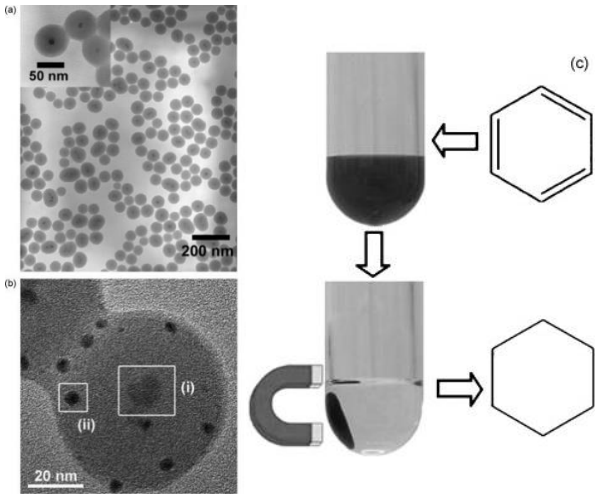

Figure 17: Recoverable rhodium nanoparticles for hydrogenation reactions. Adapted with permission from reference[111]. Copyright © 2007 Elsevier B.V.

Some major reactions in synthetic chemistry and manifacturing processes like C-C coupling reactions: Heck, Suzuki, Sonagashira couplings or hydrogenation reactions can also be performed with several recycling numbers on SiO_2 coated SPIONs[112, 113]. Increment of the effective surface area of nanoparticles can be more effective in manufacturing processes. Also those, which mimic the Pd based catalysts are relatively expensive, so recycling feasibility of MNPs are profitable.

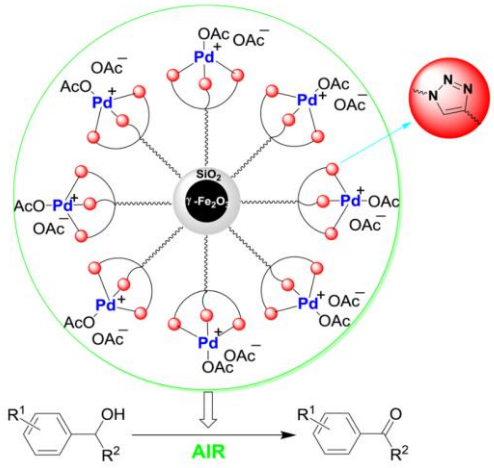

Figure 18: Magnetically recoverable palladium catalyst. Reprinted with permission from reference[114]. Copyright © 2015, American Chemical Society.

Chapter II

Experimental Procedures

2.1 General

All chemicals and reaction solvents purchased from Sigma Aldrich, Acros Organics and ABCR were used without purification. Column chromatography purifications were performed with glass columns using Merck Silica gel 60 (particle size: 0.040-0.063 mm, 230-400 mesh ASTM) and reactions were monitored by thin layer chromatography (TLC) using pre-coated silica gel plates (Merck Silica Gel PF-254). Chromatography solvents (DCM, n-hexane, EtOAc) were purchased as technical grade and were purified employing fractional distillation before use. Anhydrous THF and toluene was used freshly after refluxing over sodium (Na) in the presence of benzophenone under argon. DMF was used after keeping it over activated 4Å molecular sieves for 24 h.

NMR spectra were recorded on Bruker Spectrospin Avance DPX 400 spectrometer (operating at 400 MHz for ^{1}H NMR and 100 MHz for ^{13}C NMR) using deuterated solvents ($CDCl_3$, DMSO-d_6) with tetramethylsilane (TMS) as internal standard purchased from Merck. Spin multiplicities are reported as following: s (singlet), d (doublet), t (triplet), q (quartet), quint (quintet), sext

(sextet), dd (doublet of doublets), dt (doublet of triplets), td(triplet of doublets), m (multiplet), bs (broad signal). High Resolution Mass Spectroscopy (HRMS) experiments were done on an Agilent Technologies-6530 Accurate-Mass Q-TOF-LC/MS. Absorption and Emission measurements were acquired using Varian Cary-100 Spectrophotometer and Varian Eclipse Fluorospectrometer. Malvern NanoZS DLS was used for the determination of nanoparticle size distribution. Transmission Electron Microscopy images were recorded with FEI Technai G2F30 High-Resolution TEM on carbon grid. X-Ray Powder Diffractometry measurements were carried on PANalytical X'Pert Powder Diffractometer. Gas Chromatography Mass Spectroscopy (GCMS) experiments were performed on Agilent Technologies 7890A GC System with Agilent Technologies 5975C inert MSD with Triple-Axis Detector.

2.2 Synthesis of Photosensitizer

Synthesis of compound **2-6** was done according to the literature procedure[50].

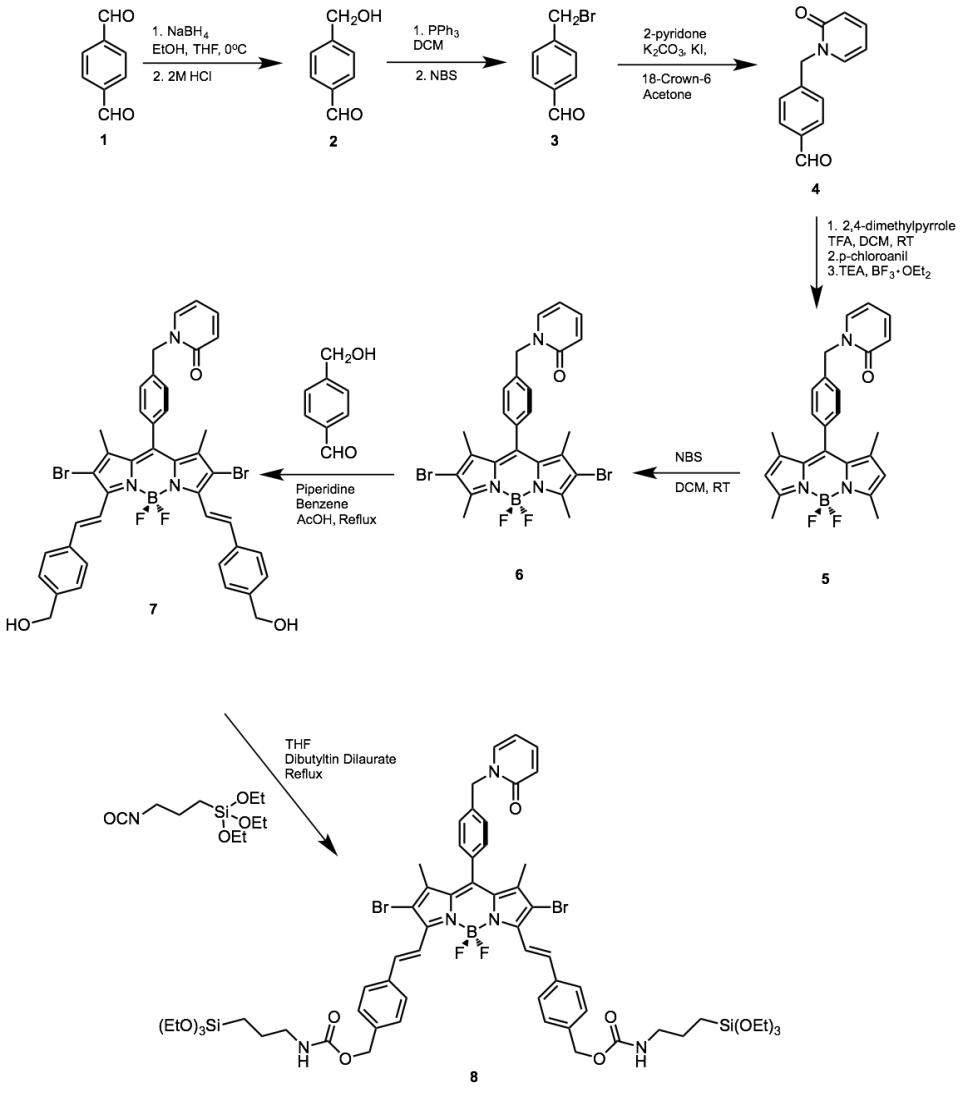

Figure 19: Synthesis scheme for photosensitizer.

2.2.1 Synthesis of 4-(hydroxymethyl) benzaldehyde (2)

Terephthalaldehyde (1.0 g, 7.46 mmol) is dissolved in 15 mL ethanol and 20 mL THF mixture. $NaBH_4$ (0.07 g, 1.85 mmol) is added in an ice bath slowly and reaction is kept in 0 °C for further 6 h. Then, pH of the mixture is adjusted to 5 by addition of 2 M HCl solution. The reaction mixture is then extracted with EtOAc and water. Organic phases are combined and dried over anhydrous Na_2SO_4. Solvent is evaporated in vacuo and the product is purified by silica gel column chromatography using DCM/MeOH (98:2, v/v) as the eluent. Compound **2** was obtained as colorless oil (0.40 g, 40%).

^{1}H NMR (400 MHz, $CDCl_3$): δ 9.92 (s, 1H), 7.80 (d, J = 8.1 Hz, 2H), 7.47 (d, J = 8.1 Hz, 2H), 4.74 (s, 2H), 3.25 (s, 1H).

^{13}C NMR (100 MHz, $CDCl_3$): δ 192.4, 148.2, 135.5, 130.0, 126.9, 64.3.

MS (TOF-ESI): m/z calculated for $C_8H_8O_2$ $[M-H]^-$: 135.04515, found for $[M-H]^-$: 135.04782, Δ= -19.75 ppm.

2.2.2 Synthesis of 4-(bromomethyl) benzaldehyde (3)

Compound **2** (0.8 g, 5.87 mmol) and triphenyl phosphine (3.11 g, 11.89 mmol) are dissolved in 50 mL DCM at room temperature. N-bromosuccinimide (2.00 g, 11.43 mmol) is added portion wise. Reaction is kept at room temperature for overnight. Then, the reaction mixture is extracted with DCM and water. Organic phases are combined and dried over anhydrous Na_2SO_4. Solvent is evaporated in vacuo and the product is purified by silica gel column chromatography using EtOAc/Hexane (1:1, v/v) as the eluent. Compound **3** was obtained as white powder (0.60 g, 38%).

^{1}H NMR (400 MHz, $CDCl_3$): δ 10.01 (s, 1H), 7.86 (d, J = 8.1 Hz, 2H), 7.55 (d, J = 8.1 Hz, 2H), 4.51 (s, 2H).

^{13}C NMR (100 MHz, $CDCl_3$): δ 191.4, 144.2, 136.2, 130.1, 129.7, 31.9.

2.2.3 Synthesis of Compound 4

Compound **3** (0.50 mg, 2.51 mmol), 2-pyridone (0.256 mg, 2.69 mmol) and potassium carbonate (1.25 g, 9.04 mmol) is dissolved in 50 mL acetone. 18-crown-6 and potassium iodide is added catalytic amount. Reaction is stirred at room temperature for overnight. The solids are filtered off and the eluent is evaporated in vacuo and the product is purified by silica gel column chromatography using DCM/Hexane (1:1, v/v) as the eluent. Compound **4** was obtained as white powder (1.2 g, 40%).

^{1}H NMR (400 MHz, $CDCl_3$): δ 10.01 (s, 1H), 7.87 (d, J = 8.3 Hz, 2H), 7.45 (d, J = 8.3 Hz, 2H), 7.41-7.34 (m, 1H), 7.30 (dd, J_{12}=6.8Hz, J_{23}=2.0 Hz, 1H), 6.66 (d, J=9.2Hz, 1H), 6.21 (dt, J_{12}=6.8Hz, J_{23}=1.4 Hz, 1H), 5.23 (s, 2H).

^{13}C NMR (100 MHz, $CDCl_3$): δ 191.7, 162.6, 143.1, 139.9, 137.4, 135.9, 130.2, 128.3, 121.4, 106.7, 52.0.

MS (TOF-ESI): m/z calculated for $C_{13}H_{11}NO_2$ $[M+H]^+$: 214.08626, found for $[M+H]^+$: 214.08808, Δ= -8.52 ppm.

2.2.4 Synthesis of Compound 5

Compound **4** (0.50 g, 2.35 mmol) and 2,4-dimethylpyrrole (0.53 mL, 5.15 mmol) are dissolved in DCM, which is degassed by Ar purging for 30 mins. Two drops of trifluoroacetic acid was added dropwise. The red solution is stirred overnight in the dark at room temperature. p-Chloranil (0.58 g, 2.35 mmol) is added and reaction mixture is stirred further for 1 h. Triethylamine (5.0 mL) and $BF_3 \bullet OEt_2$ (5.0 mL) are added dropwise to the reaction mixture consecutively and the resulting solution is stirred for one additional hour. Then, the reaction

mixture is extracted with DCM and water. Organic phases are combined and dried over anhydrous Na_2SO_4. Solvent is evaporated in vacuo and the product is purified by silica gel column chromatography using EtOAc as the eluent. Compound **5** was obtained as red powder (0.90 g, 37%).

^{1}H NMR (400 MHz, $CDCl_3$): δ 7.42 (d, J = 7.8 Hz, 2H), 7.36-7.40 (m, 1H), 7.27-7.31 (m, 3H), 6.68 (d, J = 9.2 Hz, 1H), 6.21 (t, J = 6.7 Hz, 1H), 5.99 (s, 2H), 5.26 (s, 2H), 2.56 (s, 6H), 1.37 (s, 6H).

^{13}C NMR (100 MHz, $CDCl_3$): δ 162.6, 155.6, 143.0, 141.0, 139.6, 137.6, 137.0, 134.8, 131.4, 128.62, 128.57, 121.4, 121.3, 106.6, 51.6, 14.6, 14.4.

MS (TOF-ESI): m/z calculated for $C_{25}H_{24}BF_2N_3O$ $[M-H]^-$: 429.19440, found for $[M-H]^-$: 429.19033, Δ= 9.49 ppm.

2.2.5 Synthesis of Compound 6

Compound **5** (0.10 g, 0.23 mmol) is dissolved in 20 mL of DCM. N-bromosuccinimide (0.10 g, 0.56 mmol) is dissolved in minimum volume of DCM and added dropwise to reaction mixture at room temperature. The reaction is stirred for 10 mins and extracted with DCM and water. Organic phases are combined and dried over anhydrous Na_2SO_4. Solvent is evaporated in vacuo and the product is purified by silica gel column chromatography using EtOAc as the eluent. Compound **6** was obtained as red powder (0.10 g, 75%).

^{1}H NMR (400 MHz, $CDCl_3$): 7.46 (d, J=7.9 Hz, 2H), 7.37-7.42 (m, 1H), 7.32 (dd, J_{12}=6.8 Hz, J_{23}=2.1 Hz, 1H), 7.26 (d, J=7.9 Hz ,2H), 6.70 (d, J=9.2 Hz, 1H),6.24 (t, J=6.8 Hz, 1H), 5.28 (s, 2H), 2.61 (s, 6H), 1.36 (s, 6H).

^{13}C NMR (100 MHz, $CDCl_3$): δ 162.7, 154.1, 150.0, 141.4, 140.5, 139.9, 138.3, 137.0, 134.0, 128.8, 128.4, 121.4, 106.8, 51.7, 13.8, 13.7.

MS (TOF-ESI): m/z calculated for $C_{25}H_{22}BBr_2F_2N_3O$ $[M-H]^-$: 585.01543, found for $[M-H]^-$: 585.00912, Δ= 10.79 ppm.

2.2.6 Synthesis of Compound 7

Compound **6** (0.09 g, 0.16 mmol) and 4-(hydroxymethyl)-benzaldehyde (**2**) (0.04 mg, 0.32 mmol) are dissolved in benzene (25 mL) in a round-bottomed flask. Glacial acetic acid (0.20 mL) and piperidine (0.20 mL) are added to the reaction mixture. Dean-Stark apparatus is placed on the round-bottomed flask and reaction mixture is refluxed at 100 °C until all the starting material was consumed which is confirmed by TLC using DCM as the eluent. The reaction was diluted with DCM and extracted with water. Organic phases are combined and dried over anhydrous Na_2SO_4. Solvent is evaporated in vacuo and the product is purified by silica gel column chromatography with gradient elution from DCM to DCM/MeOH (98:2, v/v). Compound **7** was obtained as naive waxy solid (0.07 g, 52%).

^{1}H NMR (400 MHz, DMSO-d_6): δ 8.08 (d, J=16.0 Hz, 2H), 7.83 (d, J= 6.6 Hz, 2H) 7.70-7.86 (m, 5H), 7.40-7.50 (m, 9H), 6.49 (d, J= 9.3 Hz, 1H), 6.31 (t, J= 6.2 Hz, 1H), 5.32 (t, J= 5.1 Hz, 2H), 5.26 (s, 2H), 4.57 (s, 4H), 1.33 (s, 6H).

^{13}C NMR (100 MHz, DMSO-d_6): δ 162.0, 148.0, 145.3, 141.8, 140.9, 140.8, 139.7, 139.5, 139.4, 134.9, 133.2, 132.2, 128.9, 127.7, 127.6, 125.4, 120.4, 117.1, 110.4, 106.2, 63.0, 51.3, 13.9.

MS (TOF-ESI): m/z calculated for $C_{41}H_{34}BBr_2F_2N_3O_3$ $[M+Na]^+$: 845.09566, found for $[M+Na]^+$: 845.09677, Δ= -1.32 ppm.

2.2.7 Synthesis of Compound 8

Compound **7** (0.10 g, 0.12 mmol) is dissolved in freshly distilled THF in an oven-dried round-bottomed flask. 3-(Triethoxysilyl)propyl isocyanate (64 µl, 0.26 mmol) and dibutyltin dilaurate (5 µl, 0.008 mmol) is added to the reaction mixture and the reaction mixture was refluxed at 70 °C overnight. Solvent is evaporated in vacuo and the product is purified by silica gel column chromatography with gradient elution from DCM to DCM/MeOH (98:2, v/v). Compound **8** was obtained as naive waxy solid (0.07 g, 52%).

^{1}H NMR (400 MHz, $CDCl_3$): δ 8.14 (d, J=16.6 Hz, 2H), 7.74 (d, J=16.6 Hz, 2H), 7.66 (d, J= 8.0 Hz, 4H), 7.47 (d, J= 8.3, 2H), 7.43 (d, J=8.0, 4H), 7.37-7.41 (m, 1H), 7.33-7.34 (m, 1H), 7.31 (d, J= 8.3, 2H), 6.69 (dt, J_{12}= 9.2 Hz, J_{23}= 0.6 Hz, 1H), 6.24 (td, J_{12}= 6.7 Hz, J_{23}= 1.4 Hz, 1H), 5.29 (s, 2H), 5.14 (s, 4H), 3.84 (q, J= 7.0 Hz, 12H), 3.24 (q, J= 6.6 Hz, 4H), 1.67 (quint, J= 7.4 Hz, 4H), 1.42 (s, 6H), 1.24 (t, J= 7.0 Hz, 18H) 0.66 (t, J= 8.1 Hz, 4H).

^{13}C NMR (100 MHz, $CDCl_3$): δ 156.3, 148.6, 143.9, 141.3, 139.7, 139.1, 139.0, 138.4, 138.0, 137.0, 136.6, 134.4, 132.2, 128.8, 128.5, 127.8, 127.3, 121.6, 118.3, 110.6, 106.6, 66.2, 58.5, 51.6, 43.5, 23.3, 18.3, 13.9, 7.6.

MS (TOF-ESI): m/z calculated for $C_{61}H_{76}BBr_2F_2N_5O_{11}Si_2$ $[M+Na]^+$: 1339.34363, found for $[M+Na]^+$: 1339.33954, Δ= 3.05 ppm.

2.3 Preparation of SPIONs

2.3.1 Synthesis of Iron Oxide Nanoparticles (9)

$FeCl_2 \cdot 4H_2O$ (2.15 g, 0.01 mol) and $FeCl_3 \cdot 6H_2O$ (5.84 g, 0.02 mol) are dissolved in argon bubbled deionized water (200 mL) at 90 °C under mechanical stirring. Aqueous ammonia (25% NH_3 in water, 7.5 mL) solution is added to the reaction medium. Instant color change from orange to black indicated the formation of iron oxide nanoparticles. Reaction medium is kept at that temperature for 30 min. Iron oxide nanoparticles are collected with neodymium magnet and washed three times with deionized water and ethanol. At the final stage iron oxide nanoparticles are dried under argon atmosphere for further functionalization.

2.3.2 Synthesis of Silica coated Iron Oxide Nanoparticles (9s)

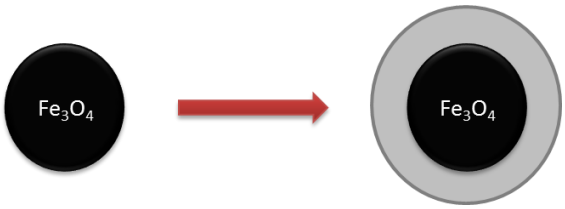

Freshly prepared iron oxide nanoparticles (2 g) are dispersed in water (60 mL), ethanol (240 mL) and ammonia (25% NH_3 in water, 7.5 mL) containing mixture with ultra-sonication for 30 min at room temperature. To this dispersion is added tetraethyl orthosilicate (TEOS) (1.6 mL, 1.5 g, 0.0072 mol). This mixture firstly ultra-sonicated for 30 min then mechanically stirred for 12 h at

room temperature. The silica coated iron oxide nanoparticles are separated with neodymium magnet and washed 3 times with water and DMF. After this washing process, nanoparticles are immersed in HCl (4 M) for 30 min to dissolve unreacted iron oxide nanoparticles. The coated nanoparticles are separated from HCl by washing with deionized water and separating with neodymium magnet until pH of the supernatant reaches 7. The coated iron oxide nanoparticles are dried under Ar atmosphere.

2.4 Preparation of Photocatalyst

2.4.1 Synthesis of BODIPY Functionalized Silica Coated Iron Oxide Nanoparticles (10)

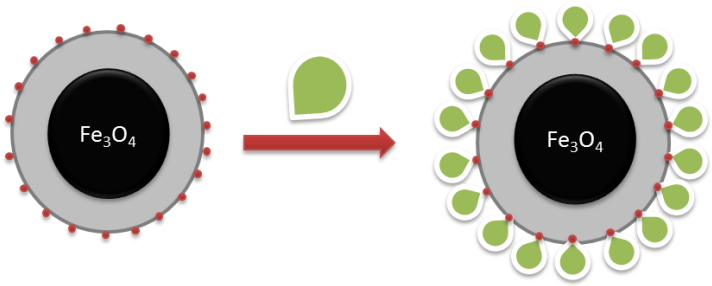

The coated iron oxide nanoparticles are dried under Ar atmosphere. Silica coated iron oxide nanoparticles (85 mg) are dispersed in dry toluene (45 mL) with ultra-sonication for 30 min under Ar atmosphere at room temperature. Compound **8** (6 mg, 0.005 mmol) is dissolved in the dispersion under mechanical stirring. Mixture is kept under mechanical stirring and reflux at 120 °C for 48 h. BODIPY functionalized nanoparticles are collected with magnetization with neodymium magnet and centrifugation (7000rpm, 20mins). To get rid of any bound BODIPY in non-covalent manner, nanoparticles dispersed in ultra-sonication for 30 min and collected by magnetization with neodymium magnet centrifuged (7000 rpm, 20 min). This procedure is applied in DCM and ethanol

repeatedly until supernatant shows any sign of existence of BODIPY under UV light.

2.4.2 Synthesis of Compound 11

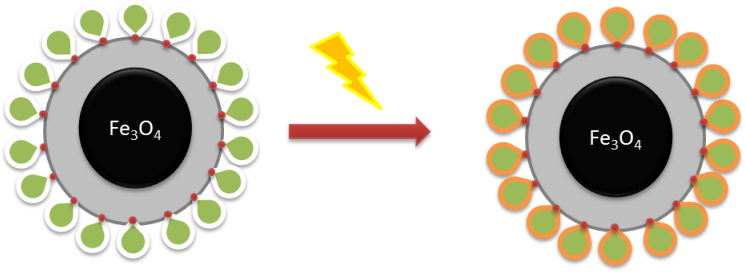

BODIPY Functionalized Silica Coated Iron Oxide Nanoparticles (0.05 g) are dissolved in $CHCl_3$ (80 mL) with ultrasonication for 15 min while bubbling solution with oxygen gas. The resulting solution is irradiated with 500 W halogen lamp while oxygen gas is bubbling through it for an h. The resulting nanoparticles are separated by neodymium magnet and nanoparticles are washed with $CHCl_3$ 3 times.

2.5 Preparation of Sulfides

2.5.1 Synthesis of Benzyl Phenyl Sulfide (12)

Thiophenol (0.26 mL, 2.5 mmol) and potassium carbonate (0.38 g, 2.75 mmol) are dissolved in 5 mL of DMF. Benzyl bromide (0.30 mL, 2.5 mmol) is added dropwise to reaction mixture at room temperature. The reaction is stirred for 4

h and extracted with EtOAc and brine. Organic phases are combined and dried over anhydrous Na_2SO_4. Solvent is evaporated in vacuo and the product is purified by silica gel column chromatography using petroleum benzine as the eluent. Benzyl phenyl sulfide **(12)** was obtained as white solid (0.430 g, 86%).

^{1}H NMR (400 MHz, $CDCl_3$): δ 7.31-7.37 (m, 7H), 7.31-7.29 (m, 1H), 7.26-7.28 (m, 1H), 4.16 (s, 2H).

^{13}C NMR (100 MHz, $CDCl_3$): δ 137.5, 136.4, 129.9, 128.8, 128.7, 128.5, 127.2, 126.4, 39.1.

MS (TOF-ESI): m/z calculated for $C_{13}H_{12}S$ $[M-H]^-$: 199.05869, found for $[M-H]^-$: 199.05911, Δ= -2.09 ppm.

2.5.2 Synthesis of Octyl Phenyl Sulfide (13)

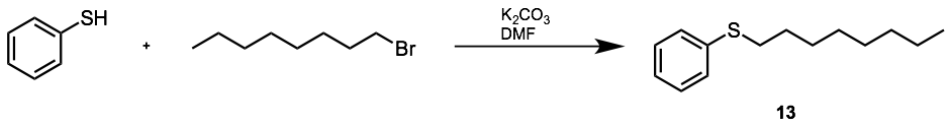

13

Thiophenol (1.86 mL, 18.2 mmol) and potassium carbonate (5.00 g, 36.4 mmol) are dissolved in 20 mL of DMF. n-octyl bromide (4.70 mL, 27.3 mmol) is added to the reaction mixture. The reaction is refluxed at 85 °C for overnight and extracted with Et_2O and water. Organic phases are combined and dried over anhydrous Na_2SO_4. Solvent is evaporated in vacuo and the product is purified by silica gel column chromatography using petroleum benzine as the eluent. Octyl phenyl sulfide (**13**) was obtained as colorless liquid (2.6 g, 64%).

^{1}H NMR (400 MHz, $CDCl_3$): δ 7.35- 7.38 (m, 1H), 7.29-7.34 (m, 2H), 7.16-7.22 (tt, J_{12}= 7.2 Hz, J_{23}= 1.4 Hz, 1H), 2.96 (t, J= 7.4 Hz, 2H), 1.69 (quint, J= 7.4 Hz, 2H), 1.47 (quint, J= 7.3 Hz, 2H), 1.30-1.33 (m, 8H), 0.93 (t, J= 6.9 Hz, 3H).

^{13}C NMR (100 MHz, $CDCl_3$): δ 137.1, 128.9, 128.8, 125.6, 33.6, 31.8, 29.2, 29.1, 28.9, 22.7, 14.1.

MS (TOF-APCI): m/z calculated for $C_{14}H_{22}S$ $[M+H]^+$: 223.1515, found for $[M+H]^+$: 223.15146, Δ= 0.17 ppm.

2.5.3 Synthesis of Benzyl Butyl Sulfide (14)

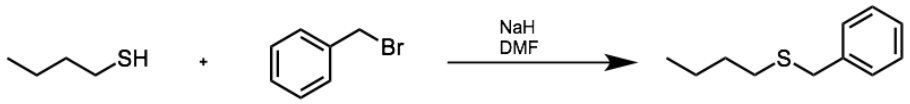

14

1-Butanethiol (1.00 mL, 9.3 mmol) and sodium hydride (60% dispersion in mineral oil, 0.37 g, 9.3 mmol) are dissolved in 10 mL of DMF under Argon atmosphere. When the starting compound is consumed by checking with TLC, benzyl bromide (1.05 mL, 8.9 mmol) is added dropwise to reaction mixture at room temperature. The reaction is stirred overnight and extracted with DCM and brine. Organic phases are combined and dried over anhydrous Na_2SO_4. Solvent is evaporated in vacuo and the product is purified by silica gel column chromatography using hexane to EtOAc/Hexane (2:98, v/v) as the eluent. Benzyl butyl sulfide (**14**) was obtained as white oil (1.4 g, 84%).

^{1}H NMR (400 MHz, $CDCl_3$): δ 7.32-7.37 (m, 4H), 7.24-7.30 (m, 1H), 3.74 (s, 2H), 2.45 (t, J= 7.4 Hz, 2H), 1.58 (quint, J= 7.3 Hz, 2H), 1.41 (sextet, J=7.4 Hz, 2H), 0.92 (t, J= 7,3 Hz, 3H).

^{13}C NMR (100 MHz, $CDCl_3$): δ 138.7, 128.8, 128.4, 126.9, 36.3, 31.3, 31.1, 22.0, 13.7.

MS (TOF-APCI): m/z calculated for $C_{11}H_{16}S$ $[M+H]^+$: 181.10455, found for $[M+H]^+$: 181.10439, Δ= 0.87 ppm.

2.5.4 Synthesis of Butyl tert-butyl Sulfide (15)

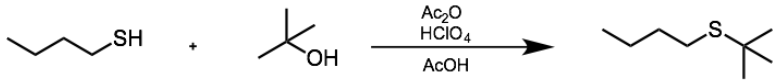

15

Perchloric acid (70% solution, 1.40 mL, 16.2 mmol) and acetic anhydride (2.40 mL, 25.4 mmol) are dissolved in 4 mL of acetic acid (glacial). The solution is stirred for 30 min at room temperature. 1-butanethiol (2.14 mL, 20.0 mmol) and tert-butanol (2.26 mL, 23.6 mmol) in 3 mL acetic acid is added dropwise to reaction mixture at room temperature. The reaction is stirred overnight at room temperature and extracted with Et_2O and brine. Organic phases are combined and dried over anhydrous Na_2SO_4. Solvent is evaporated in vacuo to yield pure butyl tert-butyl sulfide (**15**) as slightly yellowish oil (2.9 g, 99%).

^{1}H NMR (400 MHz, $CDCl_3$): δ 2.50 (t, J=7.4 Hz, 2H), 1.53 (quint, J= 7.4 Hz, 2H), 1.40 (quint, J= 7.4 Hz, 2H), 1.29 (s, 9H), 0.89 (t, J= 7.3 Hz, 3H).

^{13}C NMR (100 MHz, $CDCl_3$): δ 41.6, 31.9, 30.9, 27.9, 22.3, 13.7.

2.6 Preparation of Sulfoxides

2.6.1 General Procedure under Light Irradiation

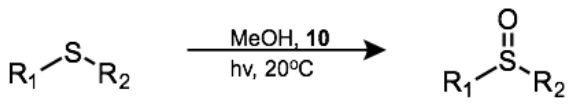

12-15 12a-15a

20 mg of BODIPY Functionalized Silica Coated Iron Oxide Nanoparticles (**10**) are dissolved by ultrasonication in 20 mL in MeOH for 5 min. Corresponding sulfide (**12-15**, 0.05 mmol) is dissolved in 5 mL of MeOH and added to the

reaction mixture. The resulting mixture is stirred with mechanical stirrer under light (500 W halogen lamp) while O_2 gas is bubbled and temperature is maintained at 20 °C. The reaction is monitored by TLC on silica with DCM as eluent, for given period of time as shown in Table **1**. The BODIPY Functionalized Silica Coated Iron Oxide Nanoparticles are collected by neodymium magnet and the supernatant solution is filtered through a pad of silica and washed with DCM/MeOH (5:1, v/v). The filtrate is dried over anhydrous Na_2SO_4 and evaporated in vacuo to yield crude product (**12a-15a**). The sulfoxide is purified by silica gel column chromatography with gradient elution from DCM to DCM/MeOH (95:5, v/v).

Benzyl Phenyl Sulfoxide (12a):

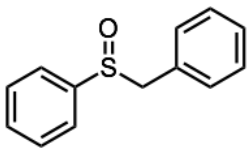

12a

^{1}H NMR (400 MHz, $CDCl_3$): δ 7.36-7.52 (m, 5H), 7.20-7.35 (m, 3H), 6.92-7.05 (m, 2H), 4.13 (d, J= 12.4 Hz, 1H), 4.02 (d, J= 12.4 Hz, 1H).

^{13}C NMR (100 MHz, $CDCl_3$): δ 142.7, 131.2, 130.4, 129.1, 128.9, 128.5, 128.3, 124.5, 63.6.

MS (TOF-APCI): m/z calculated for $C_{13}H_{12}OS$ $[M+H]^+$: 217.06816, found for $[M+H]^+$: 217.06749, Δ= 3.1 ppm.

Octyl Phenyl Sulfoxide (13a):

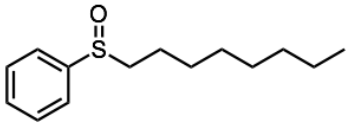

13a

^{1}H NMR (400 MHz, $CDCl_3$): δ 7.61-7.67 (m, 2H), 7.48-7.58 (m, 3H), 2.80 (td, J_{12}= 7.7 Hz, J_{23}= 1.8 Hz, 2H) 1.75 (sextet, J= 6.7 Hz, 1H), 1.64 (sextet, J=6.7 Hz, 1H) 1.38-1.46 (m, 2H), 1.23-1.31 (bs, 8H), 0.88 (t, J=6.7 Hz, 3H).

^{13}C NMR (100 MHz, $CDCl_3$): δ 144.1, 130.9, 129.2, 124.0, 57.4, 31.7, 29.1, 29.0, 28.7, 22.6, 22.2, 14.0.

MS (TOF-APCI): m/z calculated for $C_{14}H_{22}OS$ $[M+H]^+$: 239.14641, found for $[M+H]^+$: 239.14633, Δ= 0.35 ppm.

Benzyl Butyl Sulfoxide (14a)

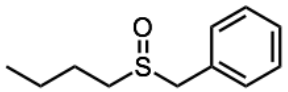

14a

^{1}H NMR (400 MHz, $CDCl_3$): δ 7.36-7.42 (m, 3H), 7.30-7.34 (m, 2H), 4.07 (d, J=12.9 Hz, 1H), 3.97 (d, J=12.9 Hz, 1H), 1.71-1.81 (m, 2H), 1.38-1.54 (m, 2H), 0.95 (t, J= 7.4 Hz, 3H).

^{13}C NMR (100 MHz, $CDCl_3$): δ 130.0, 129.0, 128.4, 128.2, 58.2, 50.6, 24.5, 22.0, 13.6.

MS (TOF-APCI): m/z calculated for $C_{11}H_{16}OS$ $[M+H]^+$: 197.09946, found for $[M+H]^+$: 197.09986, Δ= -2.02 ppm.

Butyl tert-Butyl Sulfoxide (15a):

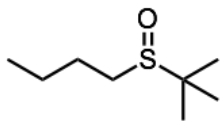

15a

^{1}H NMR (400 MHz, $CDCl_3$): δ 2.36-2.43 (m, 2H), 1.63-1.84 (m, 2H), 1.34-1.52 (m, 2H) 1.18 (s, 9H), 0.90 (t, J= 7.3 Hz, 3H).

^{13}C NMR (100 MHz, $CDCl_3$): δ 52.6, 45.3, 25.7, 22.8, 22.1, 13.7.

MS (TOF-APCI): m/z calculated for $C_8H_{18}OS$ $[M+H]^+$: 163.11511, found for $[M+H]^+$: 163.11563, Δ= -3.17 ppm.

2.6.2 Synthesis of Butyl tert-Butyl Sulfoxide by Compound 11

Compound **11** (25 mg) is dissolved in 4 mL of MeOH by ultrasonication in a 10 mL vial. Butyl tert-butyl sulfide (**15**) (2.5 mg, 0.017 mmol) and o-dichlorobenzene (internal standard for GSMS) (5 µL, 0.044 mmol) are added to the vial and the vial is sealed. The vial is placed in 50 °C heat bath. After 4 h, the nanoparticles are collected by neodymium magnet and the supernatant liquid is collected for GCMS experiment.

Chapter III

Results and Discussion

Delivery of catalytic agents to a targeted media effectively and collecting back them is a significant issue because synthesis and manufacturing procedures seek ease of usage, recovery and recycling of those agents.

At that point, BODIPY Functionalized Silica Coated Iron Oxide Nanoparticles are synthesized for oxidation of sulfoxides in the presence and absence of light, and these SPIONs can be collected easily from reaction media by magnetization.

The synthesis of the reloadable photosensitizer was shown in Figure 19. The arylaldehyde is functionalized with 2-pyridone moiety because BODIPY synthesis is facile with an aldehyde group with high yields. After the synthesis of BODIPY core, compound **5**, NBS was used for bromination in the 2^{th} and 6^{th} position. Bromine attachment enhances intersystem crossing by providing spin-forbidden S→T transition due to spin-orbit coupling, leading to the increase in singlet oxygen photosensitization. Then, compound **6** was further functionalized in the 3 and 5^{th} position by Knoevenagel condensation with 4-(hydroxymethyl) benzaldehyde to pave the way for further addition of triethoxysilyl group which is the key group for coating on Si-coated iron oxide nanoparticles. The catalysis

of dibutyltin dilaurate for the synthesis of compound was required for the reaction of isocyanate group with alcohol, because in the absence of this catalyst, the reaction does not yield any product albeit isocyanate is very reactive toward alcohols. All of the steps were characterized by NMR and HRMS measurements. All the spectra are given in the Appendix.

Iron oxide nanoparticles were prepared by co-precipitation method due to being mild and relatively easy. The reaction took place under Argon gas to prevent air oxidation of Fe^{2+} to Fe^{3+} by oxygen in the air. The reaction is stirred vigorously by a mechanical stirrer to prevent agglomeration. The freshly prepared and washed SPIONs are then coated with silica to prevent oxidation and agglomeration. Also functionalization on the surface of silica coated SPIONs are facile with the triethoxysilyl group containing compounds.

The BODIPY functionalized silica coated SPIONs (**10**) are prepared by functionalization of silica coated SPIONs with compound **8**. The characterization of SPIONs (**9**), silica coated SPIONs (**9s**) and BODIPY functionalized SPIONs (**10**) were done with XRD, TEM and size distributions of the SPIONs are determined by Zeta Size Measurements.

3.1 X-Ray Diffraction Measurements of SPIONs (9 & 9s)

The XRD measurements are performed for the characterization of SPIONs (**9**) and silica coated SPIONS (**9s**). d values, which are the specific parameters for the sets of separation between adjacent lattice planes are calculated according to Bragg's Law. Experimental d values are in consistency with the literature values, as seen in the Table 1, indicating the SPIONS are composed of inverse cubic spinel structure of magnetite, Fe_2O_3 which was desired in our preparation method. Coating of silica can be also characterized by XRD patterns. The

broadening starting from 30 to lower degrees shows the presence of silica shell on SPIONs compared to uncoated SPIONs (**9**).

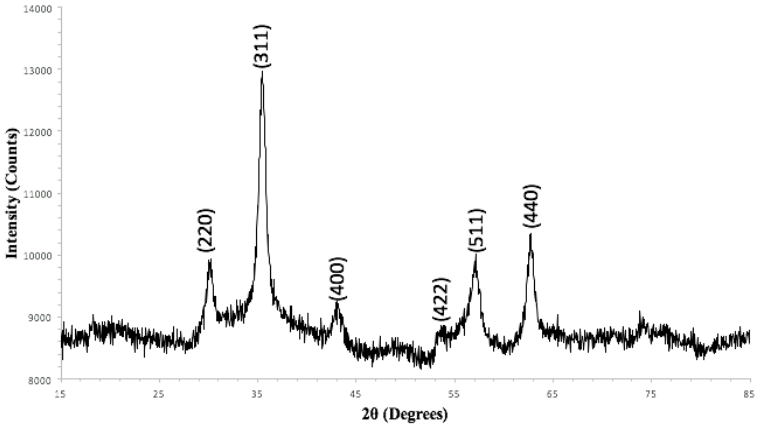

Figure 20: XRD spectrum of iron oxide nanoparticles (**9**) indicating the lattice structures.

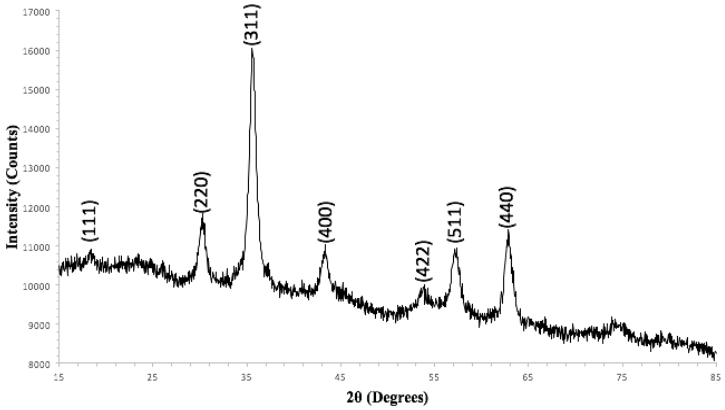

Figure 21: XRD spectrum of silica coated iron oxide nanoparticles (**9s**) indicating the lattice structures.

Table 1: d values obtained from XRD measurements and comparison with literature.

SPIONs (9)		Si-coated SPIONs (9s)		Literature
2θ(exp)	**d (exp)**	**2θ(exp)**	**d (exp)**	**d (Fe_2O_3)**
-	-	18.37	*4.82*	*4.85*
30.11	*2.96*	30.26	*2.95*	*2.97*
35.46	*2.53*	35.54	*2.52*	*2.53*
43.23	*2.09*	43.34	*2.09*	*2.10*
56.97	*1.61*	57.13	*1.61*	*1.62*
62.64	*1.48*	62.84	*1.48*	*1.48*

3.2 Transmission Electron Microscopy Analysis of SPIONs (9, 9s & 10)

The samples for TEM analysis were prepared by dropping dilute solutions of 9, 9s and 10 in ethanol on the carbon coated copper grids. The samples were hold in room temperature for 5 min to allow drying before analysis. First TEM analysis with naked SPIONs (**9**) shows that spherical SPIONs diameters have a range of 7 to 20 nm (Figure 22) which is in consistency with the literature values when the SPIONs are prepared by co-precipitation method with the given parameters in the experimental section. TEM analysis also shows that freshly prepared SPIONs aggregates easily due to the magnetic dipole attractions between them.

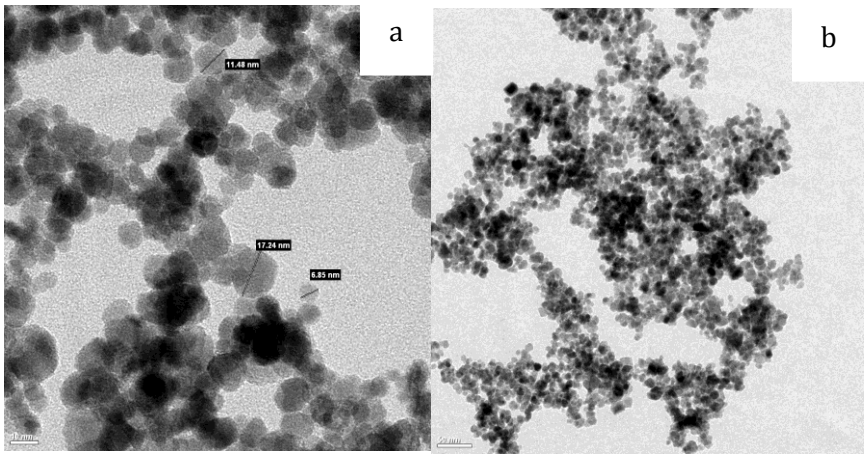

Figure 22: TEM images of SPIONs (**9**).

Secondly, silica coated SPIONs (**9s**) were analysed with TEM and the images are shown in Figure 23. Silica coating is around 1-3 nms around the small aggregates of SPIONs as seen in Figure 23b. Also the aggregation is less compared to uncoated SPIONs (**9**), which shows the stability of the silica coated SPIONs (**9s**).

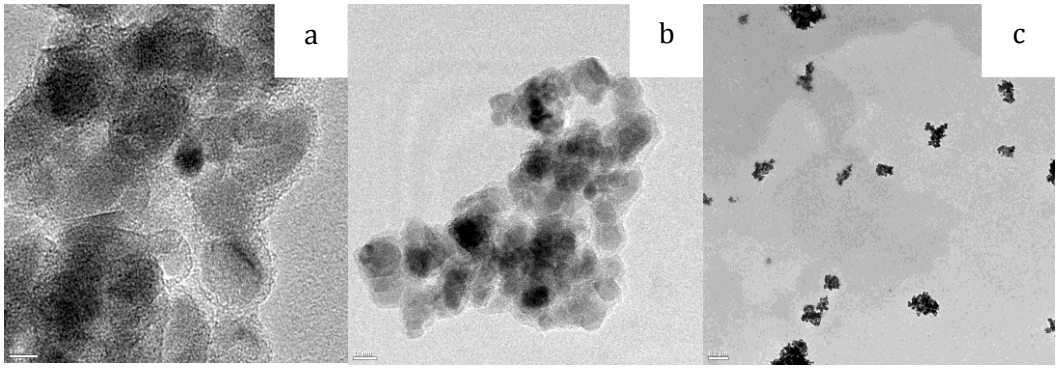

Figure 23: TEM images of silica coated SPIONs (**9s**).

Besides TEM images, EDX emission spectra shows the silica coating on the iron oxide nanoparticles as shown in the Figure 24. Presence of silica peaks as well as iron peaks shows proves the coating on SPIONs.

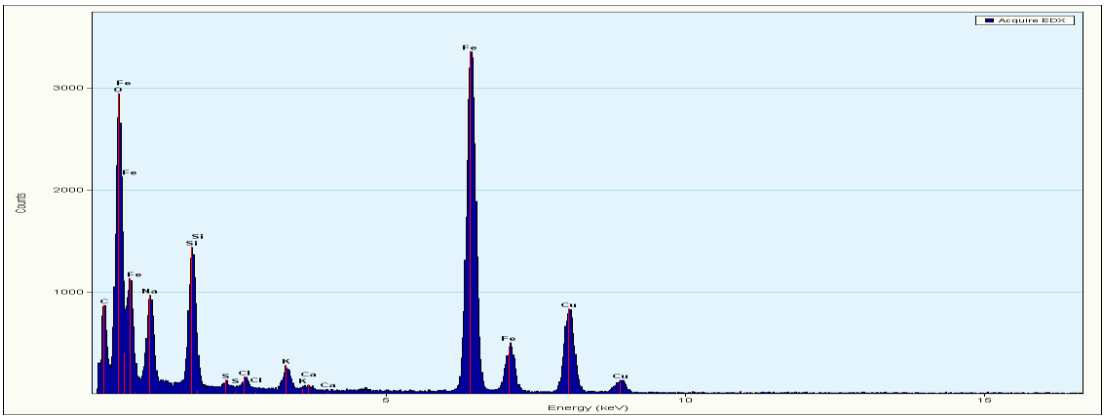

Figure 24: Energy Dispersive X-Ray analysis of silica coated SPIONs (**9s**).

Thirdly, TEM analysis was done to BODIPY functionalized silica coated SPION (**10**). The size of the nanoparticles is in consistent with the values obtained from the Zeta Size Measurements. High Angle Annular Dark Field TEM analysis combined with EDX shows boron and bromine peaks which proves the presence of BODIPY on silica coated SPIONs since BODIPY is the only source of boron and bromine atoms. Also, in order to verify the existence of BODIPY on the outer shell of SPIONs, elemental analysis on different regions of nanoparticles were compared. EDX analysis of the area marked on the edge of the nanoparticle as shown in Figure 25 (right) has higher intensity than the area marked in the middle of the nanoparticle as shown in Figure 25 (left).

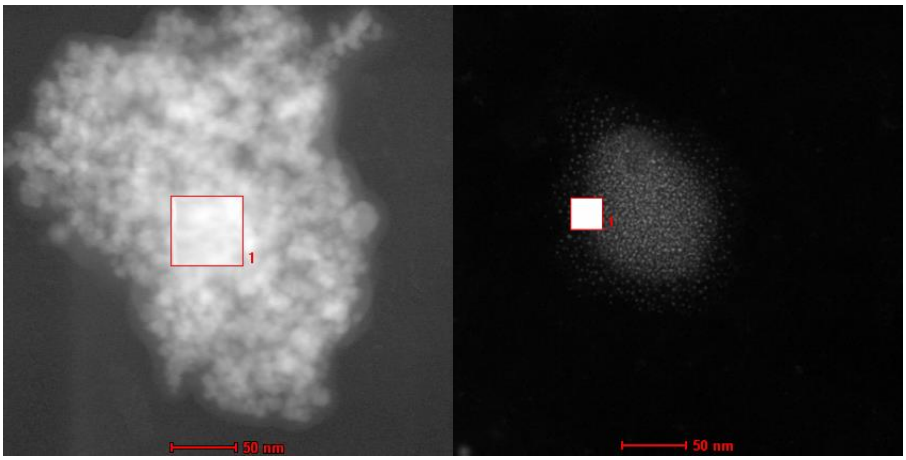

Figure 25: TEM images of BODIPY functionalized silica coated SPIONs (**10**).

In fact, iron and silica peaks are nearly invisible compared to intense major boron peak recorded on the edge of the SPION, on the other hand, iron and silica peaks can be seen if the middle of the nanoparticle is analysed. Still those peaks are less intense compared to the silica coated SPIONs (**9s**).

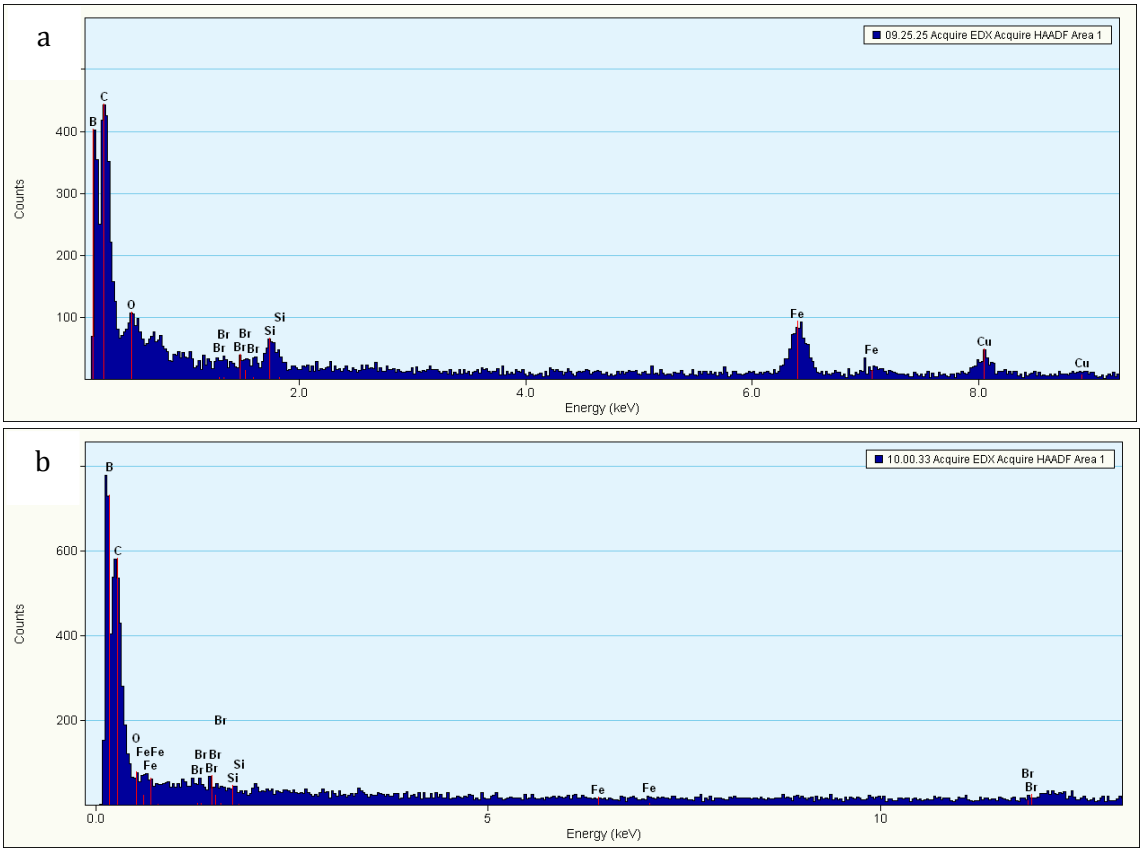

Figure 26: Energy Dispersive X-Ray analysis of BODIPY functionalized silica coated SPIONs (**10**).

3.3 Photophysical Measurements of 9s and 10

BODIPY with the triethoxysilane groups (**8**) have a maximum absorbance at 647 nm as seen in the Figure 27. It has longer wavelength compared to BODIPY core because of the extended conjugation with attached styryl groups on 3 and

5th positions. When compound **8** is coated on silica shell SPIONs (**9s**), the specific peaks of BODIPY can be observed in the absorbance spectrum of SPIONS as seen in the following:

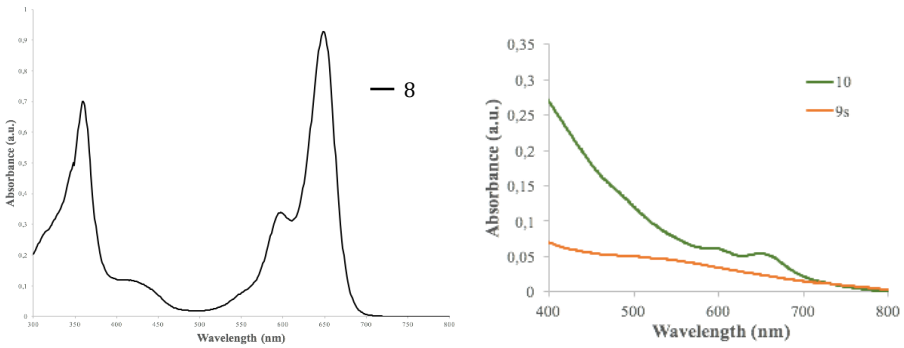

Figure 27: Absorption spectra of Compound **8**, **9s** and **10** in chloroform as solvent.

The peak at 650 nm in Figure 27 (right) also proves the presence of BODIPY on the outer shell of SPIONs. Addition of BODIPY on SPIONs also cause the color change of the nanoparticles from orange to green which can also be observed by naked eye:

Figure 28: Solutions of **9s** (left) and **10** (right) in CHCl3. The samples were ultrasonicated for 5 min.

When the solutions of silica coated SPIONs (**9s**) and BODIPY functionalized SPIONs (**10**) in chloroform are placed next to the neodymium magnet as seen in Figure 29, they can be separated from the solvent in minutes. **9s** can be separated by magnetization in 1 minute, besides **10** can be separated in 3 minutes since

solubility of SPIONs increases in organic solvents, i.e. chloroform, with the functionalization with BODIPY and it takes longer time to collect with magnet.

Figure 29: Magnetization of **9s** (left) and **10** (right) in the presence of external magnet.

3.4 Singlet Oxygen Generation and Storage Experiments:

Generation and storage capabilities of BODIPY functionalized SPIONs (**10**) are investigated with the commercially available singlet oxygen trap, 1,3-diphenylisobenzofuran (DPBF). The absorbance of DPBF decreases in the presence of singlet oxygen because singlet oxygen is highly reactive against DPBF causing the photo bleaching. Chloroform was chosen as solvent in these experiments because the SPIONs have good solubility in chloroform and lifetime of singlet oxygen is relatively high.

First, the generation capability of **10** is examined with DPBF. The solution of **10** is prepared in absorbance cuvette with oxygen bubbled chloroform for 15 minutes to saturate the solvent with molecular oxygen. Then the solution of DPBF in chloroform is added to the cuvette. The absorbance of DPBF is set around 1. The cuvette is irradiated with 653 nm LED array (1.2 W/m^2) from 10 cm distance with 1 minute time intervals and absorbance is recorded. In order to prevent the interference of the absorbance of iron oxide, the cuvette is hold on a neodymium magnet for 15 min to collect SPIONs at the bottom of cuvette before

each measurement. At the same time trap molecule is treated with same conditions as control experiment. The following spectra are obtained:

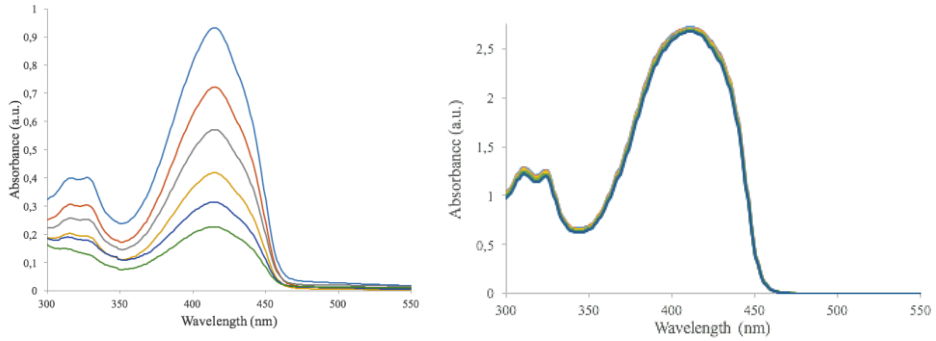

Figure 30: Left: Photobleaching of DPBF with the generation of singlet oxygen by **10**. Right: Control experiment with trap.

As shown in Figure 30, the BODIPY functionalized SPIONs (**10**) can generate singlet oxygen in high amounts in the presence of molecular oxygen.

Secondly, the storage capacity of SPIONs (**10**) with the 2-pyridone moiety was examined with DPBF. **10** is irradiated with light while oxygen gas is bubbling through it, forming **11**. Then the solution of **11** is prepared in chloroform and DPBF is added as singlet oxygen trap. From literature, the 2-pyridone moiety on 8th position of BODIPY is stable in room temperature, and undergoes thermolysis at 40 °C. The solution of **11** is placed in absorbance cuvette and the solution of DPBF in chloroform is added to the cuvette, adjusting the absorbance maxima at 0.5. The cuvette is placed in heat bath at 50 °C with 30 min time intervals and absorbance is recorded for 3.5 h. At the same time trap molecule is treated with same conditions as control experiment. Figure 31 shows the release of singlet oxygen from **11** in exponentially decreasing manner.

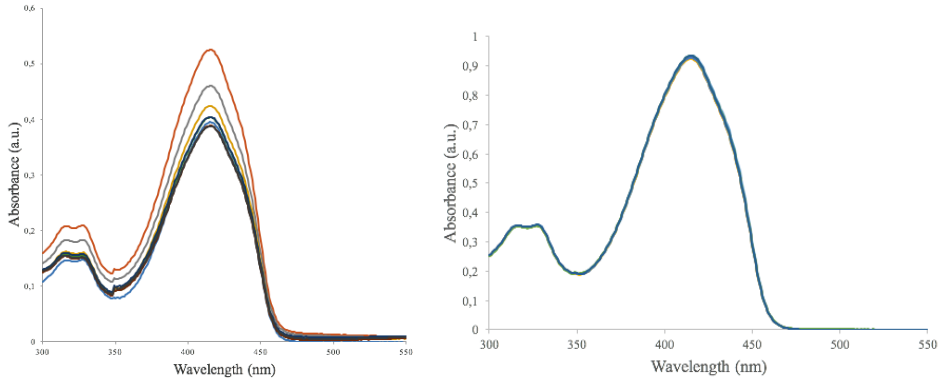

Figure 31: Left: Decrease in absorbance of DPBF with the release of singlet oxygen from pyridone moieties on **11** at 50°C. Right: Control experiment with trap.

Also the BODIPY functionalized SPIONs are rechargeable since 2-pyridone undergoes concerted cycloreversion to release singlet oxygen in high yields, with almost never producuction of side products. Thus, it can be rechargeable under light irradiation with oxygen gas bubbling. This rechargeable activity is proved by reloading of singlet oxygen to the SPIONs used in the DPBF experiment. Again, SPIONs (**11**) cause the bleaching in the absorbance of DPBF with 70% yield as shown in the Figure 32.

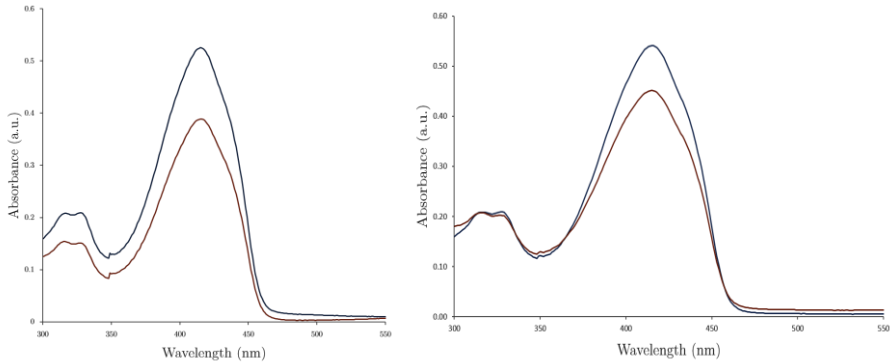

Figure 32: Recharging ability of the BODIPY functionalized silica coated SPIONs (**10**). Left: first cycle at 50 °C for 2 h. Right: second cycle at 50 °C for 2 h.

3.5 Oxidation of Sulfides

Oxidation of sulfides into sulfoxide with high yields and less side products can be done by singlet oxygen through the formation of persulfoxide. In this study, the oxidation of sulfides is performed in two courses of action. First way is the photooxidation of sulfides: magnetizable nanoparticles carrying BODIPY based photosensitizer is added to the reaction media and the reaction is performed under light irradiation while oxygen gas bubbling through it. Second approach is to load the magnetizable nanoparticles outside of the reaction media and then introduce the nanoparticles to release singlet oxygen. For both approaches, the nanoparticles can be removed from reaction media after the completion of reaction by a magnet. And both of the SPIONs are reusable in other reactions. Figure 33 is the schematic representation of the working principle of magnetizable SPIONs.

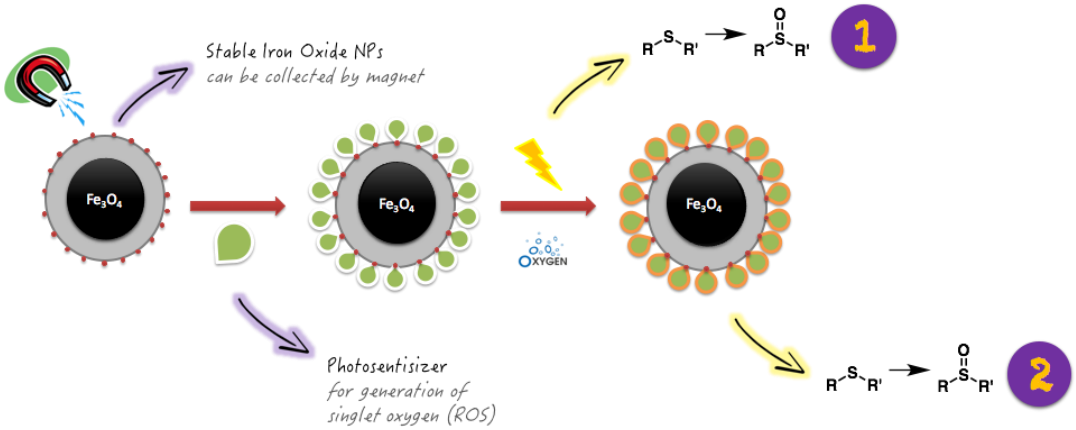

Figure 33: Schematic representation of the two working pathways of our design.

The first strategy for sulfoxide oxidation, four sulfide derivatives were used as reactants to investigate the efficiency with different functional groups bound to sulfur atom. Yields of the reactions (determined by crude NMR) and reaction

times are shown in the Table 2. Sulfides with aliphatic group attached on two sides (**14** and **15**) undergoes reaction to form sulfoxide faster than the sulfides with phenyl group attached (**12** and **13**). The reason behind is the electronic effects on the sulfide atom. Singlet oxygen has an electrophilic nature, that's why the electron withdrawing phenyl group on sulfide makes the sulfur atom more electron deficient and thus slows down the reaction 4 times. Also the bulky group, i.e. tert-butyl group, has mere effect on the photooxidation of sulfides if the yields compared for **14** and **15**. The side product sulfone is low for **12**, **13** and **14**. Sulfide **15** gives relatively higher sulfone, which shows higher reactivity toward singlet oxygen. Yet, sulfone production is pale in comparison with given high yields.

Table 2: Reaction times and sulfoxide&sulfone yields of photooxidation of sulfides **12-15**. Yields are calculated by ratio of the integration values determined by NMR.

Reactant	Reaction Time (h)	Sulfoxide Formation (%)	Sulfone Formation (%)
12	24	83	2
13	24	90	9
14	6	82	1
15	6	84	15

Second strategy, which is to load singlet oxygen by BODIPY attached on SPIONs on the 2-pyridone moiety on itself and then introducing the nanoparticles to the reaction media by heating at 50 °C. This strategy was examined on the sulfide **15**, because of the faster reaction time compared to others and being most reactive toward singlet oxygen. The reaction was studied on GCMS. o-Dichlorobenzene was used as internal standard, the reactant (**15**) and the purified product (**15a**) were loaded on the GCMS to determine the retention times to compare with the reaction.

As seen in the Figure 34, internal standard has an intense peak at 5th min in all samples. The reactant **14** comes at 4.5 mib and the product **14a** comes at 7th

min. So when the heat release of the SPIONs are studied on t-butyl butyl sulfide (**14**), the Figure 34c is obtained. The reactant sulfide production of sulfoxide can be observed at 7^{th} minute and also mass spectra of the peak is verified at the GCMS reference library. The yield is relatively lower and the reason behind it can be the diffusion problem that singlet oxygen should diffuse to the outside of the nanoparticles to reach the sulfide but quenching with nanoparticle can be the case. Also the solvent should be protic for the sulfide photooxidation, but the singlet oxygen lifetime is so low in the protic solvents, in our example MeOH. Although the yield is relatively lower than the first strategy, this method is shown to be valid for oxidation of sulfides.

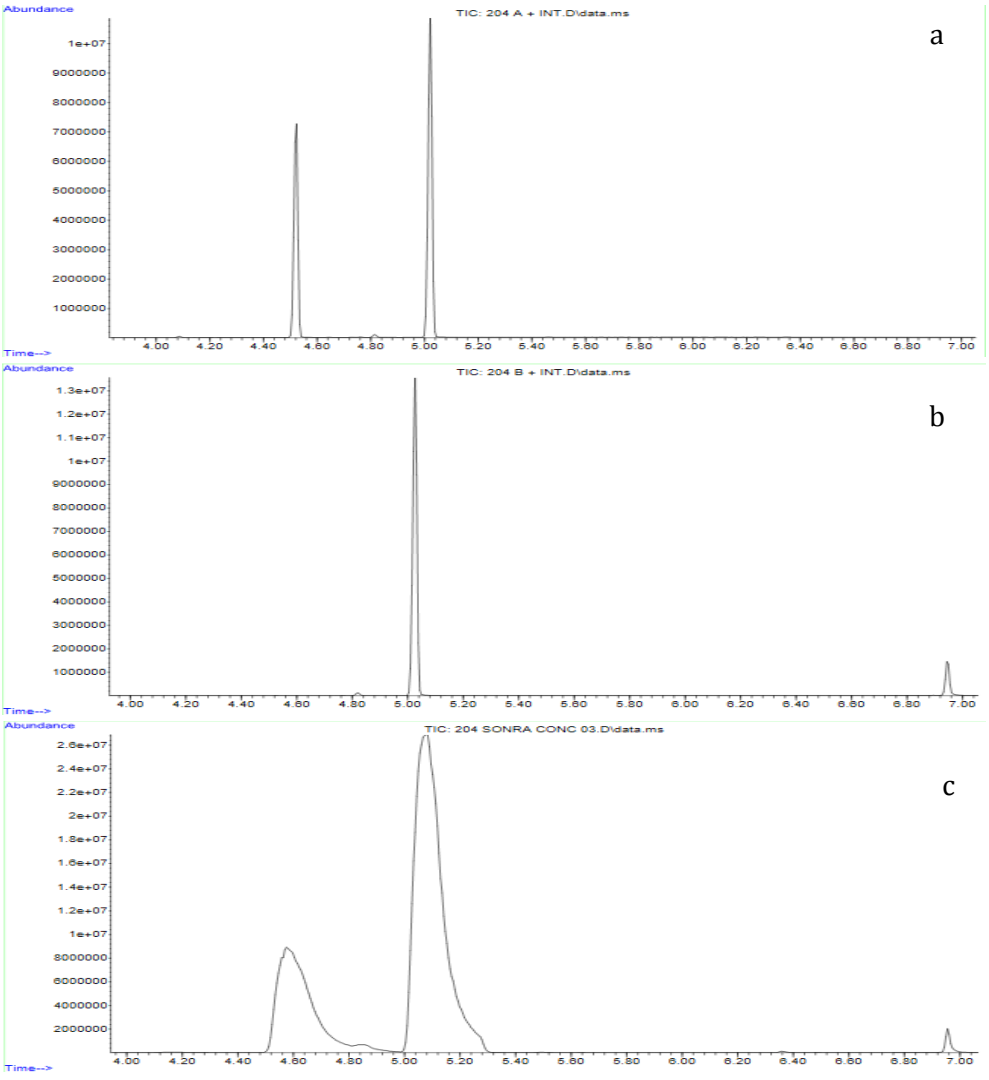

Figure 34: GCMS analysis with oxidation of sulfide **14** by release of singlet oxygen from 2-pyridone moiety. A contains starting sulfide and internal standard. B contains resulting sulfoxide and internal standard. C contains the reaction media after heating at 50 °C for 2 h.

Chapter IV

Conclusion

In this study, a magnetizable BODIPY functionalized silica coated iron oxide nanoparticles are designed and prepared for synthetic applications, i.e. oxidation of sulfide derivatives. For this purpose, iron oxide nanoparticles (**9**) are prepared by co-precipitation method and those SPIONs are coated with silica shell using tetraethoxysilane (TEOS) for high stability and ease of functionaliztion. The BODIPY, having a 2-pyridone moiety, is attached easily on the silica shell of iron oxide nanoparticles from triethoxysilane unit, forming nanostructure **10**. The structural properties of those SPIONs (**9, 9s** and **10**) are investigated and characterized by XRD and TEM. The size of the resulting SPIONs (**10**) are determined by Zeta Size and TEM analyses.

The singlet oxygen generation and storage capability of the BODIPY functionalized silica coated SPIONs (**10**) are done with the commercially available trap 1,3-Diphenylisobenzofuran (DPBF). The brominated BODIPY has high efficiency in singlet oxygen generation, and the attached 2-pyridone moiety on the 8^{th} position has the storage ability of singlet oxygen with recyclability. These features of our design are used in the oxidation of sulfides into sulfoxides.

First approach is the photooxidation of sulfides under irradiation of light in molecular oxygen saturated media. Photooxidation reactions are performed with 4 different sulfides (**12-15**) with yield of 80-90%. Sulfone production as side product is negligible, therefore this method is convenient for oxidation reactions for sulfoxides. The SPIONs can be removed from reaction media simply by a magnet at the end of the reaction.

Second approach covers the reloading of SPIONs with singlet oxygen by self-photosensitization and releasing them in the reaction media with recycling ability. The most reactive sulfide (**15**) toward singlet oxygen is used for this reaction and the reaction is analysed by GCMS. Sulfoxide production is also achieved by this strategy despite having low yields. Yet, endoperoxides can be stoichiometricly adjusted, the yields can be improved by utilisation of more endoperoxides or dealing with the problems concerning the diffusion of singlet oxygen outside of the nanoparticles toward the targeted substrates. Conclusively, our design has a significant potential for the developments in rechargable, reusable and removable nano-agents for the synthetic applications.

References

1. Fernandez, I.; Khiar, N., Recent developments in the synthesis and utilization of chiral sulfoxides. *Chemical Reviews* **2003,** *103* (9), 3651-3705.

2. Caron, S.; Dugger, R.; Ruggeri, S.; Ragan, J.; Ripin, D., Large-scale oxidations in the pharmaceutical industry. *Chemical Reviews* **2006,** *106* (7), 2943-2989.

3. Legros, J.; Dehli, J.; Bolm, C., Applications of catalytic asymmetric sulfide oxidations to the syntheses of biologically active sulfoxides. *Advanced Synthesis & Catalysis* **2005,** *347* (1), 19-31.

4. Carreno, M., Applications Of Sulfoxides To Asymmetric-Synthesis Of Biologically-Active Compounds. *Chemical Reviews* **1995,** *95* (6), 1717-1760.

5. Goldmann, S., Stereoselective Synthesis Of Alcohols. 5. Simple Regioselective Conversion Of Alkyl Ketones Into Allyl Alcohols. *Synthesis-Stuttgart* **1980,** (8), 640-642.

6. Jaxachamiec, A. A.; Sammes, P. G.; Kennewell, P. D., New Route To 5-Substituted Resorcinols And Related Systems. *Journal of the Chemical Society-Perkin Transactions 1* **1980,** (1), 170-175.

7. Maezaki, N.; Sakamoto, A.; Nagahashi, N.; Soejima, M.; Li, Y.; Imamura, T.; Kojima, N.; Ohishi, H.; Sakaguchi, K.; Iwata, C.; Tanaka, T., C-2-symmetric bis-sulfoxide: A novel chiral auxiliary for asymmetric desymmetrization of cyclic meso-1,2-diols. *Journal of Organic Chemistry* **2000,** *65* (11), 3284-3291.

8. Davies, S.; Loveridge, T.; Clough, J., Stereoselective methodology for 1-aryl-1-alkyl epoxides via chromium tricarbonyl complexes. *Synlett* **1997,** (1), 66-&.

9. Kahne, D.; Walker, S.; Cheng, Y.; Vanengen, D., Glycosylation Of Unreactive Substrates. *Journal of the American Chemical Society* **1989,** *111* (17), 6881-6882.

10. Sovová, M.; Sova, P., Pharmaceutical significance of Allium sativum L. 4. Antifungal effects. *Ceska Slov Farm* **2003,** *52* (2), 82-7.

11. Focke, M.; Feld, A.; Lichtenthaler, H., Allicin, A Naturally-Occurring Antibiotic From Garlic, Specifically Inhibits Acetyl-Coa Synthetase. *Febs Letters* **1990,** *261* (1), 106-108.

12. Agarwal, K., Therapeutic actions of garlic constituents. *Medicinal Research Reviews* **1996,** *16* (1), 111-124.

13. Yoshida, S.; Kasuga, S.; Hayashi, N.; Ushiroguchi, T.; Matsuura, H.; Nakagawa, S., Antifungal Activity Of Ajoene Derived From Garlic. *Applied and Environmental Microbiology* **1987,** *53* (3), 615-617.

14. Perez-Giraldo, C.; Cruz-Villalon, G.; Sanchez-Silos, R.; Martinez-Rubio, R.; Blanco, M.; Gomez-Garcia, A., In vitro activity of allicin against Staphylococcus epidermidis and influence of subinhibitory concentrations on biofilm formation. *Journal of Applied Microbiology* **2003,** *95* (4), 709-711.

15. Schmied, R.; Wang, G. X.; Korth, M., Intracellular Na^+ activity and positive inotropic effect of sulmazole in guinea pig ventricular myocardium. Comparison with a cardioactive steroid. *Circ Res* **1991,** *68* (2), 597-604.

16. Padmanabhan, S.; Lavin, R.; Durant, G., Asymmetric synthesis of a neuroprotective and orally active N-methyl-D-aspartate receptor ion-channel blocker, CNS 5788. *Tetrahedron-Asymmetry* **2000,** *11* (17), 3455-3457.

17. Märcker, C., Ueber einige schwefelhaltige Derivate des Toluols. *Justus Liebigs Annalen der Chemie* **1865,** *136*, 75-95.

18. Patek, M.; Drake, B.; Lebl, M., Solid-Phase Synthesis Of Small Organic-Molecules Based On Thiazolidine Scaffold. *Tetrahedron Letters* **1995,** *36* (13), 2227-2230.

19. Leonard, N. J.; Johnson, C. R., Periodate Oxidation of Sulfides to Sulfoxides. Scope of the Reaction. *The Journal of Organic Chemistry* **1962,** *27*, 282-284.

20. Sylvain, C.; Wagner, A.; Mioskowski, C., Ozone: A versatile reagent for solid phase synthesis. *Tetrahedron Letters* **1997,** *38* (6), 1043-1044.

21. Bonesi, S. M.; Manet, I.; Freccero, M.; Fagnoni, M.; Albini, A., Photosensitized oxidation of sulfides: discriminating between the singlet-oxygen mechanism and electron transfer involving superoxide anion or molecular oxygen. *Chemistry* **2006,** *12* (18), 4844-57.

22. Foote, C. S.; Peters, J. W., Chemistry of singlet oxygen. XIV. Reactive intermediate in sulfide photooxidation. *Journal of the American Chemical Society* **1971,** *93*, 3795 - 3796.

23. Liang, J.; Gu, C.; Kacher, M.; Foote, C., Chemistry Of Singlet Oxygen .45. Mechanism Of The Photo-Oxidation Of Sulfides. *Journal of the American Chemical Society* **1983,** *105* (14), 4717-4721.

24. Clennan, E., Persulfoxide: Key intermediate in reactions of singlet oxygen with sulfides. *Accounts of Chemical Research* **2001,** *34* (11), 875-884.

25. Fraile, J.; Garcia, J.; Lazaro, B.; Mayoral, J., A mild, efficient and selective oxidation of sulfides to sulfoxides. *Chemical Communications* **1998,** (17), 1807-1808.

26. Noyori, R.; Aoki, M.; Sato, K., Green oxidation with aqueous hydrogen peroxide. *Chemical Communications* **2003,** (16), 1977-1986.

27. Cope, A. C.; Morrison, D. E.; Field, L., Thermal Rearrangement of Allyl-type Sulfoxides, Sulfones and Sulfinates1. *Journal of the American Chemical Society* **1950,** *72*, 59 - 67.

28. Shriner, R. L.; Struck, H. C.; Jorison, W. J., The Preparation And Properties Of Certain Sulfoxides And Sulfones. *Journal of the American Chemical Society* **1930,** *52* (5), 2060 - 2069.

29. Drabowicz, J.; Mikolajczyk, M., An Improved Method For Oxidation Of Sulfides To Sulfoxides With Hydrogen-Peroxide In Methanol. *Synthetic Communications* **1981,** *11* (12), 1025-1030.

30. Bortolini, O.; Difuria, F.; Modena, G.; Seraglia, R., Metal Catalysis In Oxidation By Peroxides .21. Sulfide Oxidation And Olefin Epoxidation By Dilute Hydrogen-Peroxide Catalyzed By Molybdenum And Tungsten Derivatives Under Phase-Transfer Conditions. *Journal of Organic Chemistry* **1985,** *50* (15), 2688-2690.

31. Reddy, R.; Reddy, J.; Kumar, R.; Kumar, P., Sulfoxidation Of Thioethers Using Titanium Silicate Molecular-Sieve Catalysts. *Journal of the Chemical Society-Chemical Communications* **1992,** (2), 84-85.

32. Shaabani, A.; Bazgir, A.; Soleimani, K.; Salehi, P., Solvent effects in the oxidation of sulfides with $NaBrO_3/Mg(HSO_4)$. *Synthetic Communications* **2003,** *33* (17), 2935-2944.

33. Varma, R.; Saini, R.; Kumar, D., An expeditious synthesis of flavones on montmorillonite K 10 clay with microwaves. *Journal of Chemical Research-S* **1998,** (6), 348.

34. Schenck, G. O., and C. H. Krauch, Zur Photosensibilisierten O_2-Ubertragung Auf Schwefel-Verbindungen-Neuer Weg Zu Sulfoxyden. *Angewandte Chemie* **1962,** *74* (14), 510.

35. Gollnick, K., Type II photooxygenation reactions in solution. *Adv. Photochem* **1968,** *6* (1).

36. Zen, J.; Liou, S.; Kumar, A.; Hsia, M., An efficient and selective photocatalytic system for the oxidation of sulfides to sulfoxides. *Angewandte Chemie-International Edition* **2003,** *42* (5), 577.

37. Zeitler, K., Photoredox Catalysis with Visible Light. *Angewandte Chemie-International Edition* **2009,** *48* (52), 9785-9789.

38. Ravelli, D.; Dondi, D.; Fagnoni, M.; Albini, A., Photocatalysis. A multi-faceted concept for green chemistry. *Chemical Society Reviews* **2009,** *38* (7), 1999-2011.

39. Ischay, M.; Anzovino, M.; Du, J.; Yoon, T., Efficient visible light photocatalysis of [2+2] enone cycloadditions. *Journal of the American Chemical Society* **2008,** *130* (39), 12886.

40. Du, J.; Yoon, T., Crossed Intermolecular [2+2] Cycloadditions of Acyclic Enones via Visible Light Photocatalysis. *Journal of the American Chemical Society* **2009,** *131* (41), 14604.

41. Condie, A.; Gonzalez-Gomez, J.; Stephenson, C., Visible-Light Photoredox Catalysis: Aza-Henry Reactions via C-H Functionalization. *Journal of the American Chemical Society* **2010,** *132* (5), 1464.

42. Baciocchi, E.; Del Giacco, T.; Elisei, F.; Gerini, M.; Guerra, M.; Lapi, A.; Liberali, P., Electron transfer and singlet oxygen mechanisms in the photooxygenation of dibutyl sulfide and thioanisole in MeCN sensitized by N-methylquinolinium tetrafluoborate and 9,10-dicyanoanthracene. The probable involvement of a thiadioxirane intermediate in electron transfer photooxygenations. *Journal of the American Chemical Society* **2003,** *125* (52), 16444-16454.

43. Baciocchi, E.; Boschi, T.; Galli, C.; Lapi, A.; Tagliatesta, P., Epoxidation and hydroxylation reactions catalyzed by the manganese and iron complexes of 5,10,15,20-tetrakis(2,6-dimethoxyphenyl)porphyrin. *Tetrahedron* **1997,** *53* (12), 4497-4502.

44. Bonesi, S.; Fagnoni, M.; Albini, A., Photosensitized electron transfer oxidation of sulfides. A steady-state study. *European Journal of Organic Chemistry* **2008,** (15), 2612-2620.

45. Neumann, M.; Fuldner, S.; Konig, B.; Zeitler, K., Metal-Free, Cooperative Asymmetric Organophotoredox Catalysis with Visible Light. *Angewandte Chemie-International Edition* **2011,** *50* (4), 951-954.

46. Liu, H.; Feng, W.; Kee, C.; Zhao, Y.; Leow, D.; Pan, Y.; Tan, C., Organic dye photocatalyzed alpha-oxyamination through irradiation with visible light. *Green Chemistry* **2010,** *12* (6), 953-956.

47. Li, W.; Xie, Z.; Jing, X., BODIPY photocatalyzed oxidation of thioanisole under visible light. *Catalysis Communications* **2011,** *16* (1), 94-97.

48. Gorman, A.; Killoran, J.; O'Shea, C.; Kenna, T.; Gallagher, W.; O'Shea, D., In vitro demonstration of the heavy-atom effect for photodynamic therapy. *Journal of the American Chemical Society* **2004,** *126* (34), 10619-10631.

49. Atilgan, S.; Ekmekci, Z.; Dogan, A.; Guc, D.; Akkaya, E., Water soluble distyryl-boradiazaindacenes as efficient photosensitizers for photodynamic therapy. *Chemical Communications* **2006,** (42), 4398-4400.

50. Turan, I. S.; Yildiz, D.; Turksoy, A.; Gunaydin, G.; Akkaya, E. U., A Bifunctional Photosensitizer for Enhanced Fractional Photodynamic Therapy: Singlet Oxygen Generation in the Presence and Absence of Light. *Angewandte Chemie International Edition* **2016,** *55* (8), 2875-8.

51. Bozdemir, O.; Cakmak, Y.; Sozmen, F.; Ozdemir, T.; Siemiarczuk, A.; Akkaya, E., Synthesis of Symmetrical Multichromophoric Bodipy Dyes and Their Facile Transformation into Energy Transfer Cassettes. *Chemistry-a European Journal* **2010,** *16* (21), 6346-6351.

52. Rousseau, T.; Cravino, A.; Bura, T.; Ulrich, G.; Ziessel, R.; Roncali, J., BODIPY derivatives as donor materials for bulk heterojunction solar cells. *Chemical Communications* **2009,** (13), 1673-1675.

53. Kolemen, S.; Bozdemir, O.; Cakmak, Y.; Barin, G.; Erten-Ela, S.; Marszalek, M.; Yum, J.; Zakeeruddin, S.; Nazeeruddin, M.; Gratzel, M.; Akkaya, E., Optimization of distyryl-Bodipy chromophores for efficient panchromatic sensitization in dye sensitized solar cells. *Chemical Science* **2011,** *2* (5), 949-954.

54. Ozlem, S.; Akkaya, E., Thinking Outside the Silicon Box: Molecular AND Logic As an Additional Layer of Selectivity in Singlet Oxygen Generation for Photodynamic Therapy. *Journal of the American Chemical Society* **2009,** *131* (1), 48.

55. Wood, T.; Thompson, A., Advances in the chemistry of dipyrrins and their complexes. *Chemical Reviews* **2007,** *107* (5), 1831-1861.

56. Huang, L.; Zhao, J.; Guo, S.; Zhang, C.; Ma, J., Bodipy Derivatives as Organic Triplet Photosensitizers for Aerobic Photoorganocatalytic Oxidative Coupling of Amines and Photooxidation of Dihydroxylnaphthalenes. *Journal of Organic Chemistry* **2013,** *78* (11), 5627-5637.

57. Yang, P.; Zhao, J.; Wu, W.; Yu, X.; Liu, Y., Accessing the Long-Lived Triplet Excited States in Bodipy-Conjugated 2-(2-Hydroxyphenyl) Benzothiazole/Benzoxazoles and Applications as Organic Triplet Photosensitizers for Photooxidations. *Journal of Organic Chemistry* **2012,** *77* (14), 6166-6178.

58. Treibs, A.; ., K. F.-H., Difluorboryl-Komplexe von Di- und Tripyrrylmethenen. *Justus Liebigs Annalen der Chemie* **1968,** *718* (1), 208-223.

59. Jiao, L.; Yu, C.; Li, J.; Wang, Z.; Wu, M.; Hao, E., beta-Formyl-BODIPYs from the Vilsmeier-Haack Reaction. *Journal of Organic Chemistry* **2009,** *74* (19), 7525-7528.

60. Knoevenagel, E., Ueber eine Darstellungsweise der Glutarsäure. *Ber. Dtsch. Chem. Ges.* **1894,** *27* (2), 2346 - 2346.

61. Buyukcakir, O.; Bozdemir, O.; Kolemen, S.; Erbas, S.; Akkaya, E., Tetrastyryl-Bodipy Dyes: Convenient Synthesis and Characterization of Elusive Near IR Fluorophores. *Organic Letters* **2009,** *11* (20), 4644-4647.

62. Zhu, S.; Zhang, J.; Vegesna, G.; Tiwari, A.; Luo, F.; Zeller, M.; Luck, R.; Li, H.; Green, S.; Liu, H., Controlled Knoevenagel reactions of methyl groups of 1,3,5,7-tetramethyl BODIPY dyes for unique BODIPY dyes. *Rsc Advances* **2012,** *2* (2), 404-407.

63. Lawrentz, U.; Grahn, W.; Lukasznk, K.; Klein, C.; Wortmann, R.; Feldner, A.; Scherer, D., Donor-acceptor oligoenes with a locked all-trans conformation: Synthesis and linear and nonlinear optical properties. *Chemistry-a European Journal* **2002,** *8* (7), 1573-1590.

64. Wang, L.; Cao, J.; Wang, J.; Chen, Q.; Cui, A.; He, M., Facile synthesis of dimeric BODIPY and its catalytic activity for sulfide oxidation under visible light. *Rsc Advances* **2014,** *4* (28), 14786-14790.

65. Zhou, Y.; Zhou, Z.; Li, Y.; Yang, W., Synthesis and properties of BODIPY polymers and their photocatalytic performance for aerobic oxidation of benzylamine. *Catalysis Communications* **2015,** *64*, 96-100.

66. Wang, X.; Yu, S.; Wang, C.; Xue, D.; Xiao, J., BODIPY catalyzed amide synthesis promoted by BHT and air under visible light. *Organic & Biomolecular Chemistry* **2016,** *14* (29), 7028-7037.

67. Wang, X.; Meng, Q.; Zhong, J.; Gao, X.; Lei, T.; Zhao, L.; Li, Z.; Chen, B.; Tung, C.; Wu, L., The singlet excited state of BODIPY promoted aerobic cross-dehydrogenative-coupling reactions under visible light. *Chemical Communications* **2015,** *51* (56), 11256-11259.

68. Huang, L.; Zhao, J., Iodo-Bodipys as visible-light-absorbing dual-functional photoredox catalysts for preparation of highly functionalized organic compounds by formation of C-C bonds via reductive and oxidative quenching catalytic mechanisms. *Rsc Advances* **2013,** *3* (45), 23377-23388.

69. Moan, J.; Berg, K., The Photodegradation Of Porphyrins In Cells Can Be Used To Estimate The Lifetime Of Singlet Oxygen. *Photochemistry and Photobiology* **1991,** *53* (4), 549-553.

70. Ogilby, P., Singlet oxygen: there is still something new under the sun, and it is better than ever. *Photochemical & Photobiological Sciences* **2010,** *9* (12), 1543-1560.

71. Dai, T.; Fuchs, B.; Coleman, J.; Prates, R.; Astrakas, C.; St Denis, T.; Ribeiro, M.; Mylonakis, E.; Hamblin, M.; Tegos, G., Concepts and principles of photodynamic therapy as an alternative antifungal discovery platform. *Frontiers in Microbiology* **2012,** *3*.

72. Nakano, M.; Kambayashi, Y.; Tatsuzawa, H.; Komiyama, T.; Fujimori, K., Useful $^1O_2$ $^1\Delta_g$ generator, 3-(4'-methyl-1'-naphthyl)-propionic acid, 1',4'-endoperoxide (NEPO), for dioxygenation of squalene (a skin surface lipid) in an organic solvent and bacterial killing in aqueous medium. *Febs Letters* **1998,** *432* (1-2), 9-12.

73. Nakano, M.; Kambayashi, Y.; Tatsuzawa, H., 3-(4'-methyl-1'-naphthyl)propionic acid, 1',4'-endoperoxide for dioxygenation of squalene and for bacterial killing. *Singlet Oxygen, Uv-A, and Ozone* **2000,** *319*, 216-222.

74. Pellieux, C.; Dewilde, A.; Pierlot, C.; Aubry, J., Bactericidal and virucidal activities of singlet oxygen generated by thermolysis of naphthalene endoperoxides. *Singlet Oxygen, Uv-A, and Ozone* **2000,** *319*, 197-207.

75. Moureu, C.; Dufraisse, C.; Dean, P.M. Sur un Hydrocarbure Solore: Le Rubrene. Comptes Rendus de l'Academie des Sciences **1926,** *182*, 1584.

76. Wasserman, H. H. S., John R., Singlet oxygen reactions from photoperoxides. **1967,** *89*, 3073-3075.

77. Matsumoto, M.; Yamada, M.; Watanabe, N., Reversible 1,4-cyclo addition of singlet oxygen to N-substituted 2-pyridones: 1,4-endoperoxide as a versatile chemical source of singlet oxygen. *Chemical Communications* **2005,** (4), 483-485.

78. Benz, S.; Notzli, S.; Siegel, J.; Eberli, D.; Jessen, H., Controlled Oxygen Release from Pyridone Endoperoxides Promotes Cell Survival under Anoxic Conditions. *Journal of Medicinal Chemistry* **2013,** *56* (24), 10171-10182.

79. Changtong, C.; Carney, D.; Luo, L.; Zoto, C.; Lombardi, J.; Connors, R., A porphyrin molecule that generates, traps, stores, and releases singlet oxygen. *Journal of Photochemistry and Photobiology A-Chemistry* **2013,** *260*, 9-13.

80. Pissuwan, D.; Valenzuela, S.; Cortie, M.; Harding, S.; Tombs, M., Prospects for Gold Nanorod Particles in Diagnostic and Therapeutic Applications. *Biotechnology and Genetic Engineering Reviews, Vol 25* **2008,** *25*, 93-112.

81. Jang, B.; Park, J.; Tung, C.; Kim, I.; Choi, Y., Gold Nanorod-Photosensitizer Complex for Near-Infrared Fluorescence Imaging and Photodynamic/Photothermal Therapy In Vivo. *Acs Nano* **2011,** *5* (2), 1086-1094.

82. Liu, J.; Wang, H.; Yan, X., A gold nanorod based colorimetric probe for the rapid and selective detection of Cu^{2+} ions. *Analyst* **2011,** *136* (19), 3904-3910.

83. Chu, Z.; Yin, C.; Zhang, S.; Lin, G.; Li, Q., Surface plasmon enhanced drug efficacy using core-shell Au@SiO2 nanoparticle carrier. *Nanoscale* **2013,** *5* (8), 3406-3411.

84. Hone, D.; Walker, P.; Evans-Gowing, R.; FitzGerald, S.; Beeby, A.; Chambrier, I.; Cook, M.; Russell, D., Generation of cytotoxic singlet oxygen via phthalocyanine-stabilized gold nanoparticles: A potential delivery vehicle for photodynamic therapy. *Langmuir* **2002,** *18* (8), 2985-2987.

85. Wang, B.; Wang, J.; Liu, Q.; Huang, H.; Chen, M.; Li, K.; Li, C.; Yu, X.; Chu, P., Rose-bengal-conjugated gold nanorods for in vivo photodynamic and photothermal oral cancer therapies. *Biomaterials* **2014,** *35* (6), 1954-1966.

86. Kolemen, S.; Ozdemir, T.; Lee, D.; Kim, G.; Karatas, T.; Yoon, J.; Akkaya, E., Remote-Controlled Release of Singlet Oxygen by the Plasmonic Heating of Endoperoxide-Modified Gold Nanorods: Towards a Paradigm Change in Photodynamic Therapy. *Angewandte Chemie-International Edition* **2016,** *55* (11), 3606-3610.

87. Erbas, S.; Gorgulu, A.; Kocakusakogullari, M.; Akkaya, E., Non-covalent functionalized SWNTs as delivery agents for novel Bodipy-based potential PDT sensitizers. *Chemical Communications* **2009,** (33), 4956-4958.

88. Wojtoniszak, M.; Roginska, D.; Machalinski, B.; Drozdzik, M.; Mijowska, E., Graphene oxide functionalized with methylene blue and its performance in singlet oxygen generation. *Materials Research Bulletin* **2013,** *48* (7), 2636-2639.

89. Wang, Y.; Wang, H.; Liu, D.; Song, S.; Wang, X.; Zhang, H., Graphene oxide covalently grafted upconversion nanoparticles for combined NIR mediated imaging

and photothermal/photodynamic cancer therapy. *Biomaterials* **2013,** *34* (31), 7715-7724.

90. Li, F.; Park, S.; Ling, D.; Park, W.; Han, J.; Na, K.; Char, K., Hyaluronic acid-conjugated graphene oxide/photosensitizer nanohybrids for cancer targeted photodynamic therapy. *Journal of Materials Chemistry B* **2013,** *1* (12), 1678-1686.

91. Bulte, J.; Kraitchman, D., Iron oxide MR contrast agents for molecular and cellular imaging. *Nmr in Biomedicine* **2004,** *17* (7), 484-499.

92. Weissleder, R.; Elizondo, G.; Wittenberg, J.; Rabito, C.; Bengele, H.; Josephson, L., Ultrasmall Superparamagnetic Iron-Oxide - Characterization Of A New Class Of Contrast Agents For Mr Imaging. *Radiology* **1990,** *175* (2), 489-493.

93. Gupta, A.; Gupta, M., Synthesis and surface engineering of iron oxide nanoparticles for biomedical applications. *Biomaterials* **2005,** *26* (18), 3995-4021.

94. Reiss, G.; Hutten, A., Magnetic nanoparticles - Applications beyond data storage. *Nature Materials* **2005,** *4* (10), 725-726.

95. Wu, W.; He, Q.; Jiang, C., Magnetic Iron Oxide Nanoparticles: Synthesis and Surface Functionalization Strategies. *Nanoscale Research Letters* **2008,** *3* (11), 397-415.

96. Yen, S.; Varma, D.; Guo, W.; Ho, V.; Vijayaragavan, V.; Padmanabhan, P.; Bhakoo, K.; Selvan, S., Synthesis of Small-Sized, Porous, and Low-Toxic Magnetite Nanoparticles by Thin POSS Silica Coating. *Chemistry-a European Journal* **2015,** *21* (10), 3914-3918.

97. Wan, S.; Huang, J.; Guo, M.; Zhang, H.; Cao, Y.; Yan, H.; Liu, K., Biocompatible superparamagnetic iron oxide nanoparticle dispersions stabilized with poly(ethylene glycol)oligo(aspartic acid) hybrids. *Journal of Biomedical Materials Research Part a* **2007,** *80A* (4), 946-954.

98. Gole, A.; Agarwal, N.; Nagaria, P.; Wyatt, M.; Murphy, C., One-pot synthesis of silica-coated magnetic plasmonic tracer nanoparticles. *Chemical Communications* **2008,** (46), 6140-6142.

99. Wang, F.; Chen, X.; Zhao, Z.; Tang, S.; Huang, X.; Lin, C.; Cai, C.; Zheng, N., Synthesis of magnetic, fluorescent and mesoporous core-shell-structured nanoparticles

for imaging, targeting and photodynamic therapy. *Journal of Materials Chemistry* **2011,** *21* (30), 11244-11252.

100. Tada, D.; Vono, L.; Duarte, E.; Itri, R.; Kiyohara, P.; Baptista, M.; Rossi, L., Methylene blue-containing silica-coated magnetic particles: A potential magnetic carrier for photodynamic therapy. *Langmuir* **2007,** *23* (15), 8194-8199.

101. Parham, H.; Zargar, B.; Heidari, Z.; Hatamie, A., Magnetic Solid-Phase Extraction of Rose Bengal Using Iron Oxide Nanoparticles Modified with Cetyltrimethylammonium Bromide. *Journal of the Iranian Chemical Society* **2011,** *8*, S9-S16.

102. Gu, H.; Xu, K.; Yang, Z.; Chang, C.; Xu, B., Synthesis and cellular uptake of porphyrin decorated iron oxide nanoparticles - a potential candidate for bimodal anticancer therapy. *Chemical Communications* **2005,** (34), 4270-4272.

103. Stuchinskaya, T.; Moreno, M.; Cook, M. J.; Edwards, D. R.; Russell, D. A., Targeted photodynamic therapy of breast cancer cells using antibody-phthalocyanine-gold nanoparticle conjugates. *Photochemical & Photobiological Sciences* **2011,** *10* (5), 822-831.

104. Rihter, B.; Kenney, M.; Ford, W.; Rodgers, M., Photochromic Reactions Involving Palladium(II) Octabutoxynaphthalocyanine And Molecular-Oxygen. *Journal of the American Chemical Society* **1993,** *115* (18), 8146-8152.

105. Filatov, M.; Heinrich, E.; Busko, D.; Ilieva, I.; Landfester, K.; Baluschev, S., Reversible oxygen addition on a triplet sensitizer molecule: protection from excited state depopulation. *Physical Chemistry Chemical Physics* **2015,** *17* (9), 6501-6510.

106. Filatov, M.; Baluschev, S.; Ilieva, I.; Enkelmann, V.; Miteva, T.; Landfester, K.; Aeshchenkov, S.; Cheprakov, A., Tetraaryltetraanthra[2,3]porphyrins: Synthesis, Structure, and Optical Properties. *Journal of Organic Chemistry* **2012,** *77* (24), 11119-11131.

107. O' Dalaigh, C.; Corr, S.; Gun'ko, Y.; Connon, S., A magnetic-nanoparticle-supported 4-N,N-dialkylaminopyridine catalyst: Excellent reactivity combined with facile catalyst recovery and recyclability. *Angewandte Chemie-International Edition* **2007,** *46* (23), 4329-4332.

108. Gill, C.; Price, B.; Jones, C., Sulfonic acid-functionalized silica-coated magnetic nanoparticle catalysts. *Journal of Catalysis* **2007,** *251* (1), 145-152.

109. Ghorbani-Choghamarani, A.; Ghasemi, B.; Safari, Z.; Azadi, G., Schiff base complex coated Fe3O4 nanoparticles: A highly reusable nanocatalyst for the selective oxidation of sulfides and oxidative coupling of thiols. *Catalysis Communications* **2015,** *60*, 70-75.

110. Hajjami, M.; Kolivand, S., New metal complexes supported on Fe3O4 magnetic nanoparticles as recoverable catalysts for selective oxidation of sulfides to sulfoxides. *Applied Organometallic Chemistry* **2016,** *30* (5), 282-288.

111. Jacinto, M.; Kiyohara, P.; Masunaga, S.; Jardim, R.; Rossi, L., Recoverable rhodium nanoparticles: Synthesis, characterization and catalytic performance in hydrogenation reactions. *Applied Catalysis a-General* **2008,** *338* (1-2), 52-57.

112. Ghotbinejad, M.; Khosropour, A.; Mohammadpoor-Baltork, I.; Moghadam, M.; Tangestaninejad, S.; Mirkhani, V., SPIONs-bis(NHC)-palladium(II): A novel, powerful and efficient catalyst for Mizoroki-Heck and Suzuki-Miyaura C-C coupling reactions. *Journal of Molecular Catalysis a-Chemical* **2014,** *385*, 78-84.

113. Stevens, P.; Li, G.; Fan, J.; Yen, M.; Gao, Y., Recycling of homogeneous Pd catalysts using superparamagnetic nanoparticles as novel soluble supports for Suzuki, Heck, and Sonogashira cross-coupling reactions. *Chemical Communications* **2005,** (35), 4435-4437.

114. Wang, D.; Deraedt, C.; Ruiz, J.; Astruc, D., Magnetic and Dendritic Catalysts. *Accounts of Chemical Research* **2015,** *48* (7), 1871-1880.

Appendix

NMR, HRMS Spectra and Zeta Size Analysis

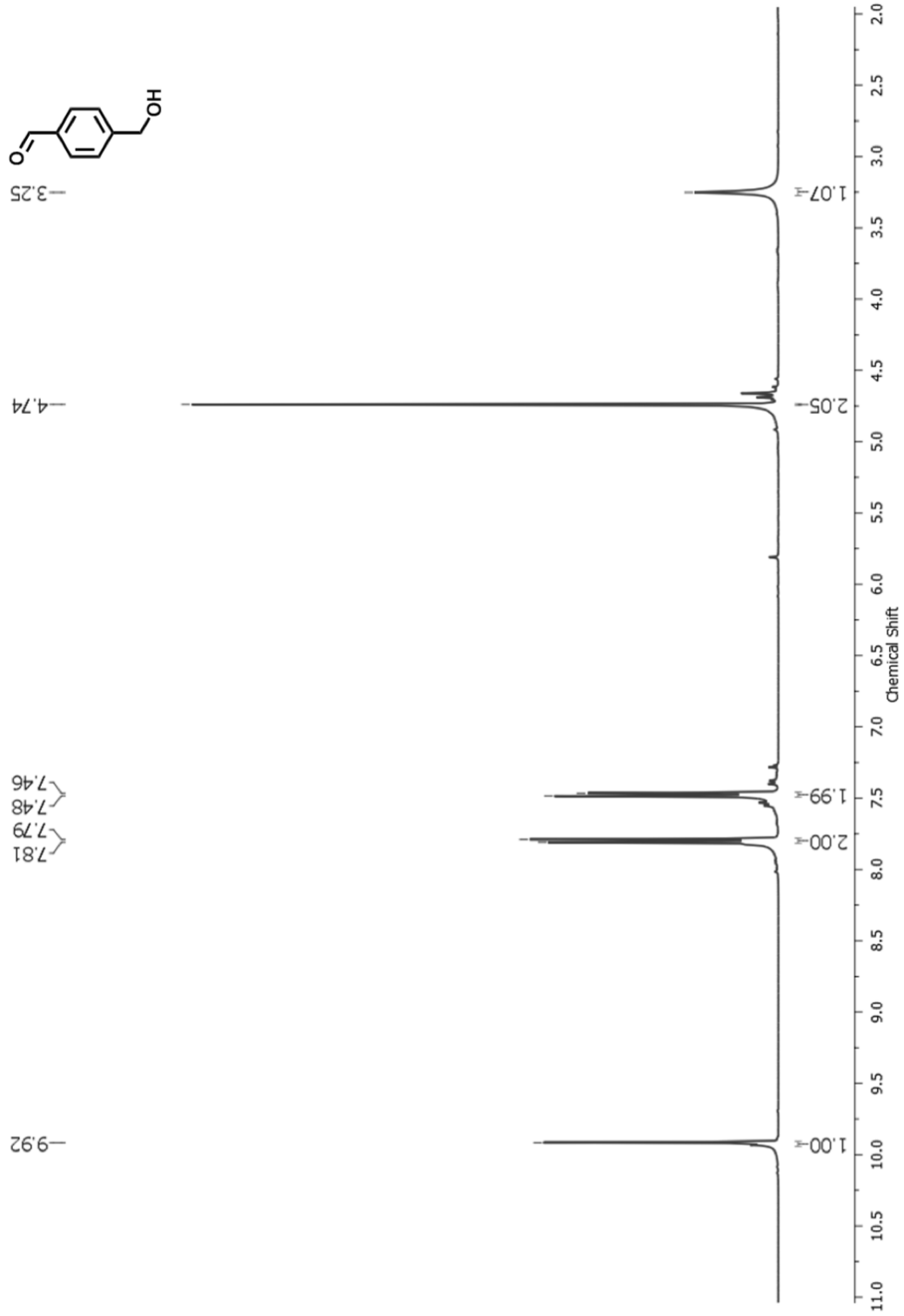

Figure 35: ^{1}H NMR of compound **2** in $CDCl_3$.

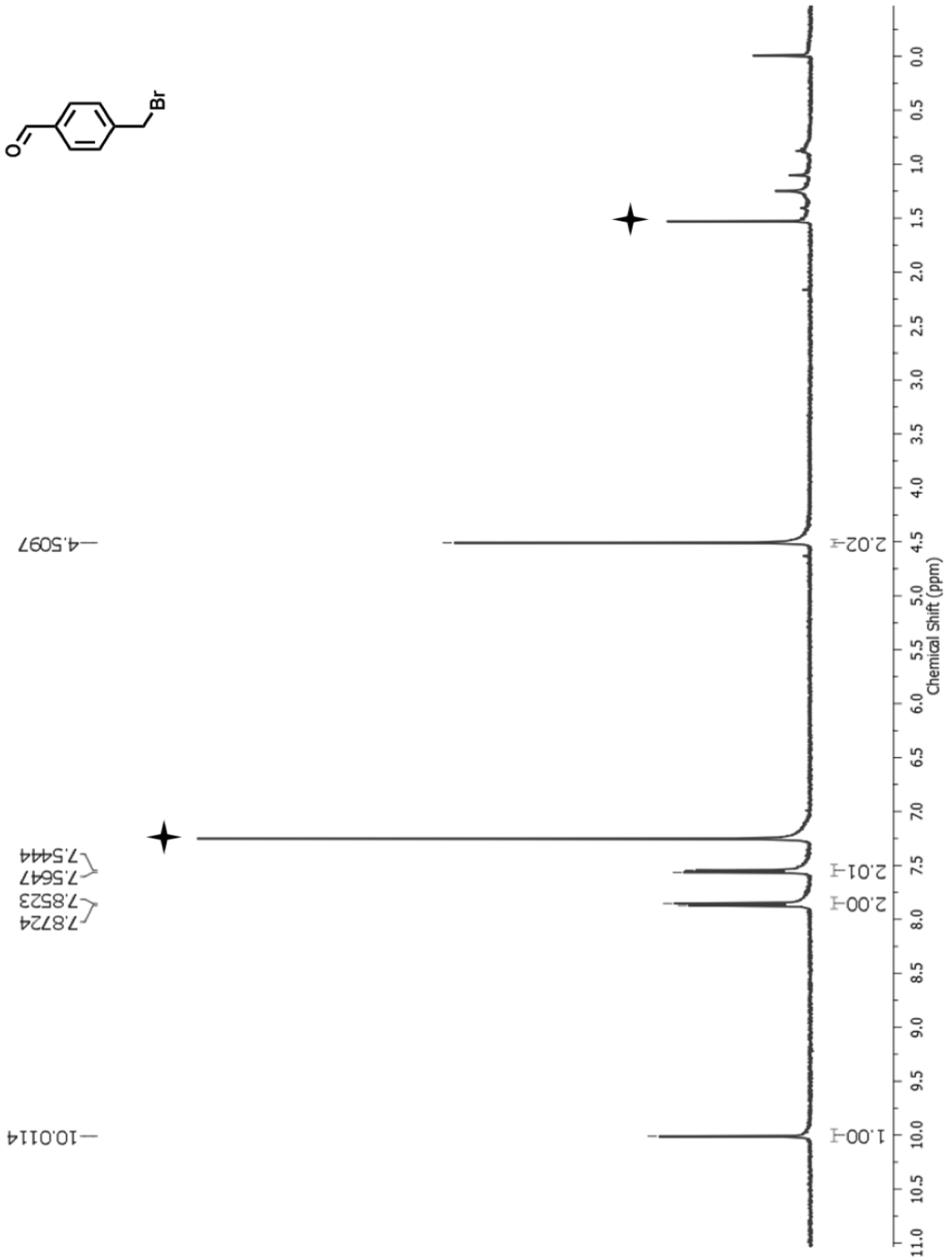

Figure 36: ^{1}H NMR of compound **3** in $CDCl_3$.

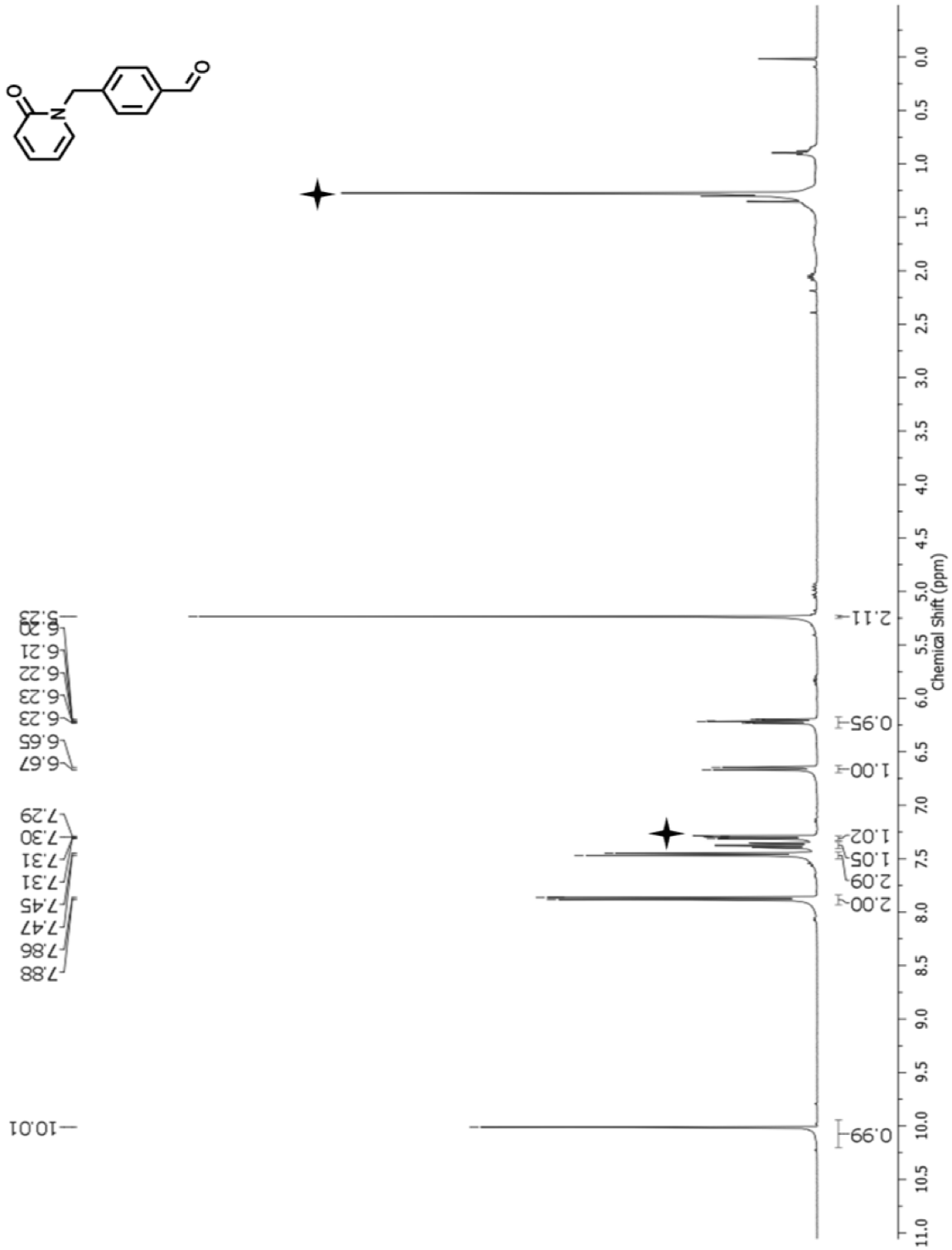

Figure 37: ^{1}H NMR of compound **4** in $CDCl_3$.

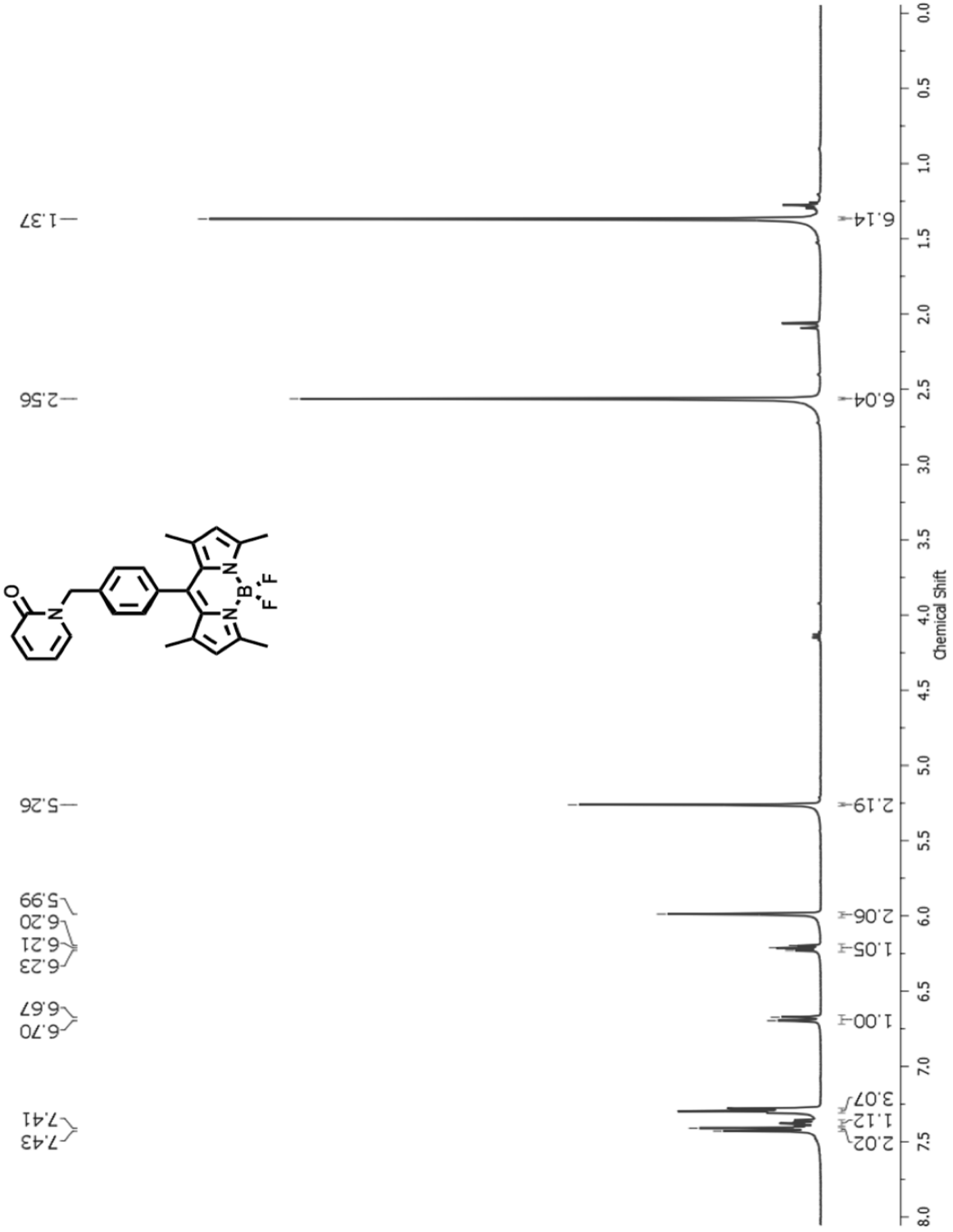

Figure 38: ^{1}H NMR of compound **5** in $CDCl_3$.

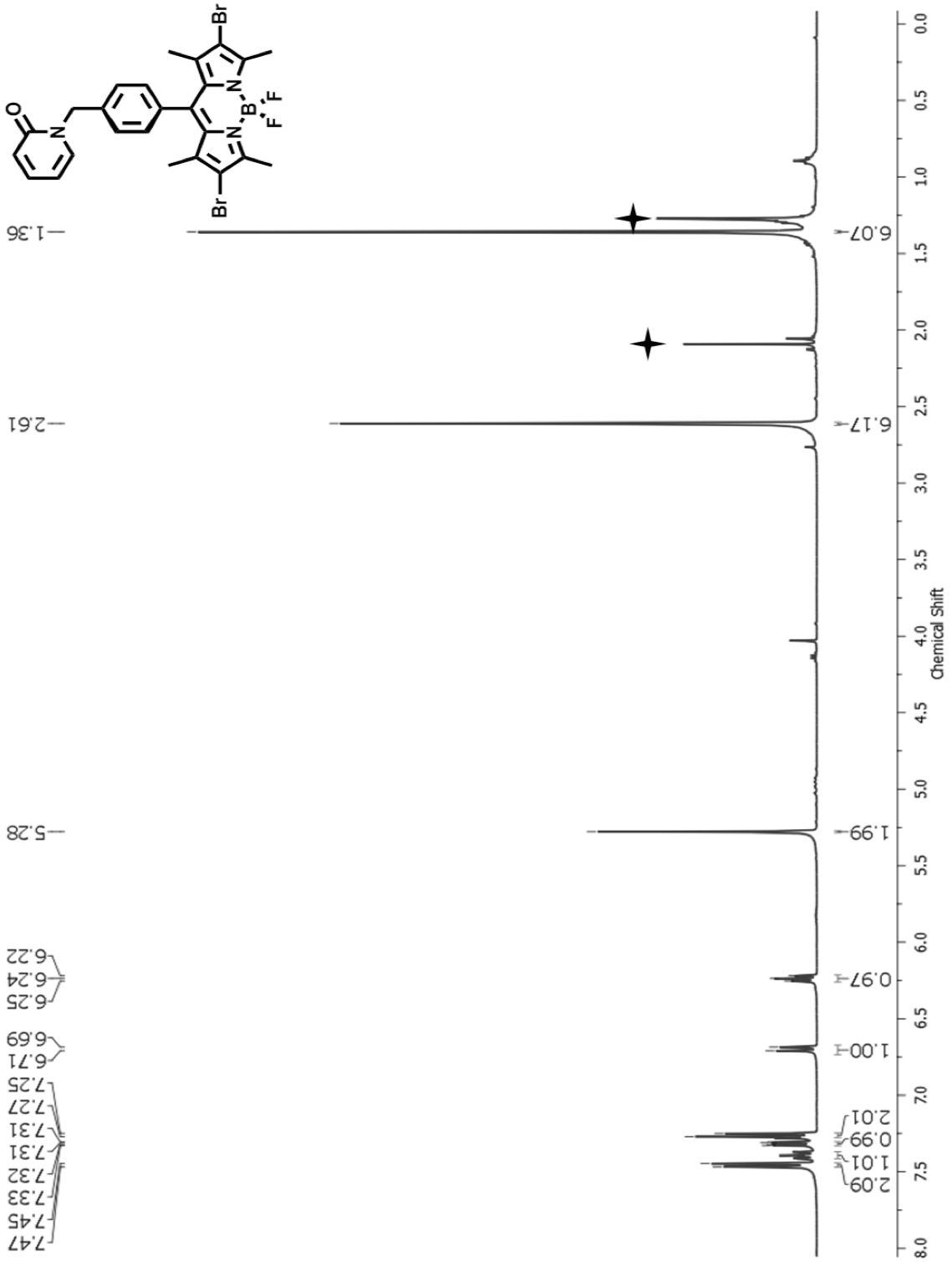

Figure 39: ^{1}H NMR of compound **6** in $CDCl_3$.

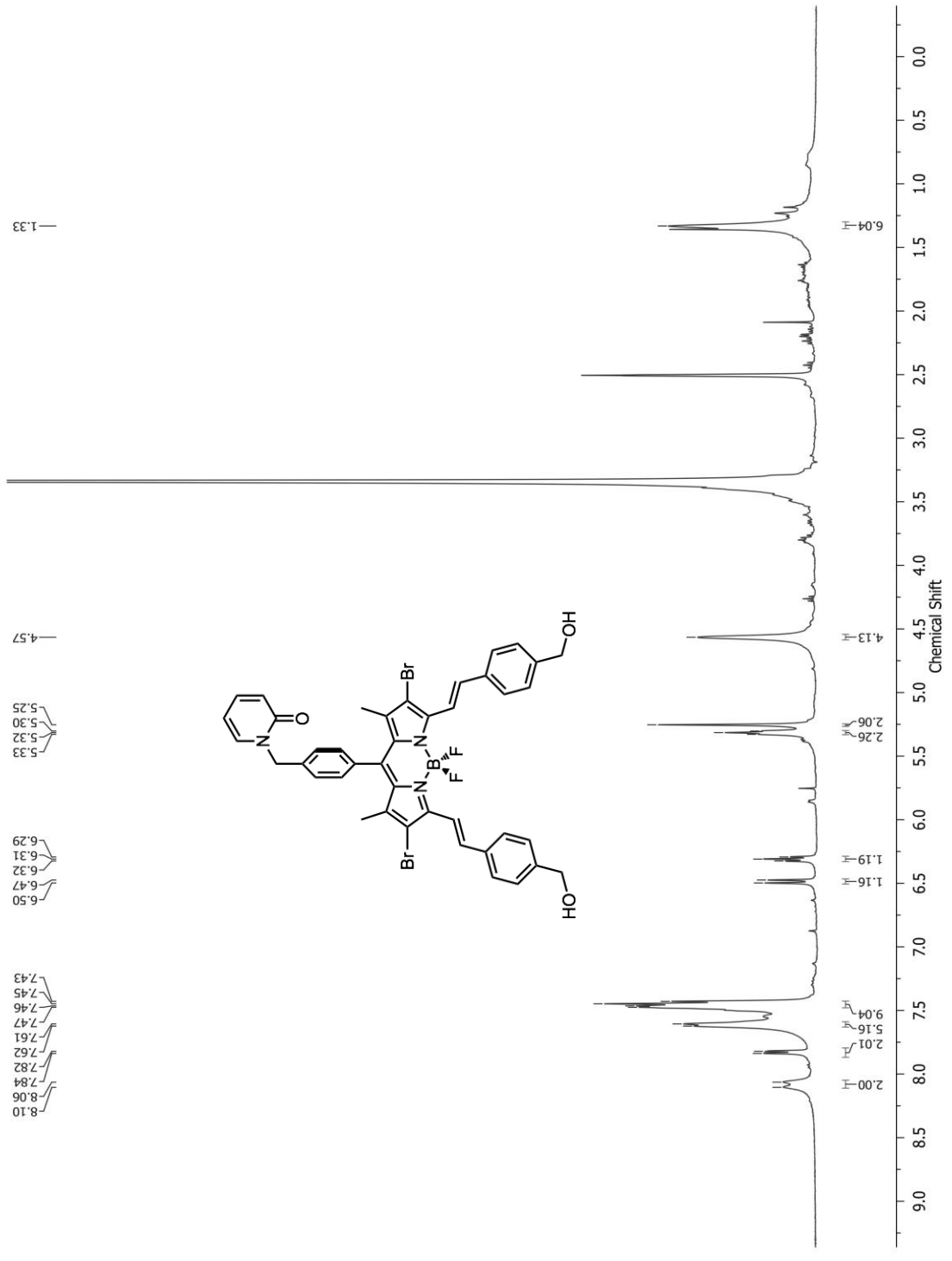

Figure 40: ^{1}H NMR of compound **7** in DMSO-d_6.

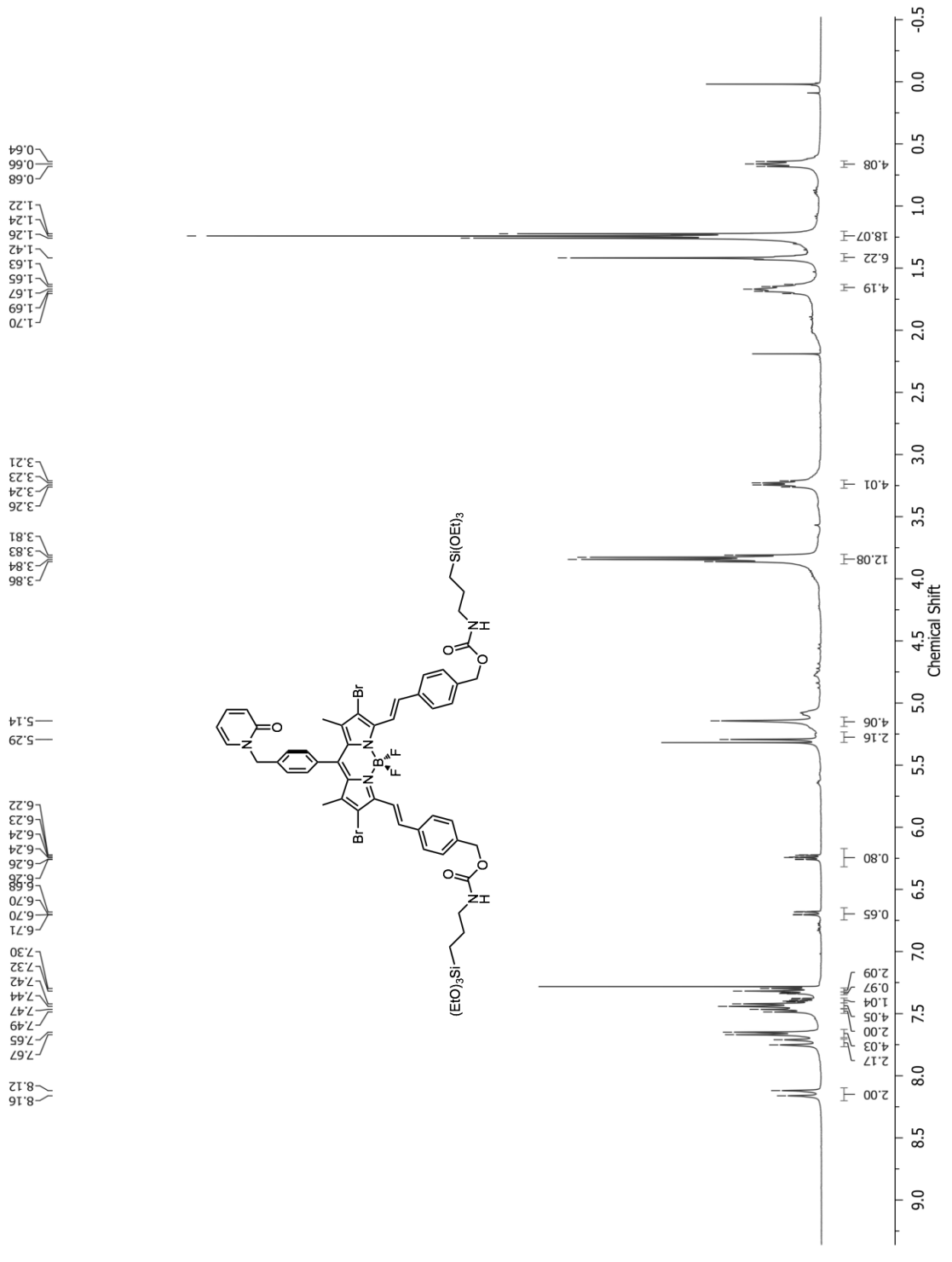

Figure 41: ^{1}H NMR of compound **8** in $CDCl_3$.

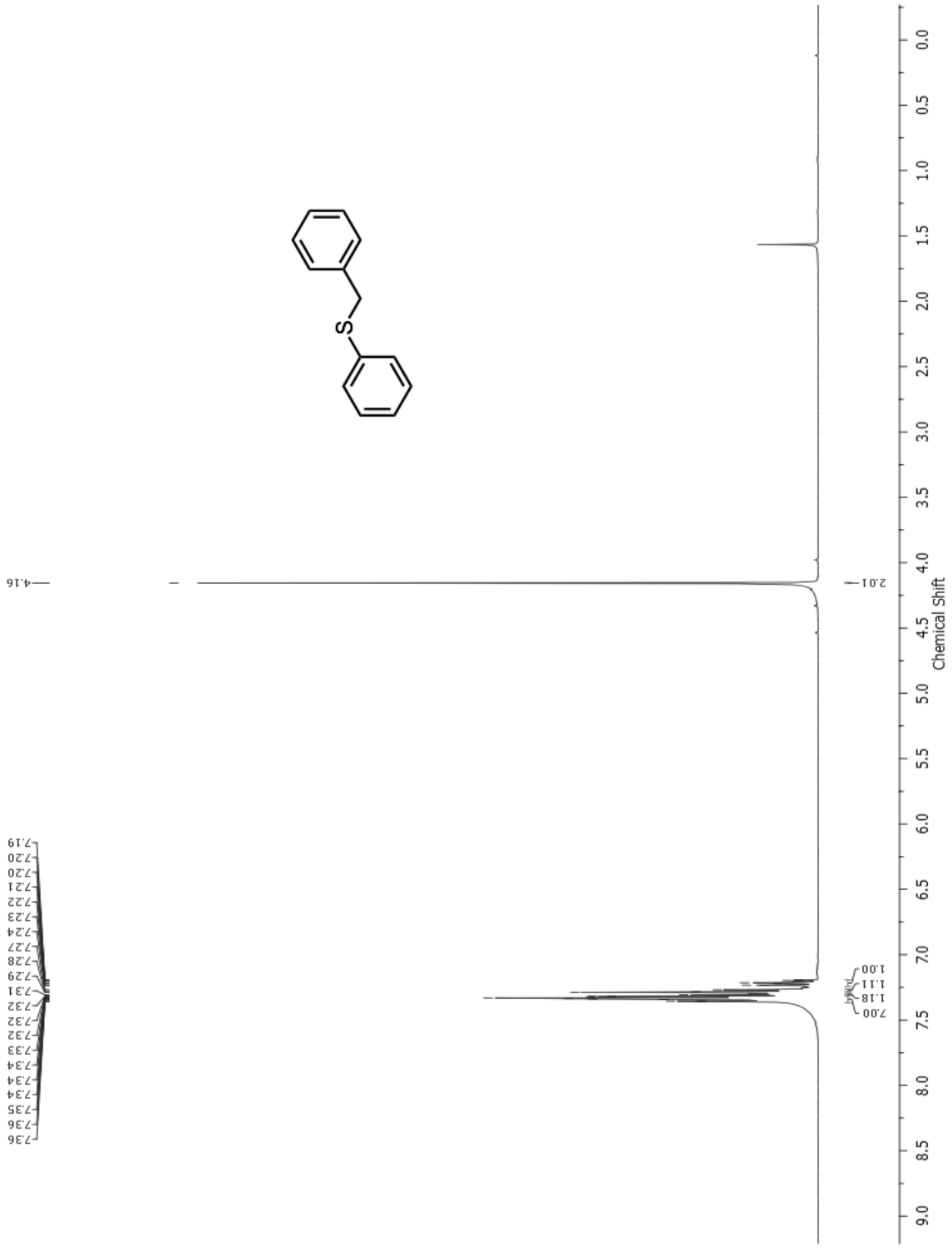

Figure 42: ^{1}H NMR of compound **12** in $CDCl_3$.

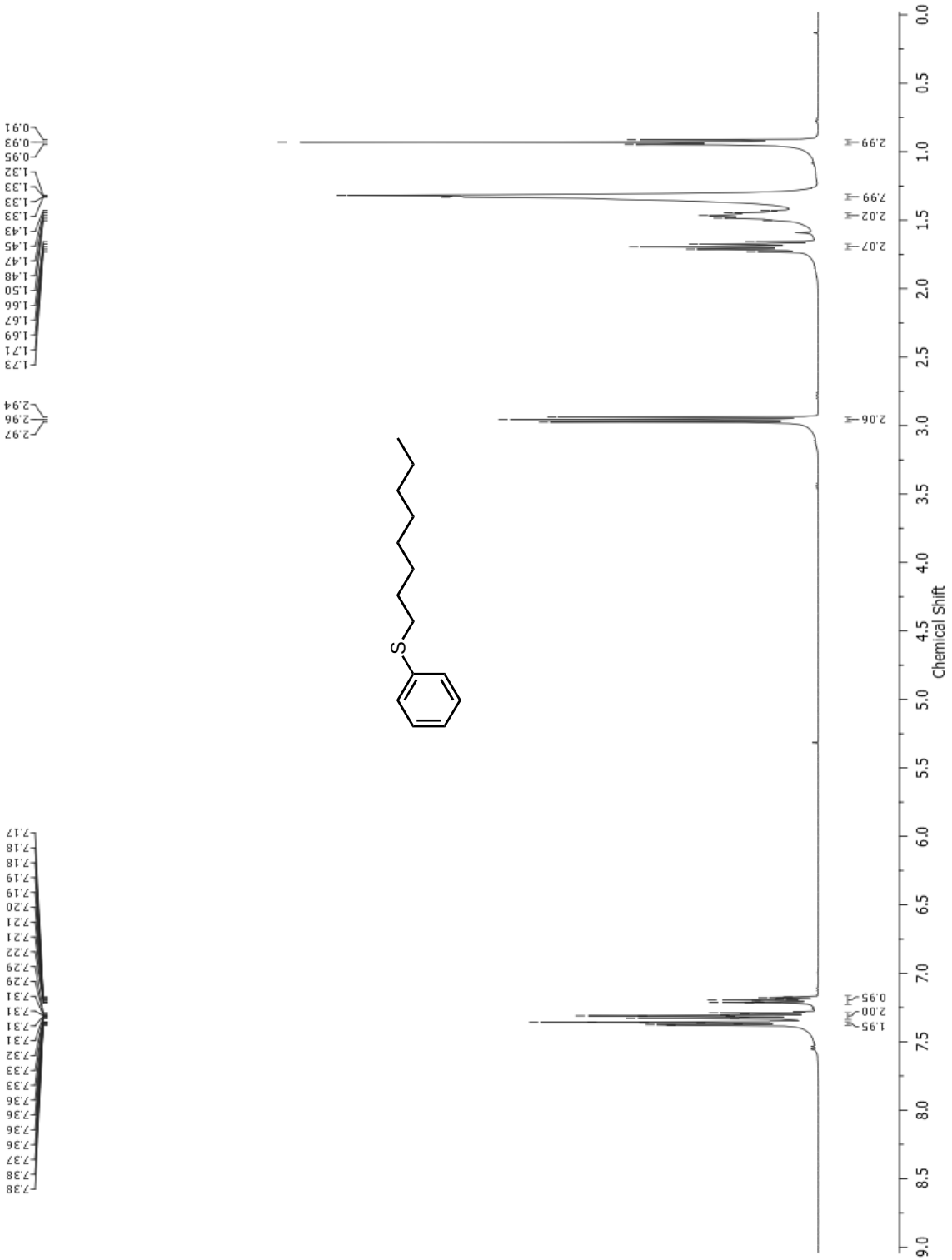

Figure 43: ^{1}H NMR of compound **13** in $CDCl_3$.

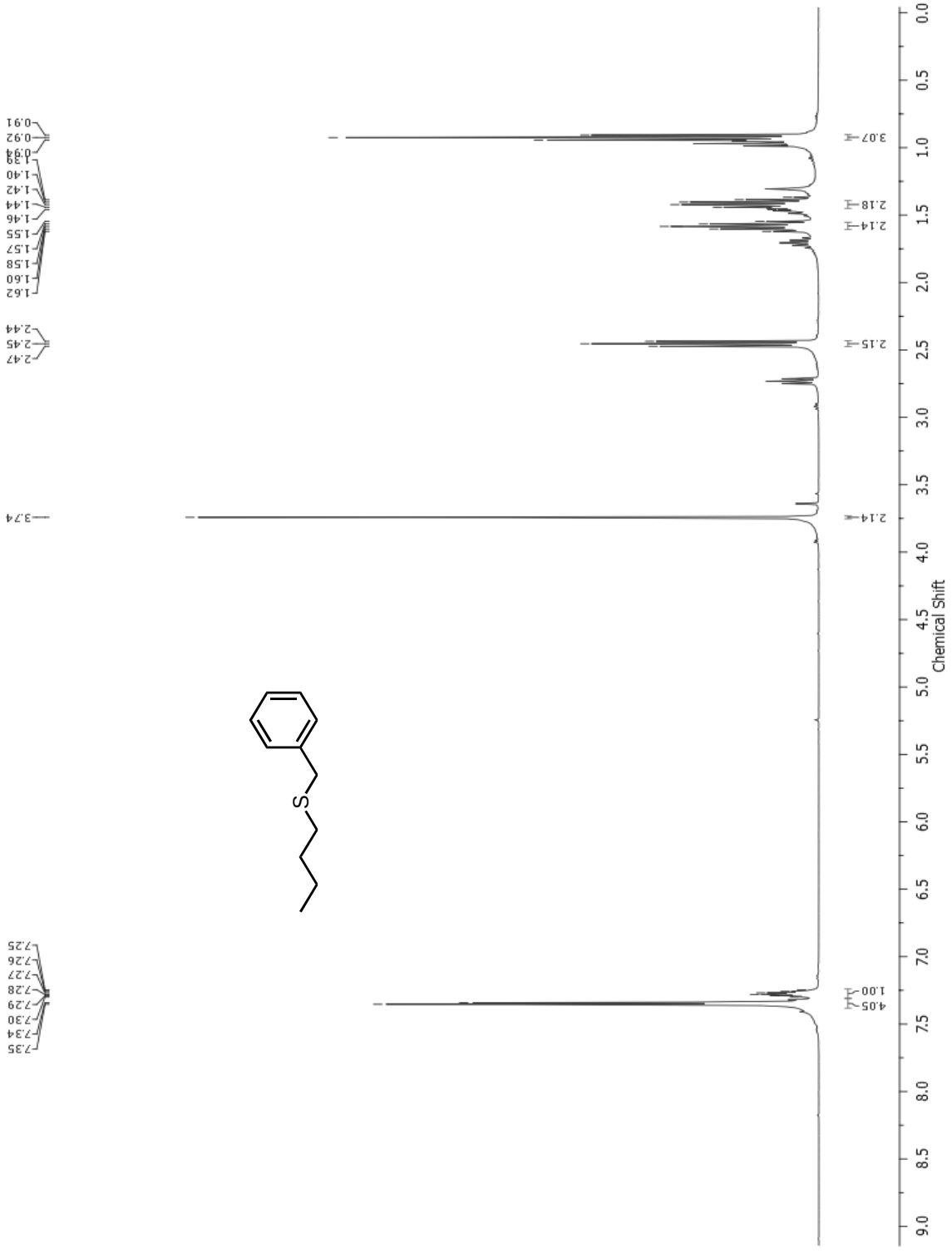

Figure 44: ^{1}H NMR of compound **14** in $CDCl_3$.

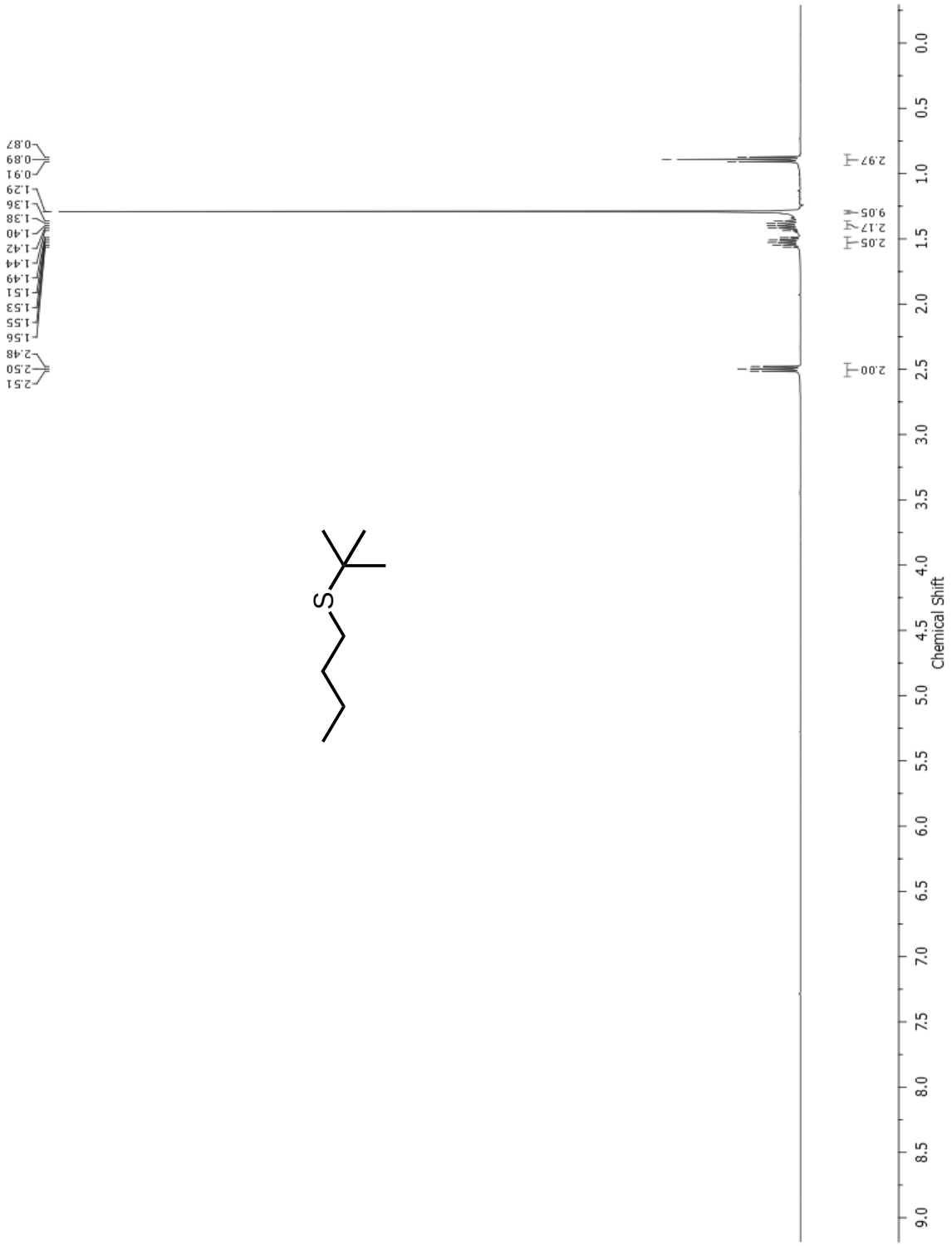

Figure 45: ^{1}H NMR of compound **15** in $CDCl_3$.

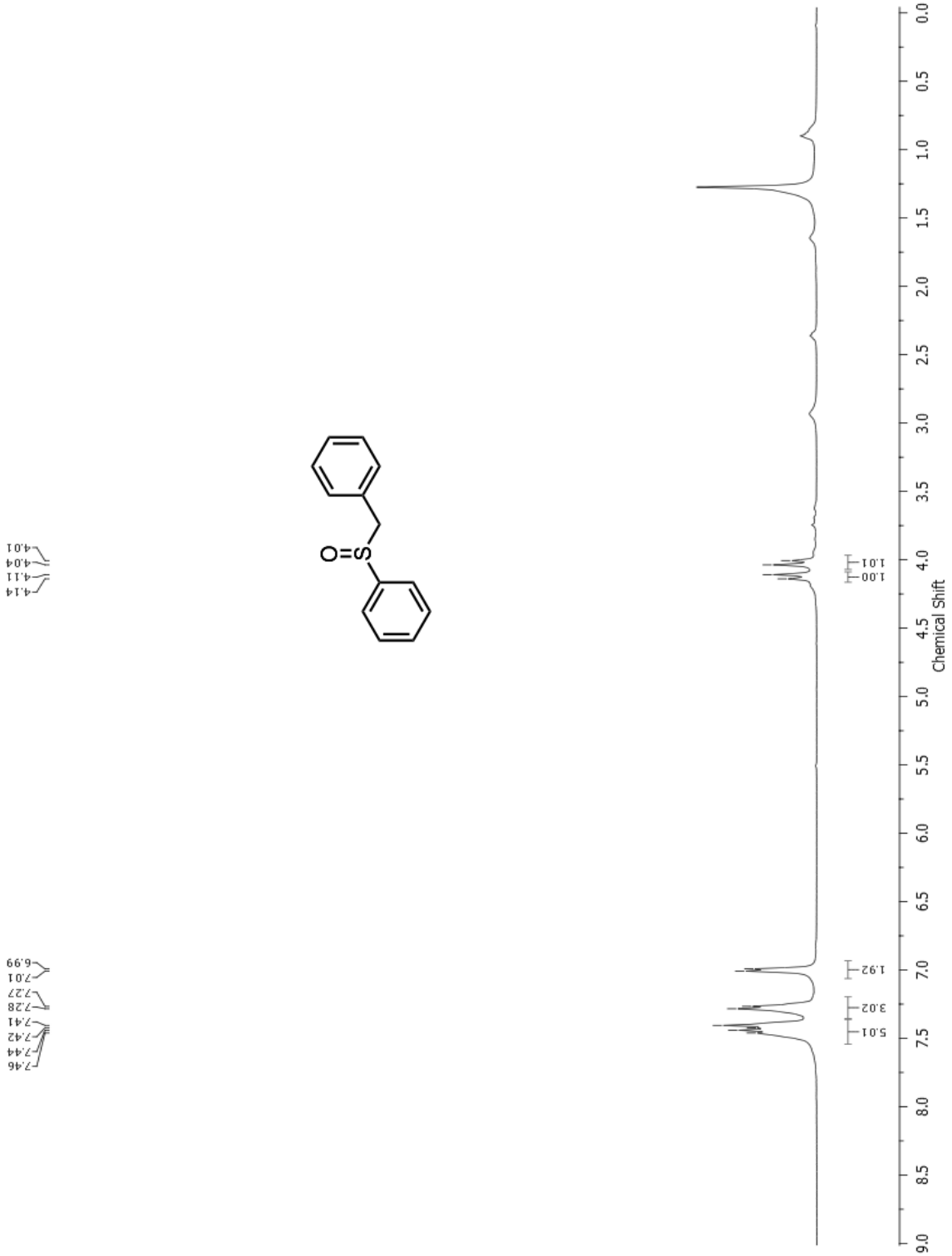

Figure 46: ^{1}H NMR of compound **12a** in $CDCl_3$.

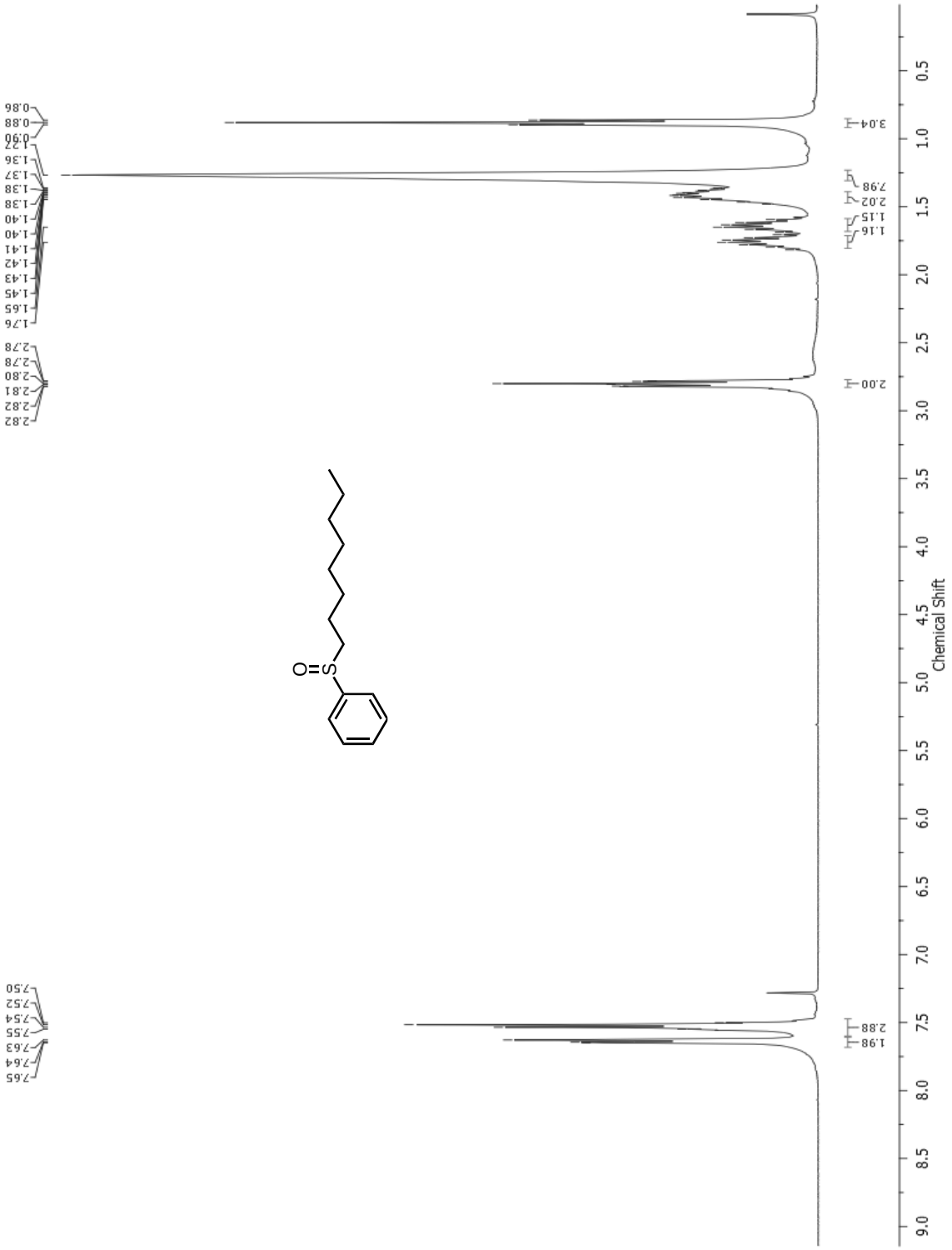

Figure 47: ^{1}H NMR of compound **13a** in $CDCl_3$.

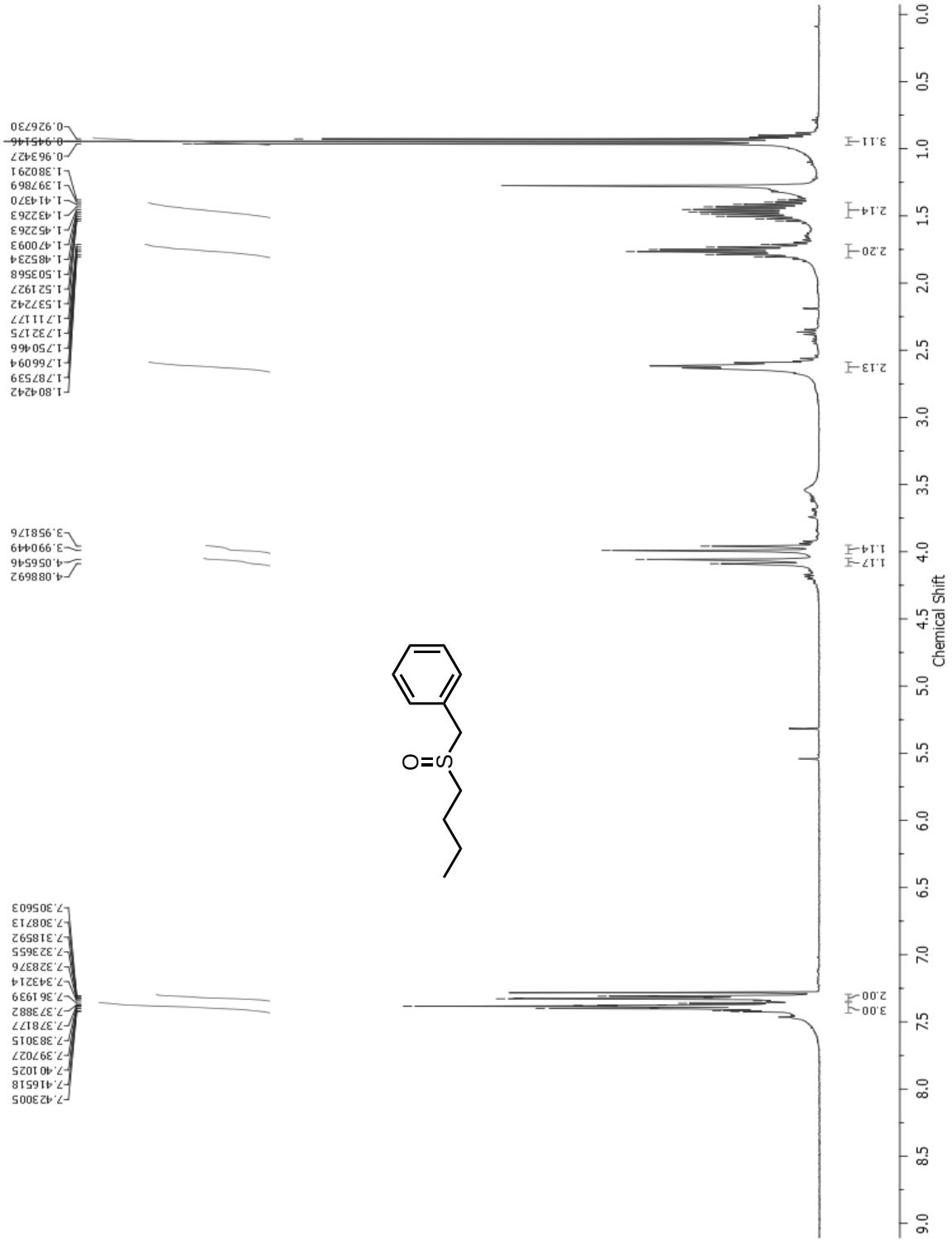

Figure 48: ^{1}H NMR of compound **14a** in $CDCl_3$.

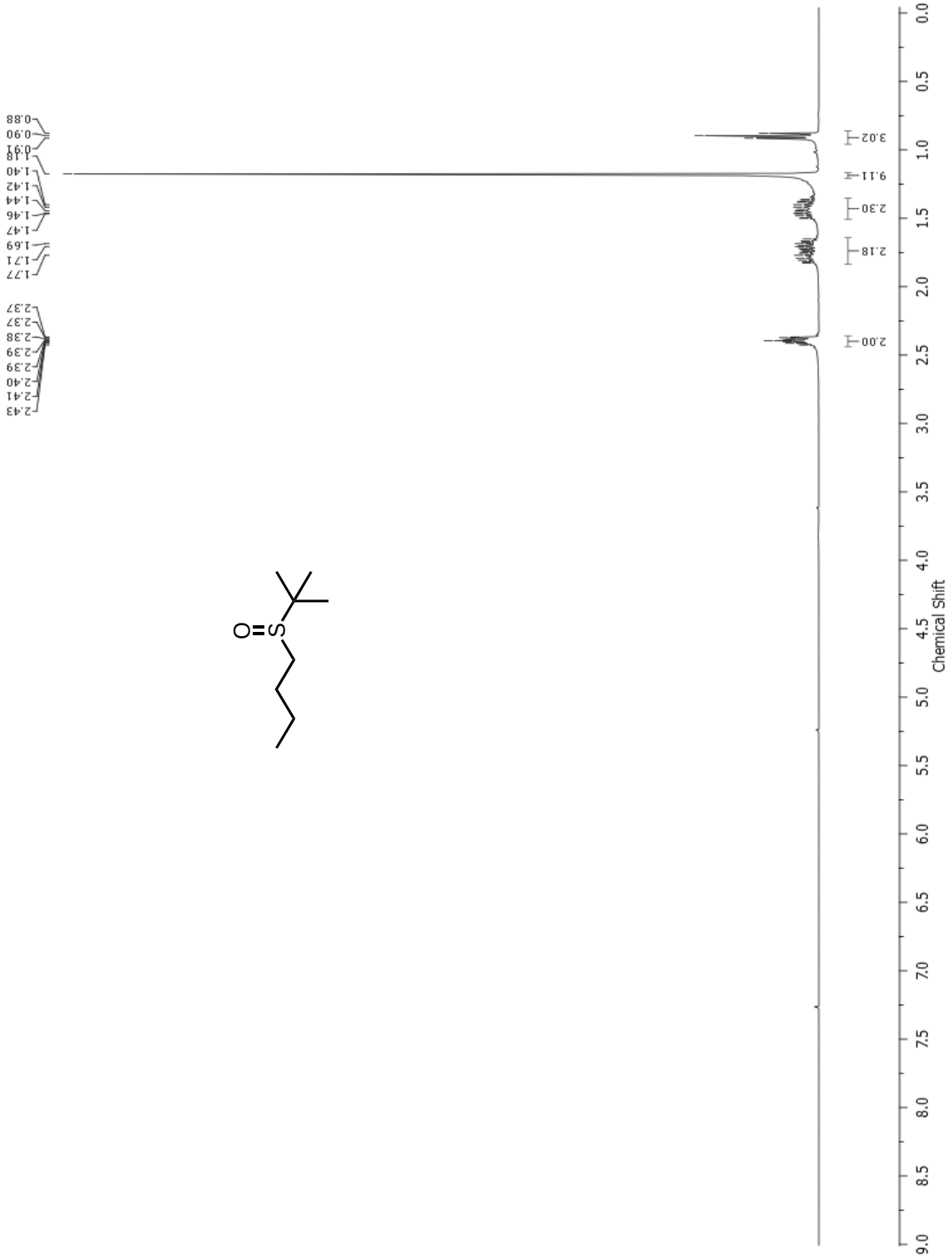

Figure 49: ^{1}H NMR of compound **15a** in $CDCl_3$.

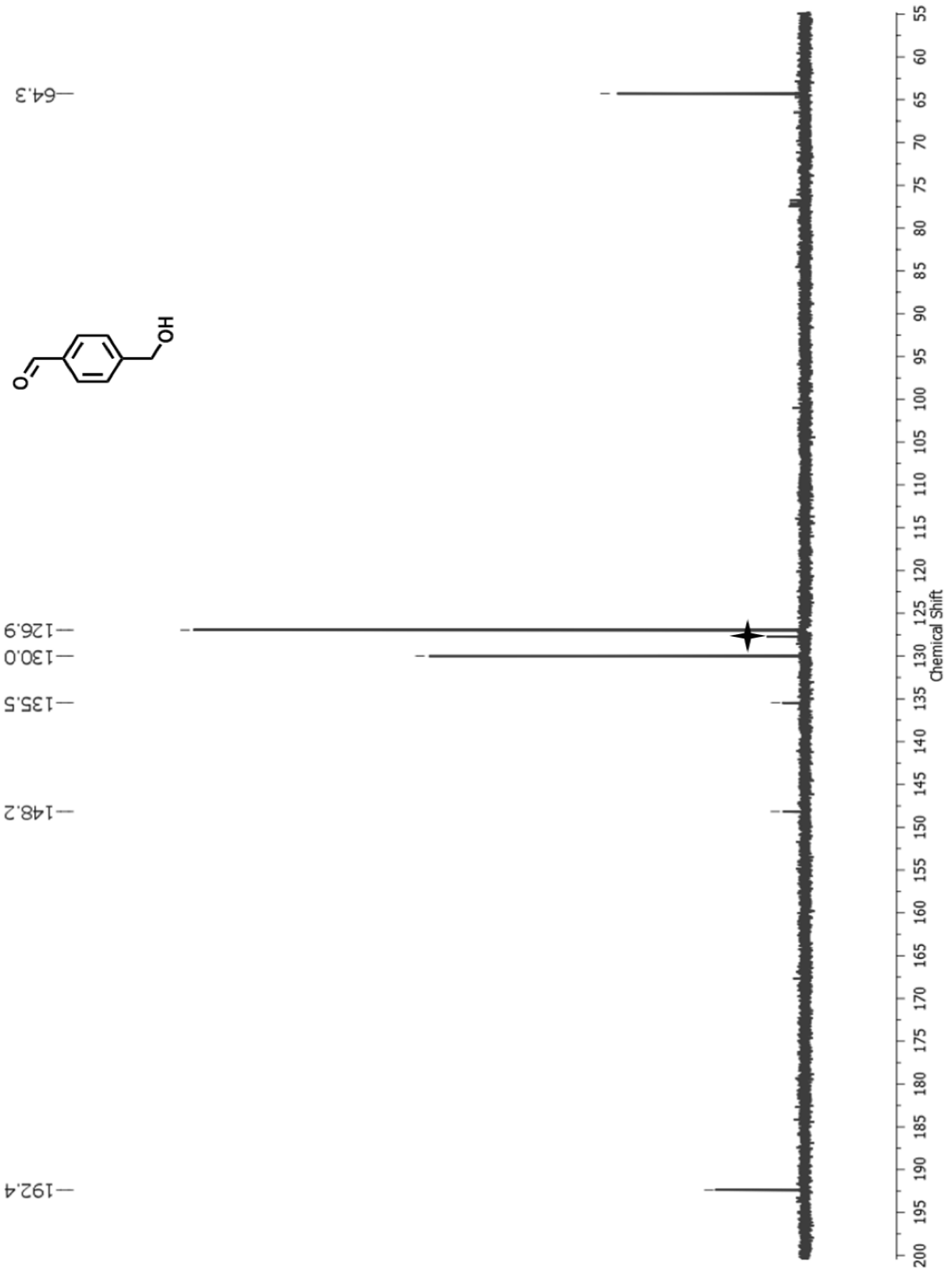

Figure 50: ^{13}C NMR of compound **2** in $CDCl_3$.

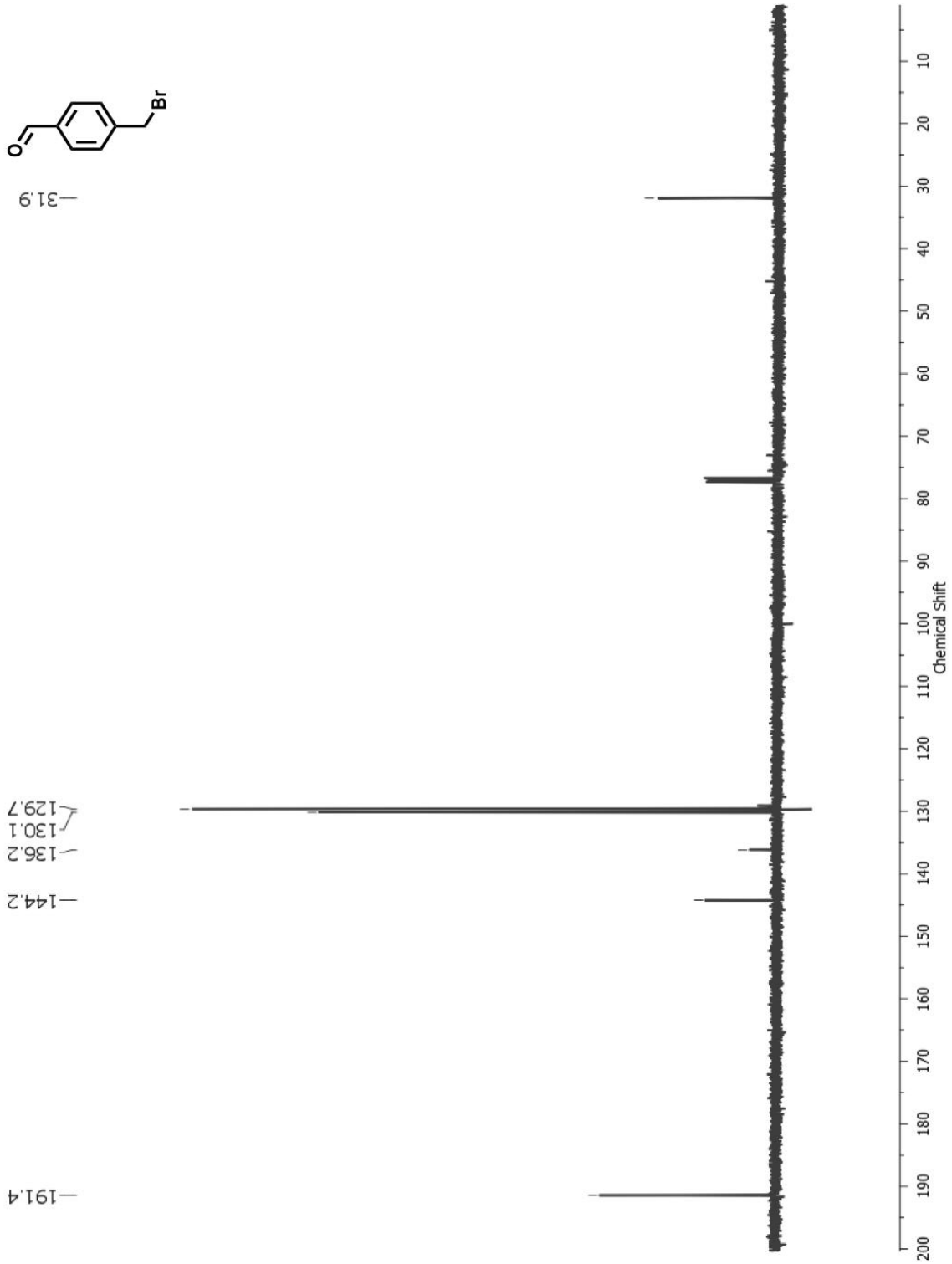

Figure 51: ^{13}C NMR of compound **3** in $CDCl_3$.

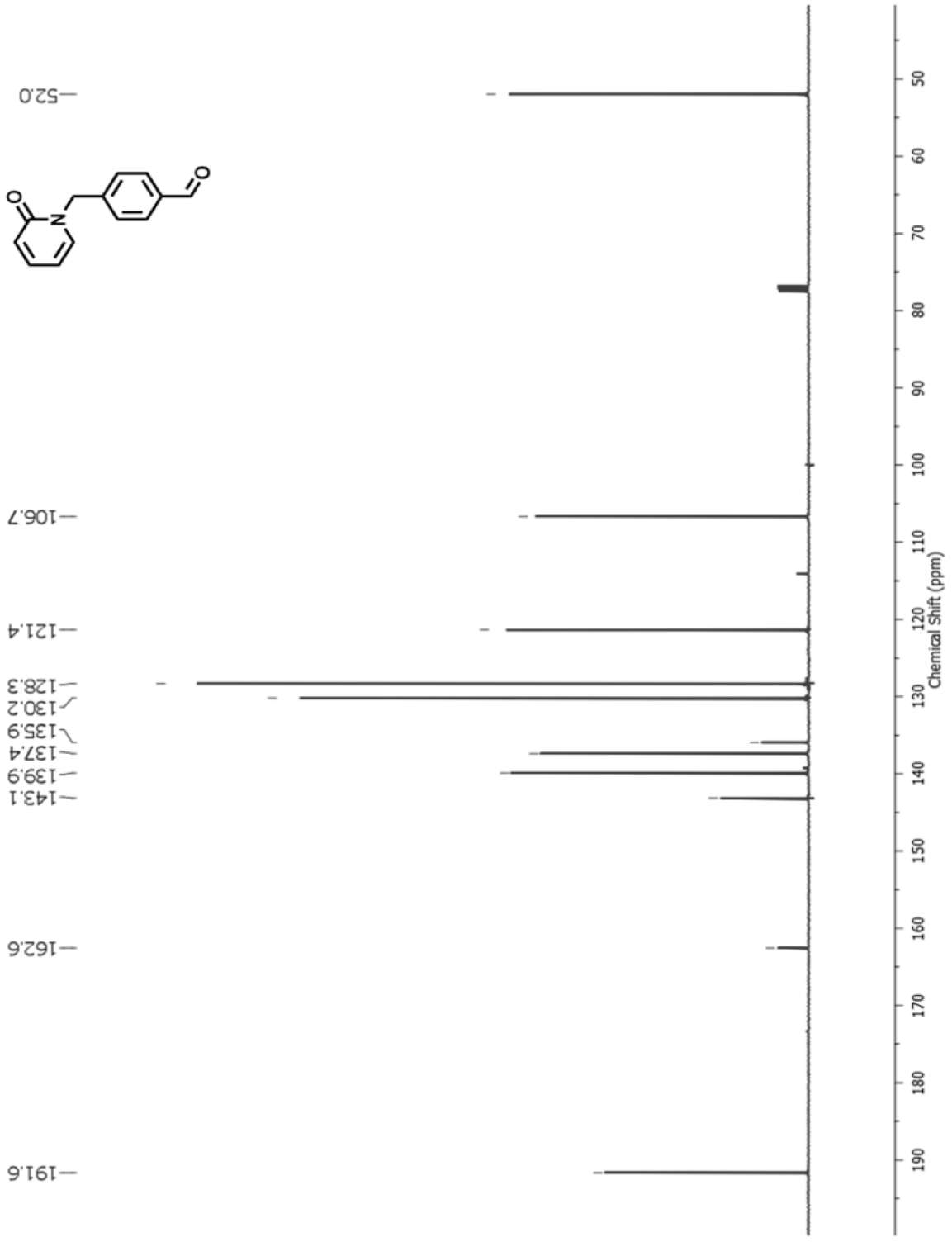

Figure 52: ^{13}C NMR of compound **4** in $CDCl_3$.

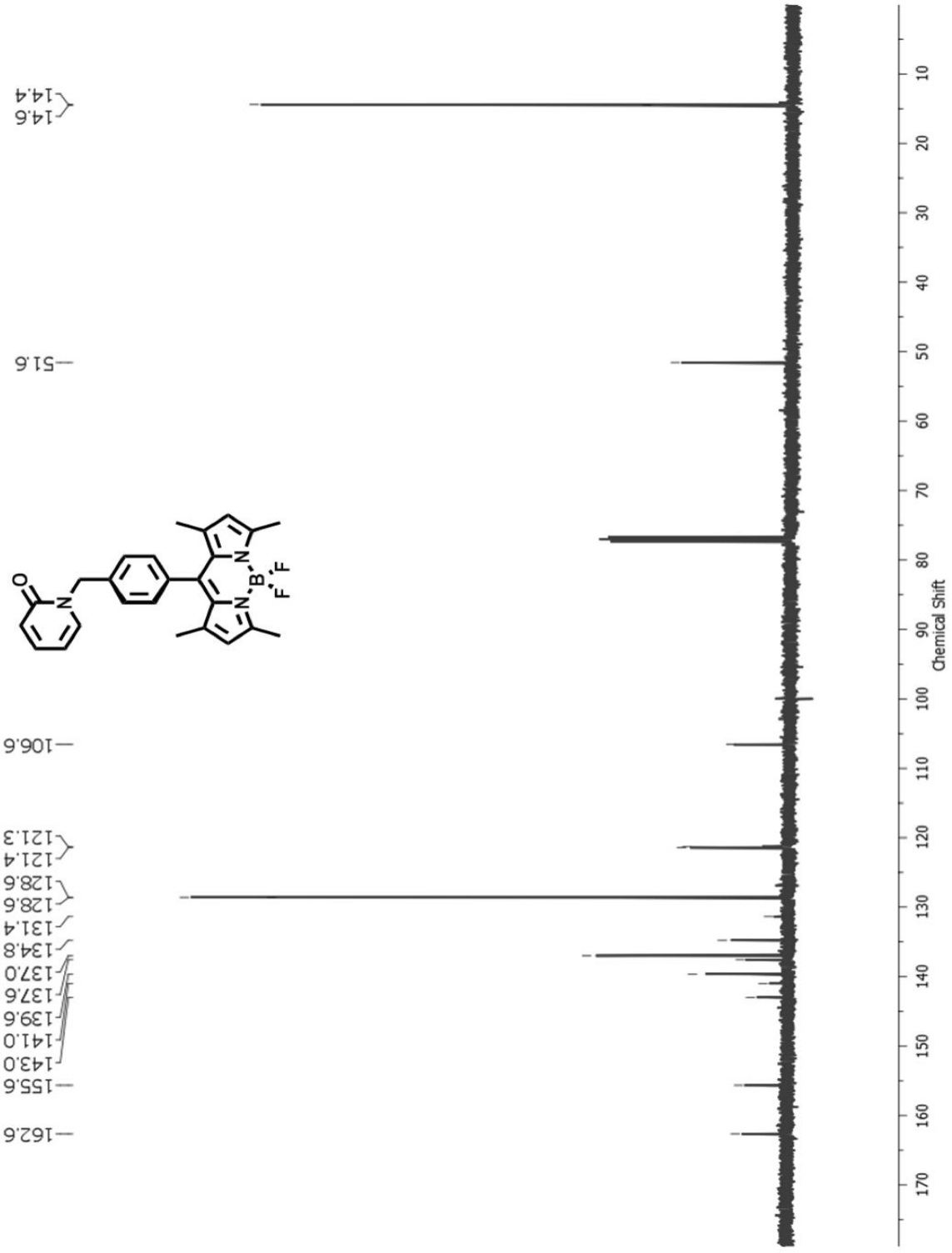

Figure 53: ^{13}C NMR of compound **5** in $CDCl_3$.

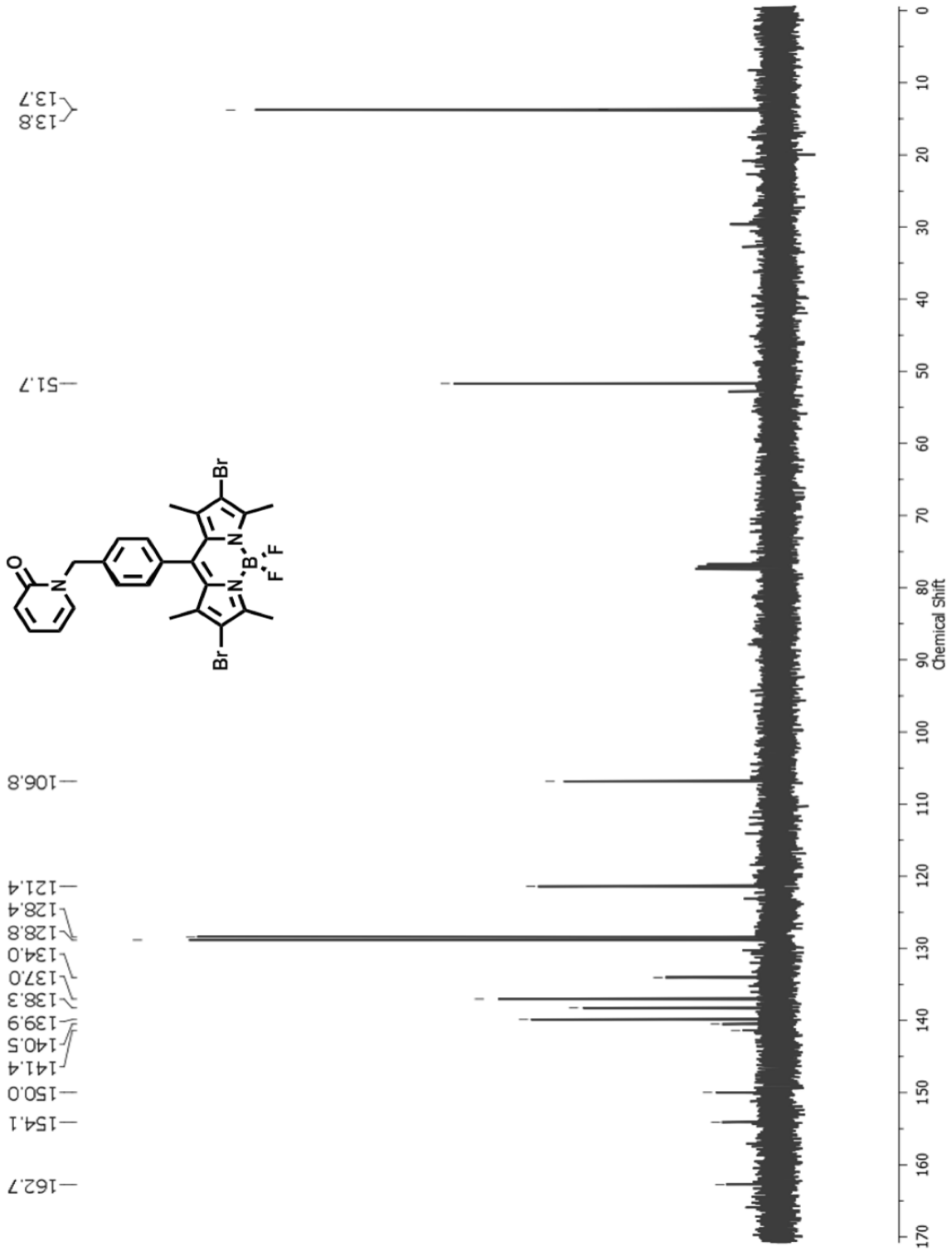

Figure 54: ^{13}C NMR of compound **6** in $CDCl_3$.

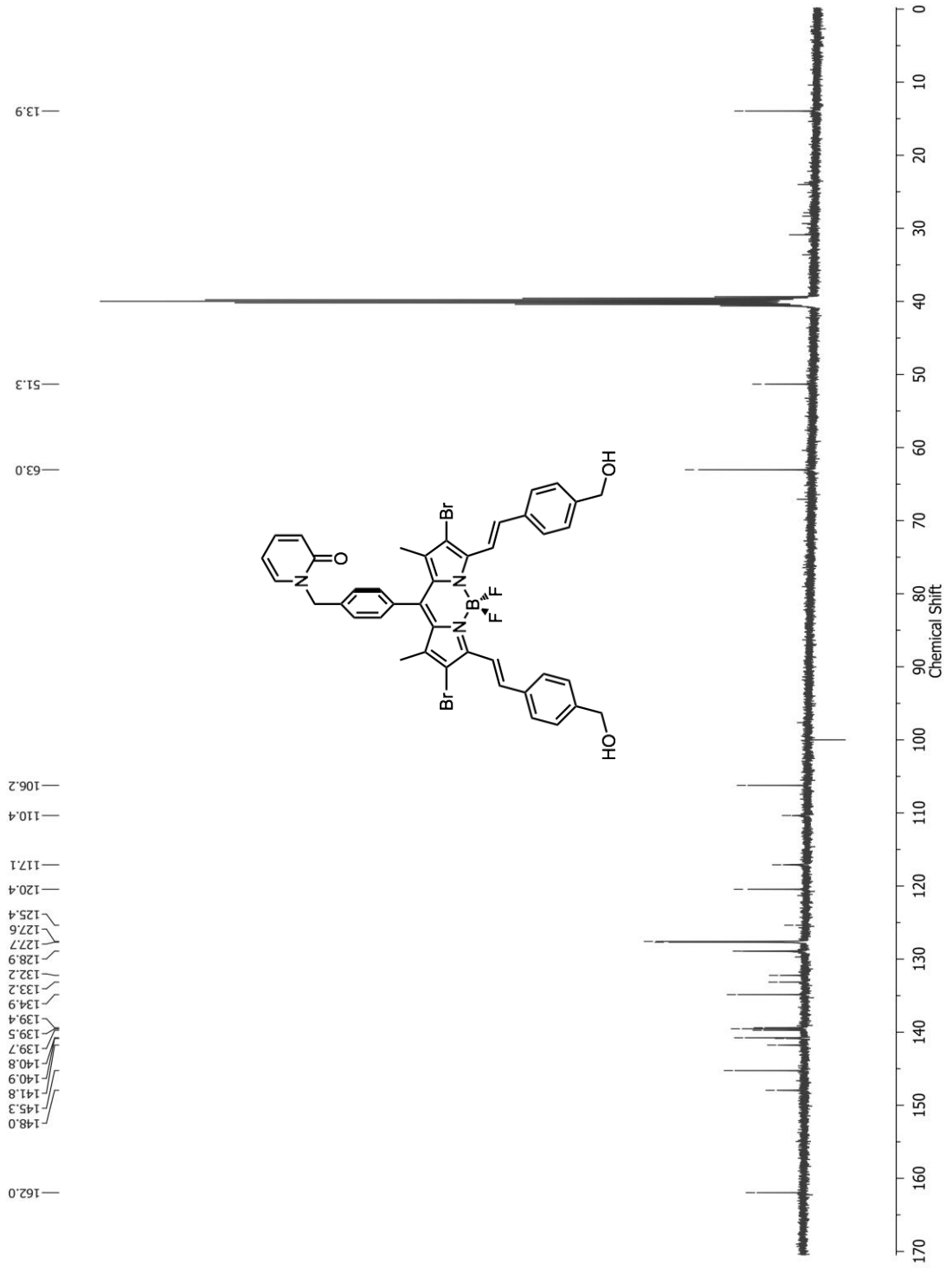

Figure 55: ^{13}C NMR of compound **7** in DMSO-d_6.

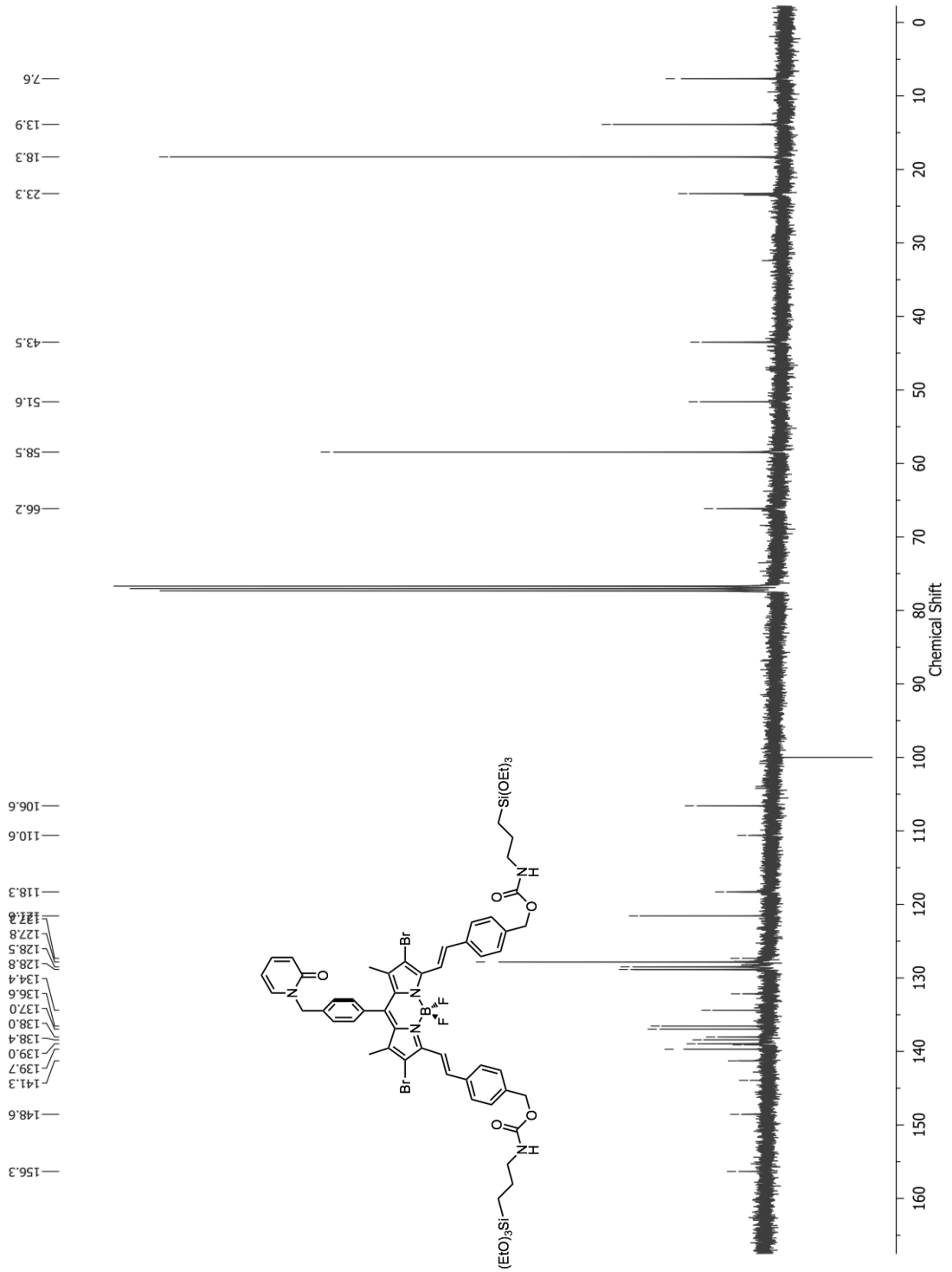

Figure [56]: ^{13}C NMR of compound **8** in $CDCl_3$.

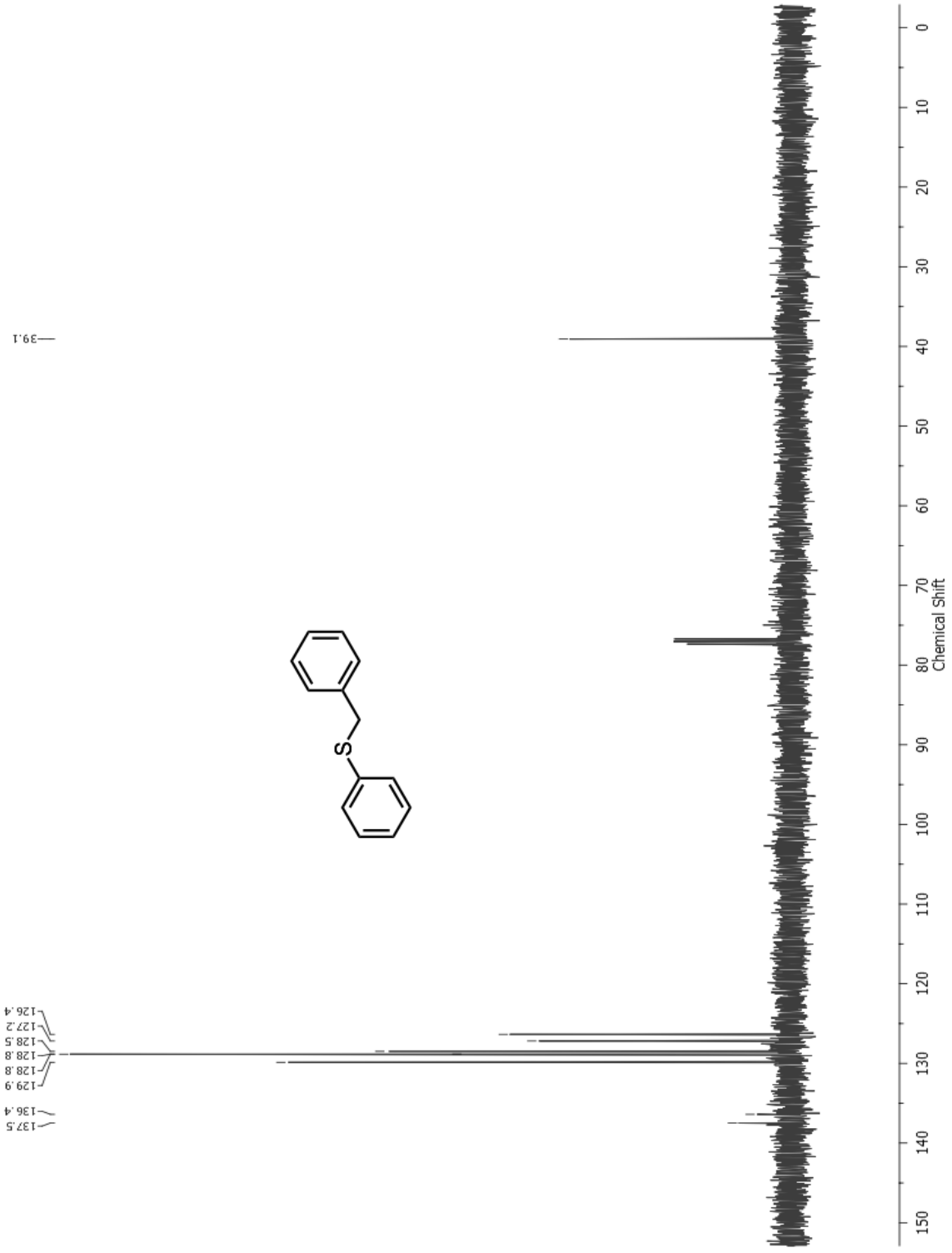

Figure 57: ^{13}C NMR of compound **12** in $CDCl_3$.

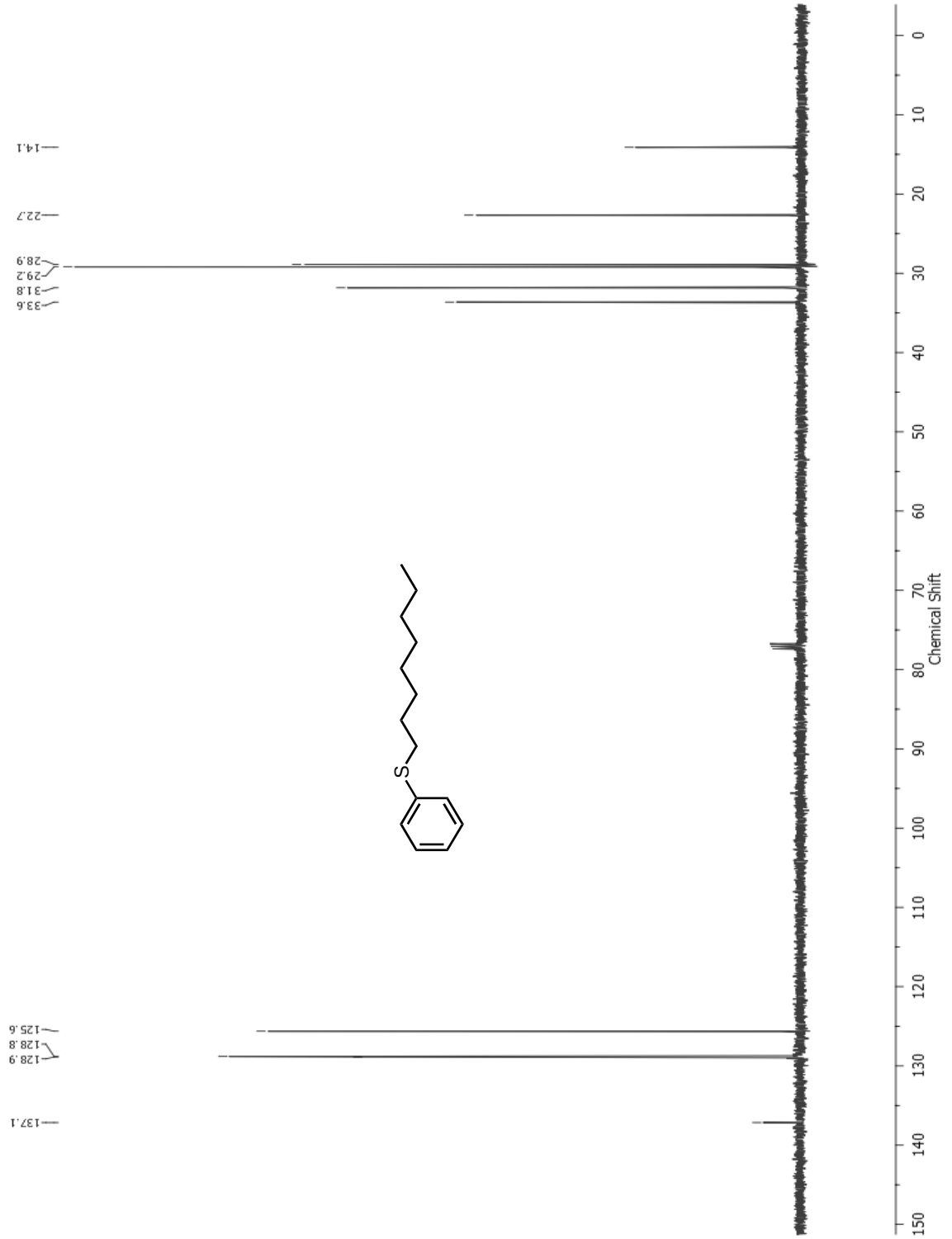

Figure 58: ^{13}C NMR of compound **13** in $CDCl_3$.

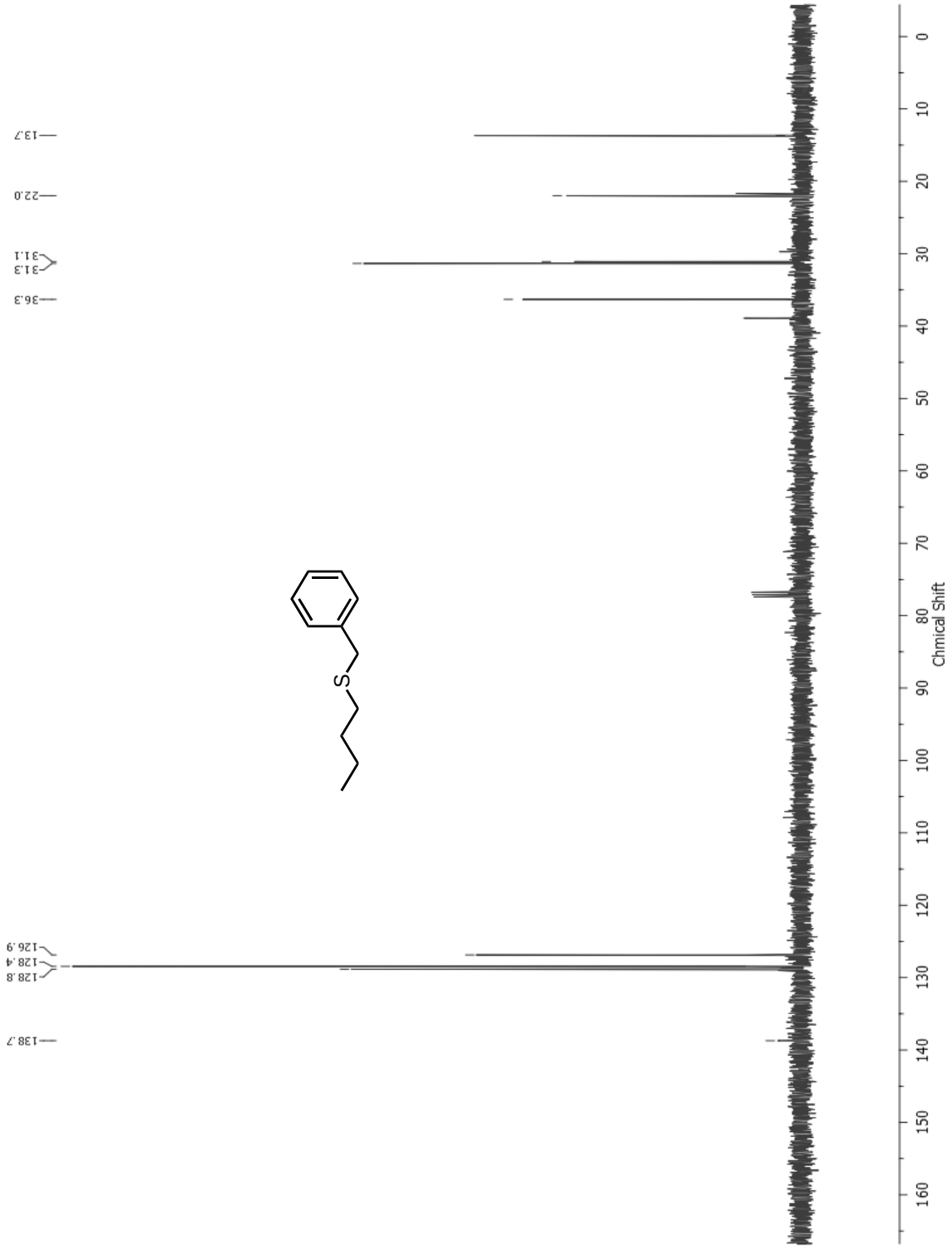

Figure 59: ^{13}C NMR of compound **14** in $CDCl_3$.

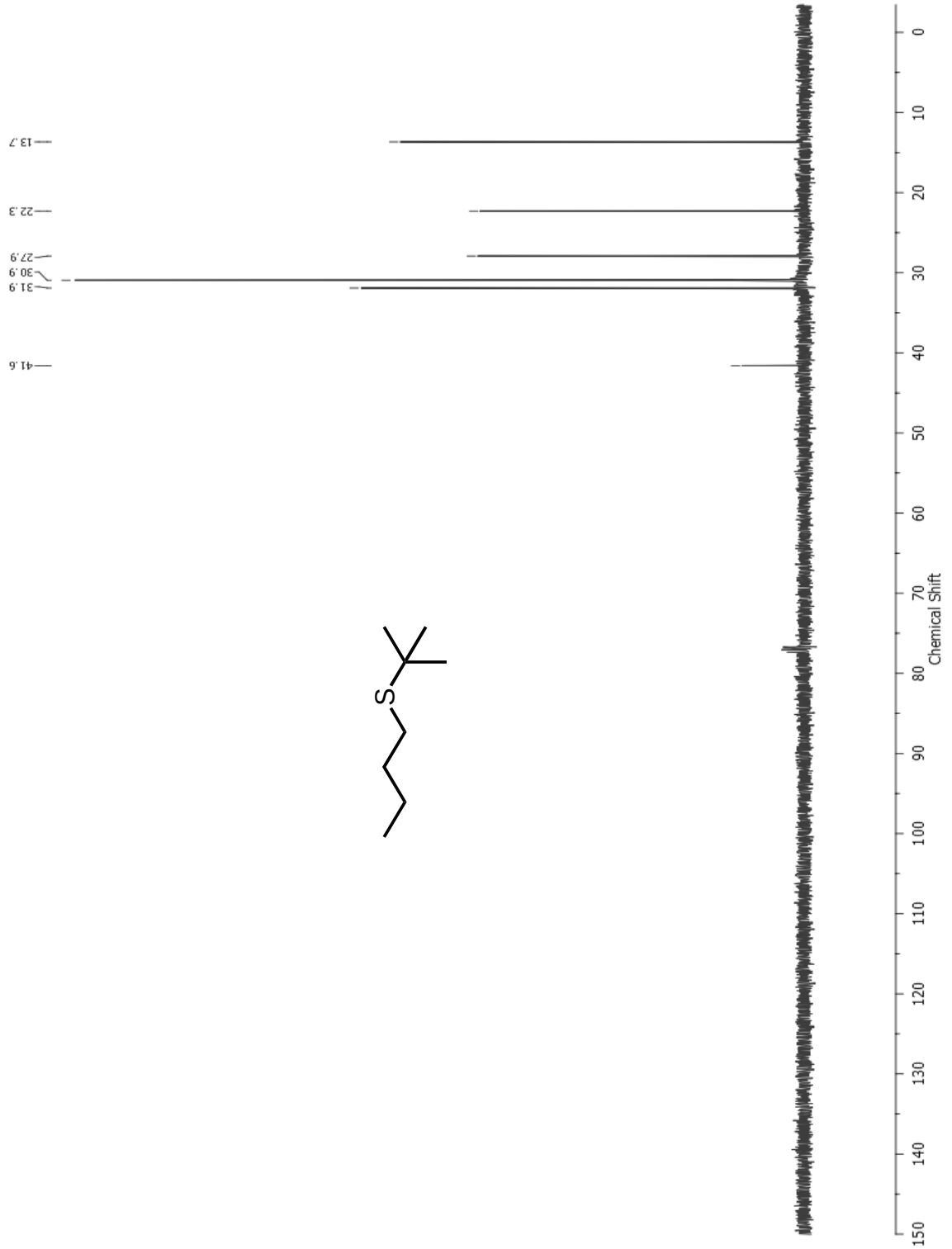

Figure 60: ^{13}C NMR of compound **15** in $CDCl_3$.

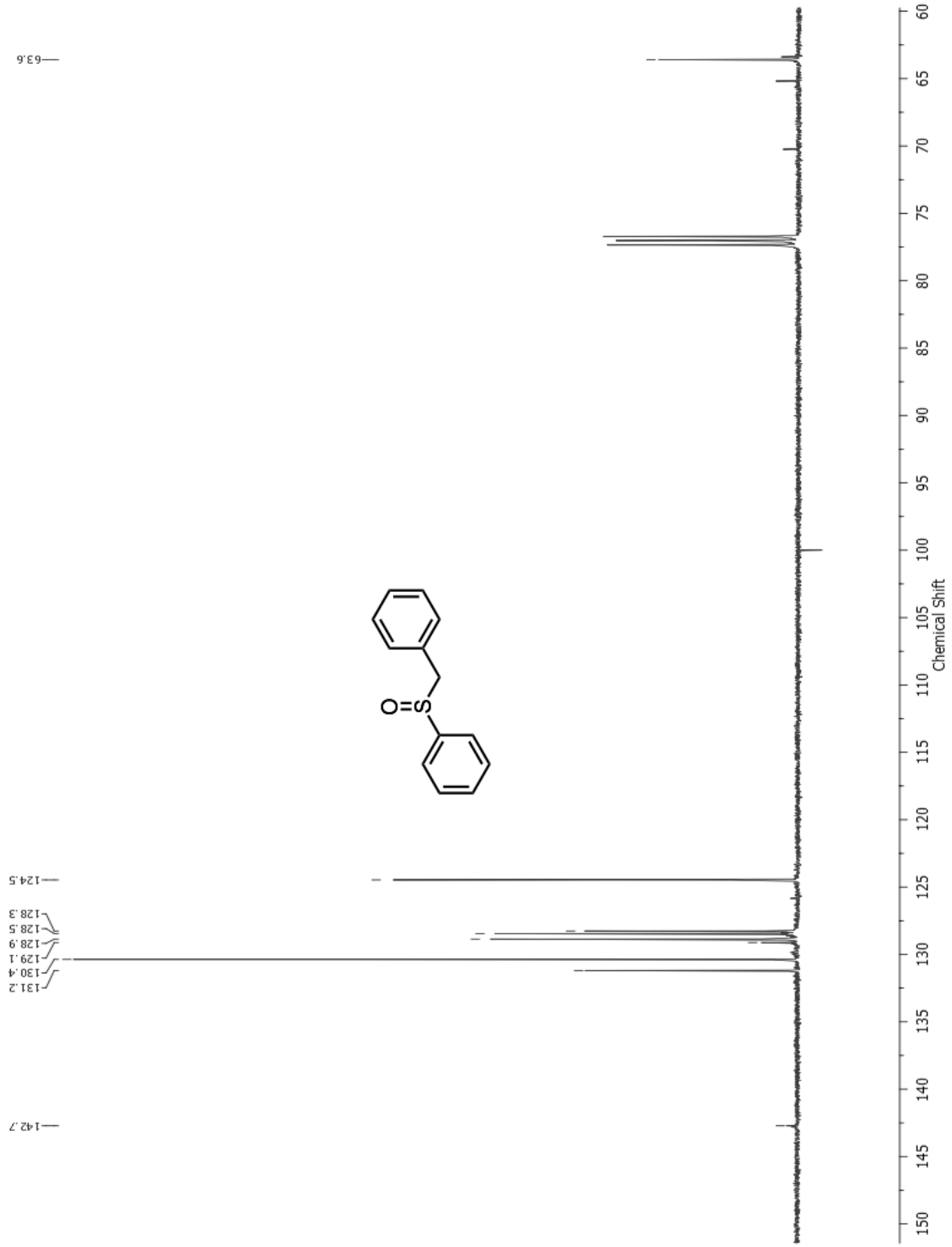

Figure 61: ^{13}C NMR of compound **12a** in $CDCl_3$.

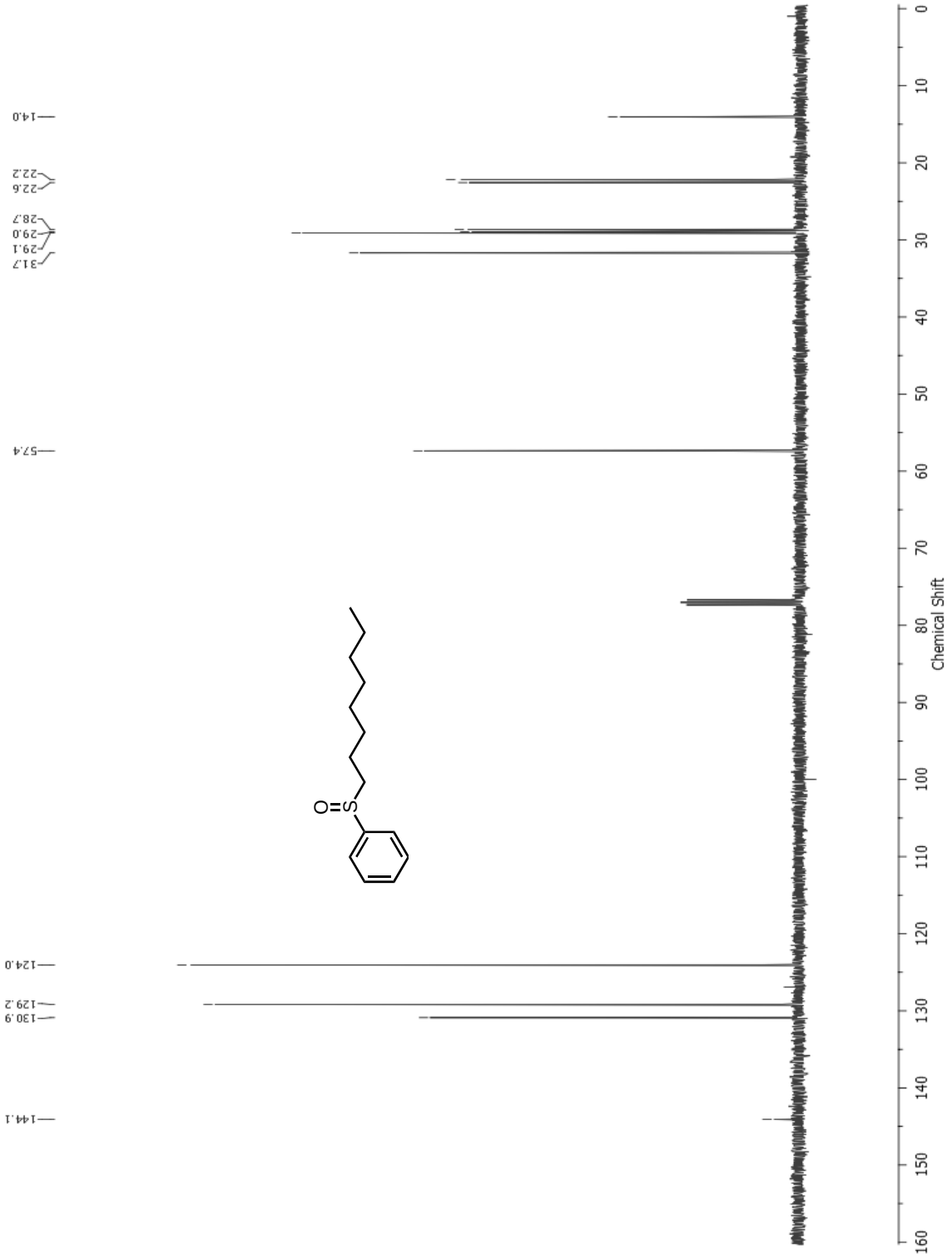

Figure 62: ^{13}C NMR of compound **13a** in $CDCl_3$.

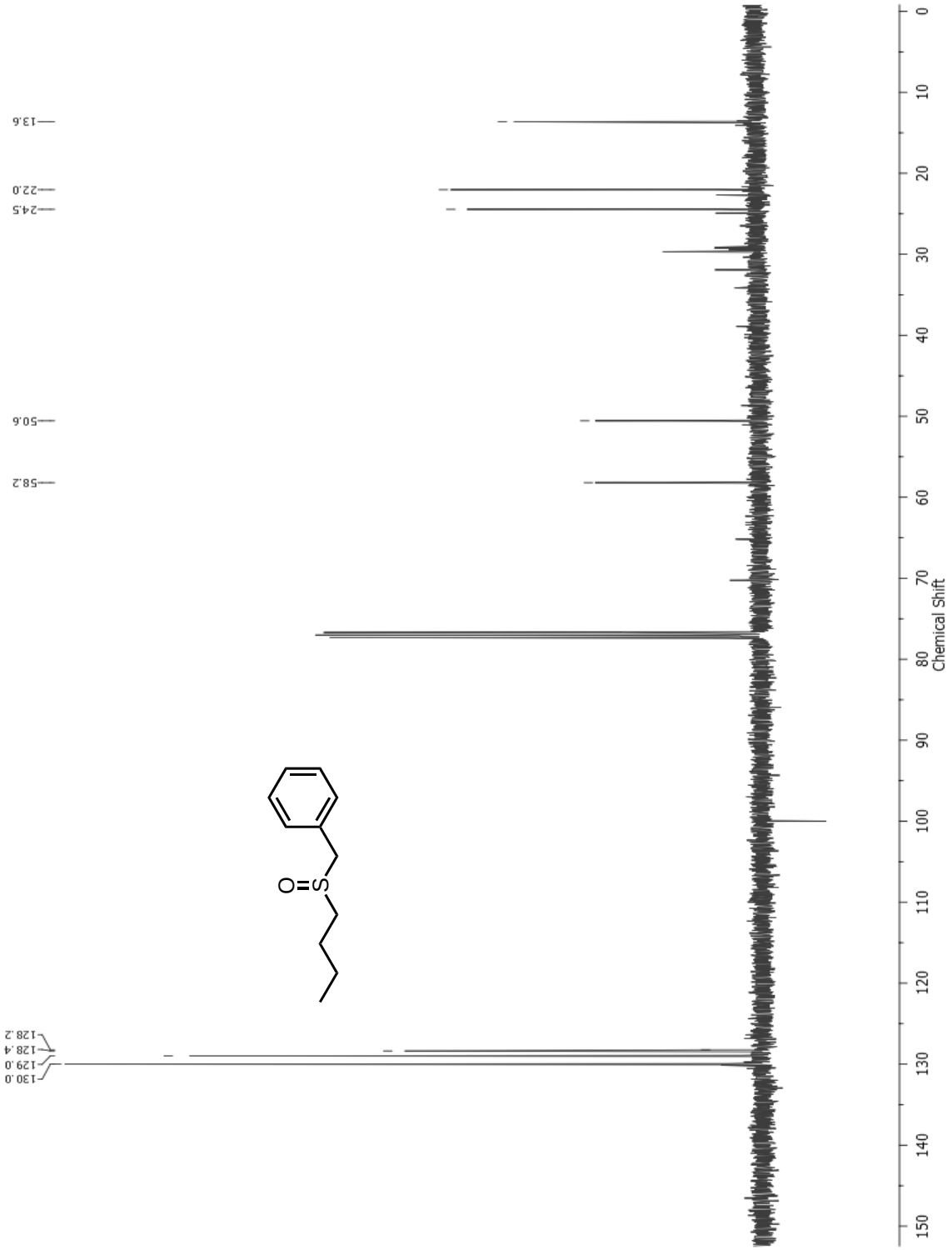

Figure 63: ^{13}C NMR of compound **14a** in $CDCl_3$.

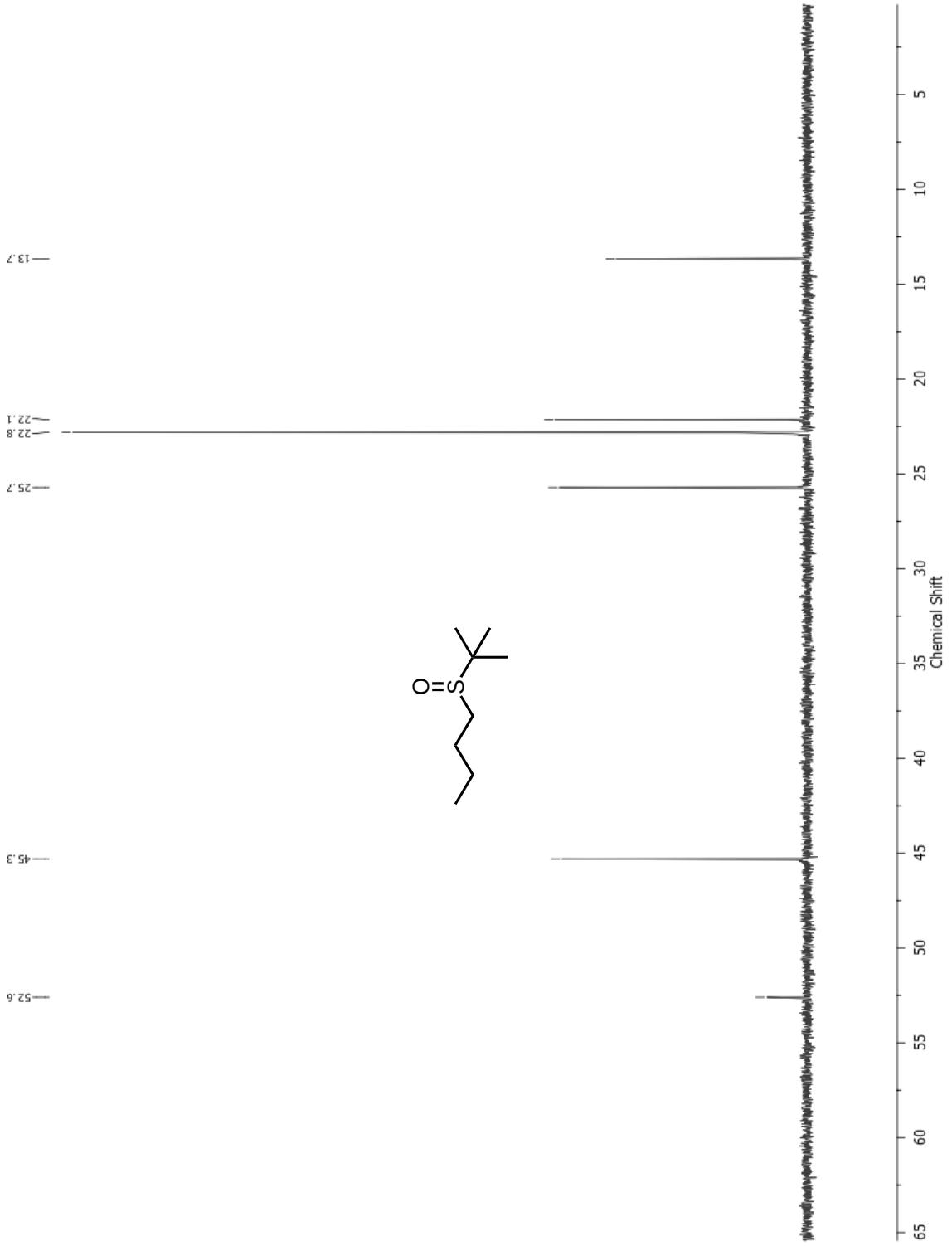

Figure 64: ^{13}C NMR of compound **15a** in $CDCl_3$.

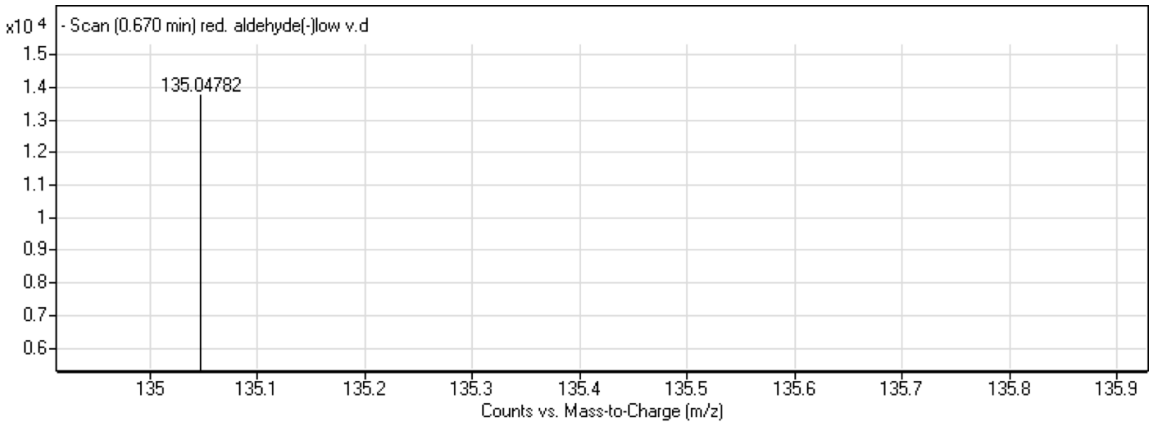

Figure 65: ESI - HRMS of compound **2**.

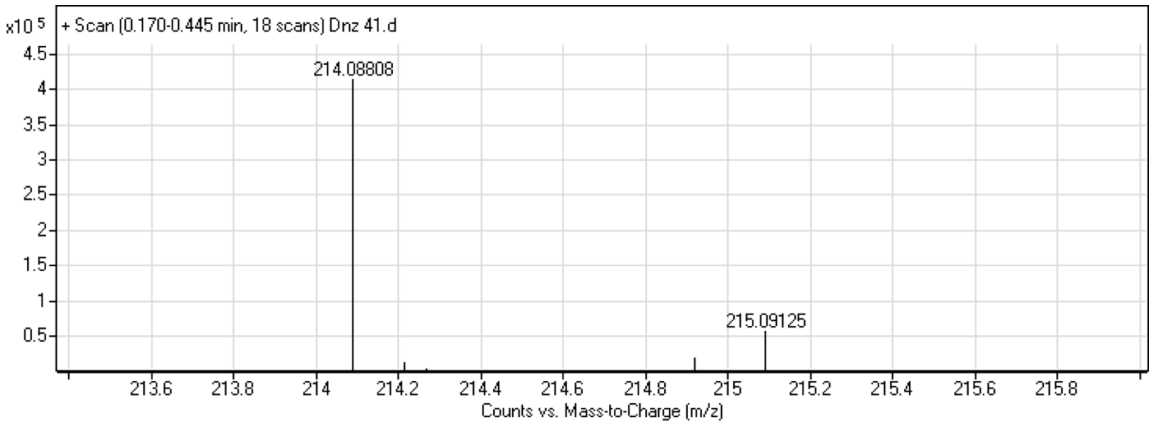

Figure 66: ESI - HRMS of compound **4**.

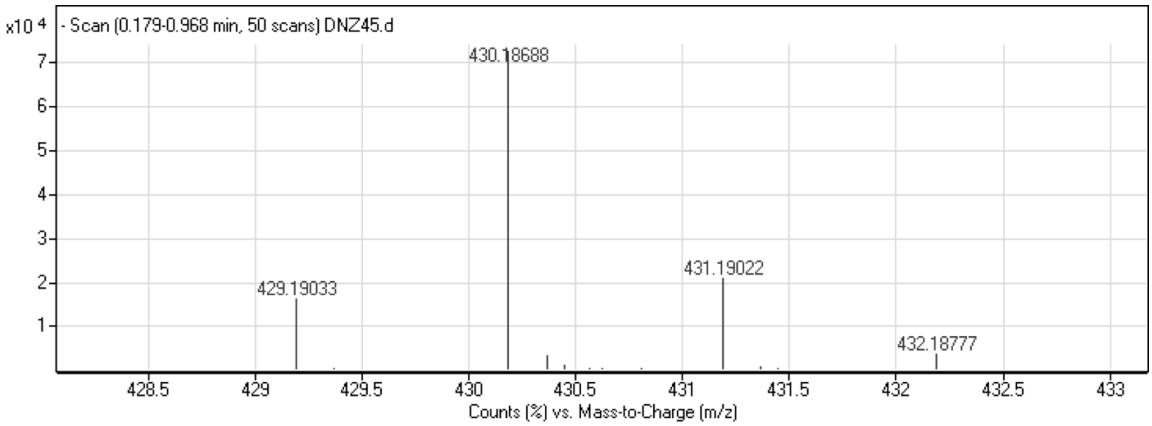

Figure 67: ESI - HRMS of compound **5**.

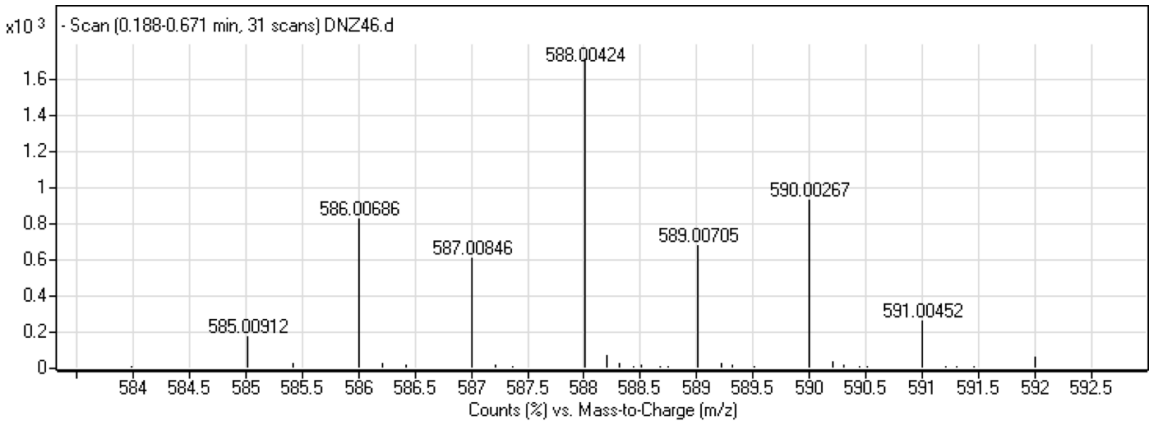

Figure 68: ESI - HRMS of compound **6**.

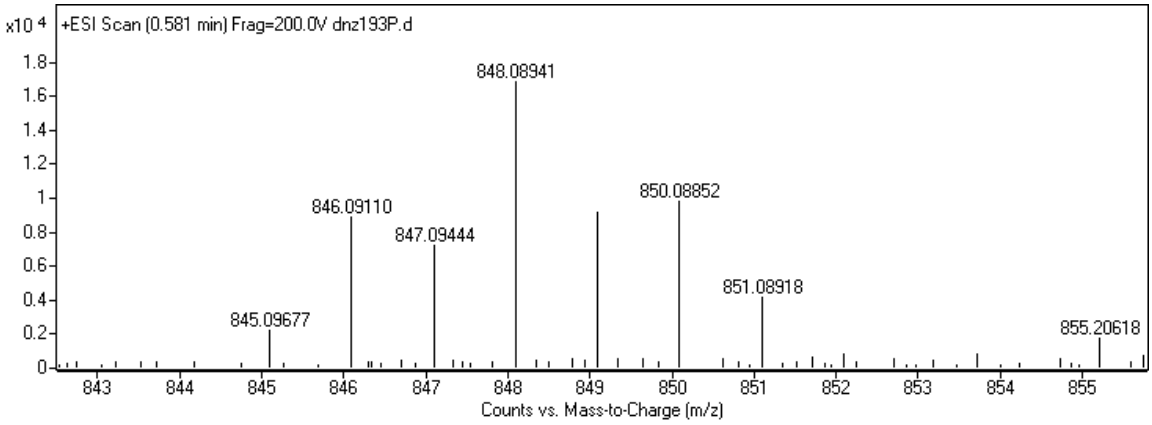

Figure 69: ESI - HRMS of compound **7**.

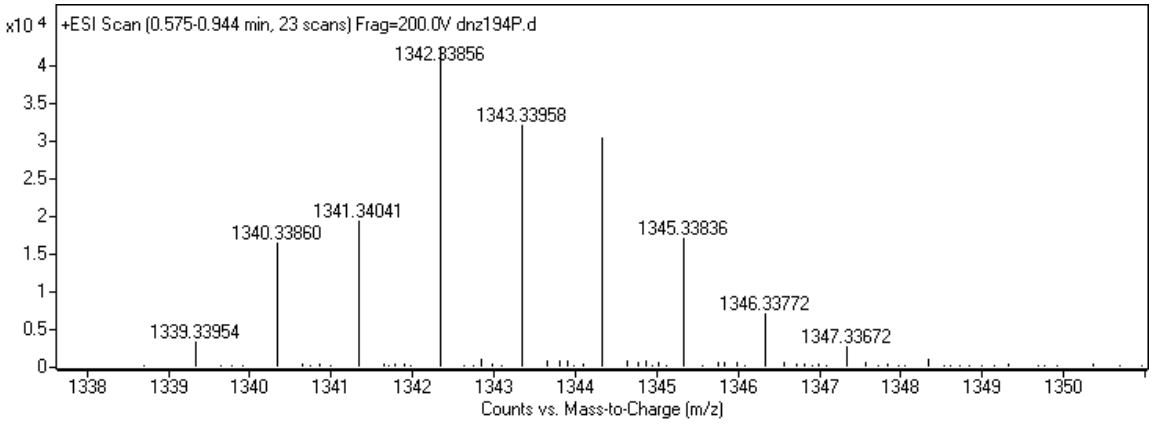

Figure 70: ESI - HRMS of compound **8**.

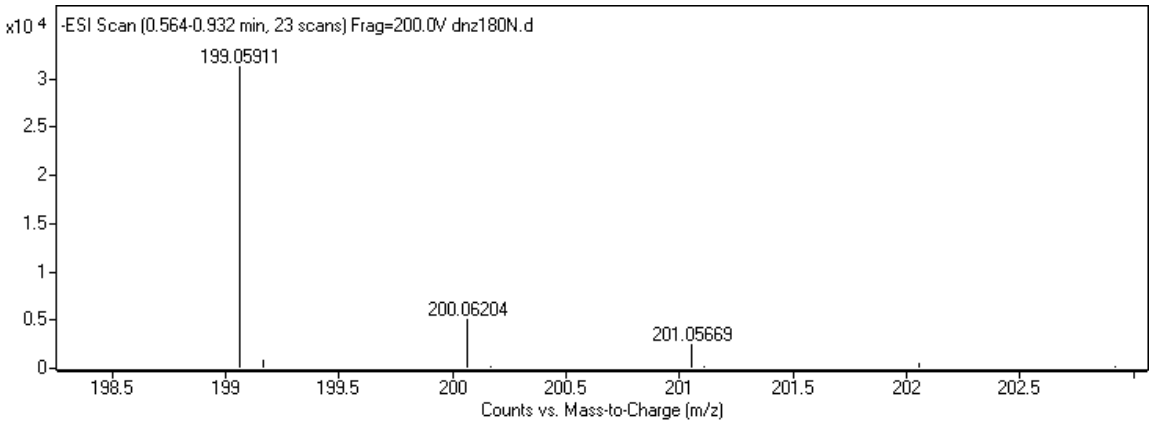

Figure 71: ESI - HRMS of compound **12**.

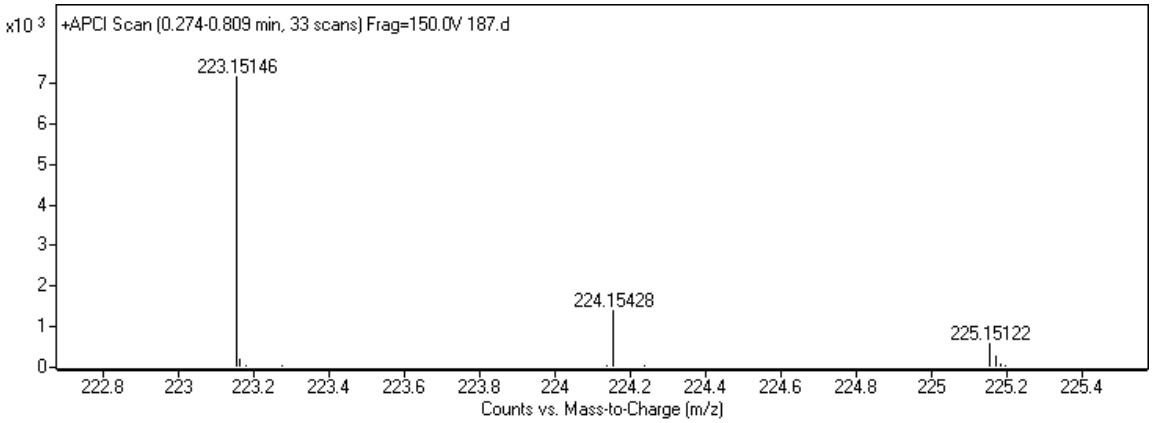

Figure 72: APCI - HRMS of compound **13**.

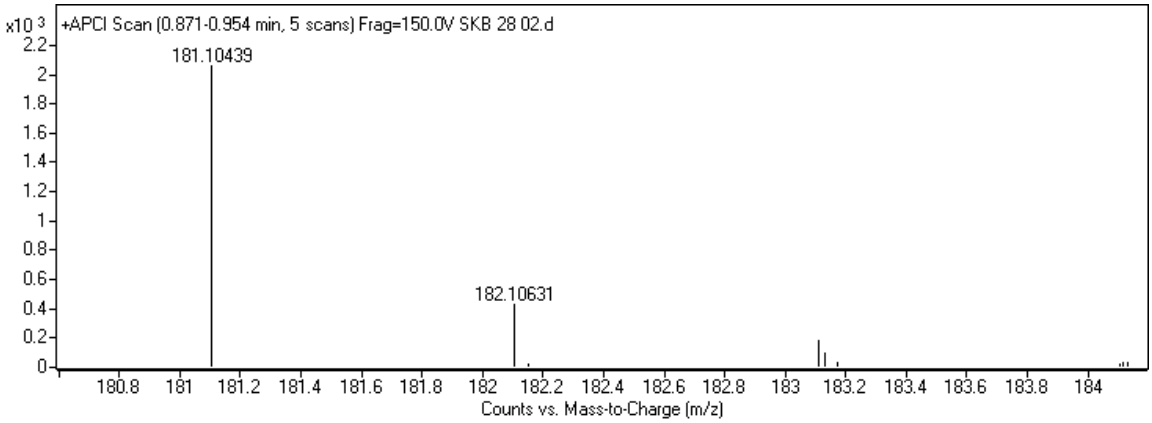

Figure 73: APCI - HRMS of compound **14**.

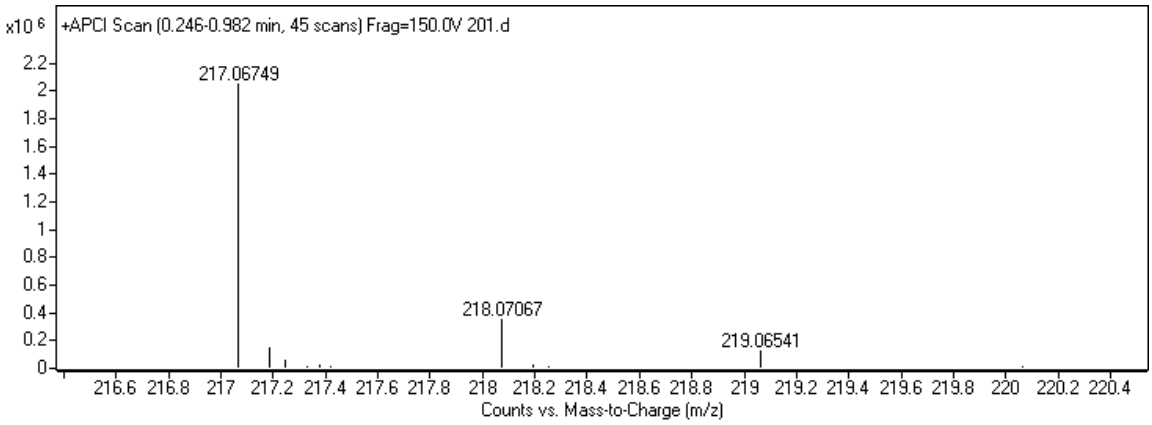

Figure 74: APCI - HRMS of compound **15**.

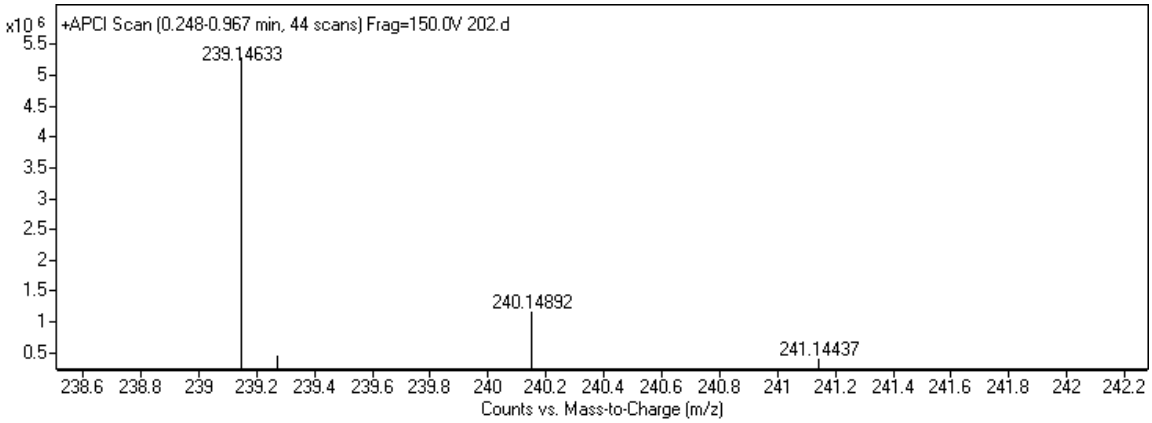

Figure 75: APCI - HRMS of compound **12a**.

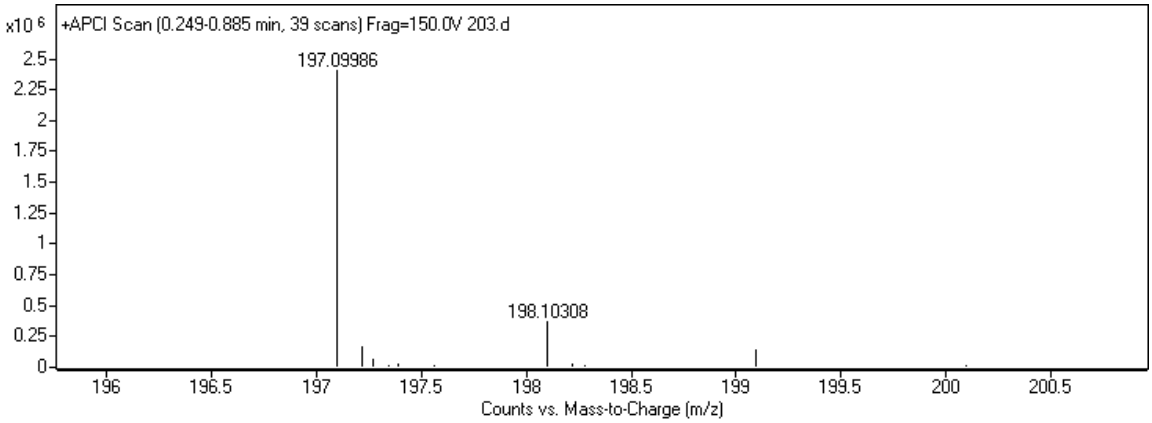

Figure 76: APCI - HRMS of compound **13a**.

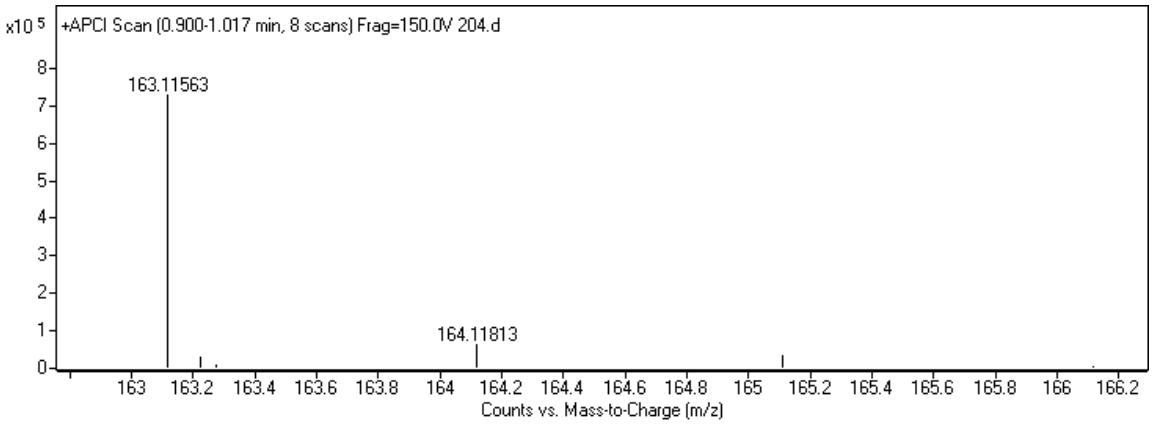

Figure 77: APCI - HRMS of compound **14a**.

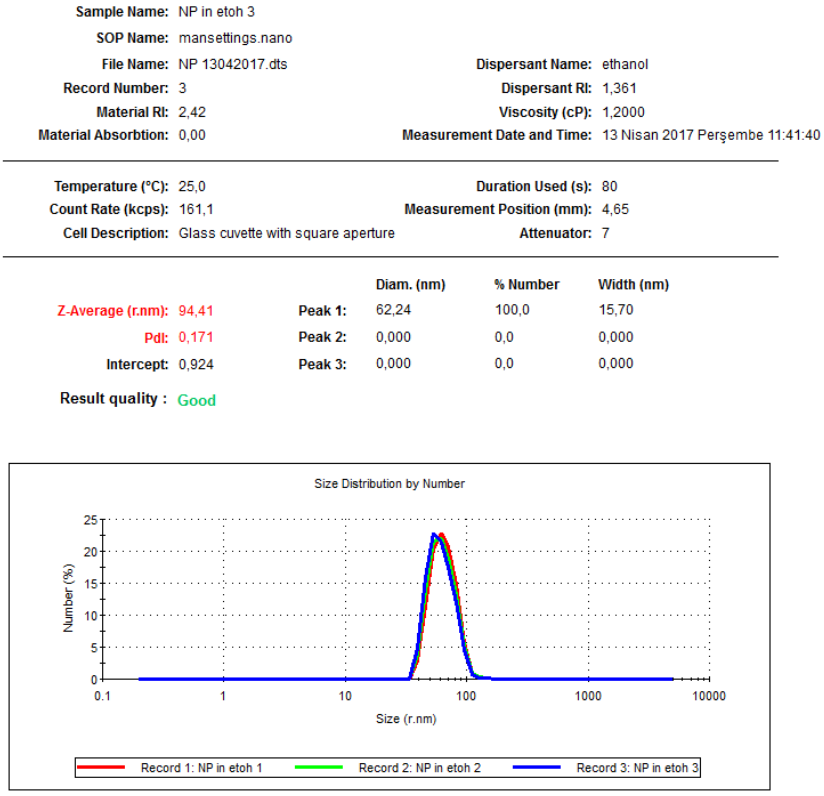

Figure 78: Size Distribution of BODIPY functionalized silica coated SPIONs (**10**) in EtOH.